Optimizing Electric Vehicle Charging Networks: Adaptive Placement and Energy Management in Uncertain Environments

by

Faraz Zargari

A thesis submitted in partial fulfillment of the requirements for the degree of

Master of Science

in

Energy Systems

Department of Electrical and Computer Engineering
University of Alberta

Abstract

With the emerging proliferation of electric vehicles (EVs) in traffic, the optimal deployment of EV charging stations has become a critical issue due to the foreseeable significant impact on conventional power distribution systems and traffic networks. With the complex coupling between time-varying traffic flow demand and power demand during a day, it is challenging to intelligently compromise the infrastructure cost and service quality to ensure cost-effective investment as well as customers' comfort. To deal with this particular challenge, in this study, an iterative algorithm comprising three stages with comprehensive formulations is presented to optimize the locations and sizing of charging stations, considering the EVs' behavior and customers' perspective in the composite transportation and power network. To verify the proposed algorithm, a case study based on a 25-node transportation network integrated with IEEE 33-bus system is done. Numerical results show that our algorithm can efficiently solve the problem in power-traffic coupled networks while accounting for time-varying flow demand and power demand.

Additionally, we addressed the high power needs of charging stations by treating them as microgrids capable of generating their own power from renewable sources. This new approach aims to make the system more robust and dependable. To do this, we introduced a sophisticated online algorithm based on thresholds. This algorithm is crucial in managing the energy storage in each microgrid, finding the best balance between charging, discharging, and interactions with the main grid. We conducted a thorough mathematical analysis to understand how well this algorithm performs in worst-case scenarios. Then, we tested it with two detailed case studies: one using

generated data and the other using real-world information. In both cases, our model consistently showed strong performance, often reaching nearly optimal results.

Preface

This thesis is an original work by Faraz Zargari. A version of **Chapter 2** and **3** is published as Zargari, F., Li, Y., Jiang, H., & Li, Y. (2023). "Electric-Vehicle Charging Station Optimization in Power-Traffic Coupled Networks: Problem Formulations and A Three-Stage Iterative Algorithm." IEEE Transactions on Transportation Electrification.

I dedicate this thesis to my significant other, whose unwavering love and support have served as a guiding beacon throughout my research journey. To my cherished family, your boundless love, encouragement, and sacrifices have shaped the person I've become today. Thank you for everything.

Acknowledgements

I extend my heartfelt thanks to Professor Yunwei (Ryan) Li, my supervisor, and Yuzhuo Li, my friend and colleague, for their invaluable guidance, support, and expertise during the entirety of this research endeavor. Professor Li's unwavering dedication to academic excellence and exceptional mentorship profoundly influenced the outcome of this work.

I am profoundly grateful for the extensive time and effort he invested in offering insightful feedback, constructive criticism, and invaluable suggestions that significantly improved the quality and coherence of this paper. His expertise in the field and commitment to fostering my intellectual growth have been genuinely inspiring.

Table of Contents

List of Tables

List of Figures

Chapter 1

Introduction

1.1 Motivation and Problem Statement

Addressing urgent global challenges such as climate change and energy scarcity has led to a significant emphasis on replacing fossil fuels with cleaner energy sources across various sectors. Embracing renewable energy, such as photovoltaic or wind power, presents a compelling opportunity to achieve the zero-emission goal pursued by many countries. This initiative aligns with the increasing adoption of electric vehicles (EVs), seen as an effective solution to reduce fossil fuel consumption and mitigate noise pollution (Boucher, 2019).

Despite the feasibility of using EVs to combat fossil fuel consumption, several challenges persist, including battery design technologies, electric vehicle safety, installation of charging facilities, load balancing, and more. One major issue is the need for meticulously orchestrated infrastructure capable of seamlessly integrating into existing transportation systems while reinforcing long-term sustainability goals. Strategically placing this infrastructure becomes crucial to alleviate range anxiety, enhance efficiency, and minimize environmental impact. Predictions indicate that the projected surge in EV usage, aiming for a 30% replacement of conventional vehicles with EVs, could result in an 18% increase in energy demand on a typical summer day in the US [1]. Furthermore, this 30% of replaced EVs lead to a 7% demand increase in peak hours and a 20% increase in off-peak hours in the Netherlands [2].

Hence, designing charging station facilities should consider factors such as customer welfare, installation costs, and compatibility with existing infrastructure. This raises questions about the ideal location and size of the charging stations (CSs), an area of

significant focus among researchers in recent years.

Furthermore, the escalating power demand in recent years has prompted considerations for a more resilient approach to address power shortages. Major power outages affecting millions highlight the need for alternative solutions. Installing equipment in charging stations capable of generating their own energy could contribute to more resilient power networks. Simultaneously, the exploration of Microgrids (MGs) as a means to harness renewable energy sources (RES) has gained traction. MGs, with the capacity for self-generation and ESSs, offer a promising solution. However, due to the intermittent nature of RES, MGs need to maintain connectivity with the main power grid or be equipped with adequate energy storage system (ESS) to ensure consistent supply. Functioning in two distinct modes – *connected* and *islanded* – MGs have the capability to operate independently, but uncertainties regarding energy demand, pricing fluctuations, and resource availability influence decision-making.

Enhanced cooperation among MGs, particularly during blackouts, is vital to meet collective energy demands. The convergence of increasing EV adoption and the evolution of MGs presents multifaceted challenges and opportunities in energy management, supply dynamics, and grid resilience. This study aims to explore the intricate interplay between optimal EV charging infrastructure deployment and the evolving landscape of MGs. Its goal is to navigate complexities and uncover potential synergies between these domains within the evolving energy paradigm.

1.2 Background and Literature Review

1.2.1 Electric Vehicle Charging Infrastructure: Challenges and Optimization Approaches

Since constructing a new charging station needs a considerable amount of investment based on its charging technology, which can affect the charging time, locating and sizing these charging stations need to be optimized to cope with the foreseeable dramatically increasing EV load.

Many publications try to deal with the above challenge by considering different aspects, e.g., planner side perspectives, and customer side perspectives, which led to two main solutions to this problem are flow-based optimization (FBO) and node-based

optimization (NBO) formulations [3]. Fig. 1.1 summarizes the formulations.

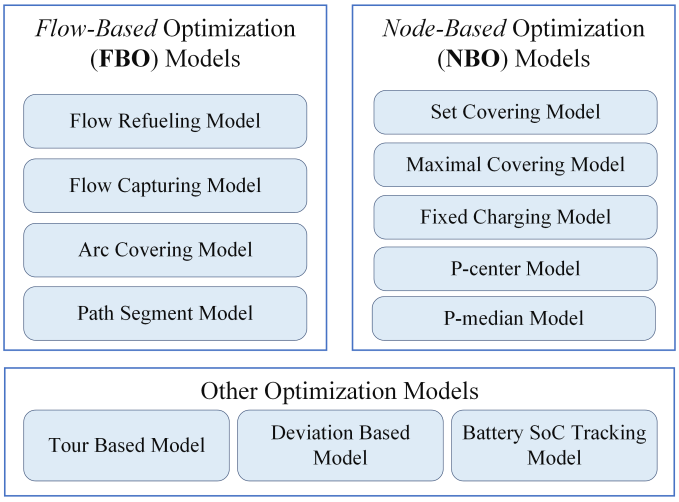

Figure 1.1: A summary of charging station placement problem algorithms.

In the FBO, a set of flows is often selected to be covered by a certain number of stations where the flows pass by, and the objective is normally to maximize the covered flows. The objective can be set to find the optimal locations of the charging facilities in a way that all vehicles can reach their destination points without running out of energy [4]. There are several algorithms based on FBO that try to find the optimal locations of the charging stations, such as the flow capturing model, flow refueling model, arc covering model, etc. In the FBO formulation, the driving range plays a significant role since the distance between charging stations should be less than the driving range. Many different publications have been working on this type of formulation.

The work in [5] is one of the first research efforts that propose FBO as a possible solution to the charging station placement problem and call it the Flow Refueling Location Method (FRLM). In this work, they consider various possible combinations of location sets and then find the optimal set based on traffic constraints. However, the complexity can soar for a large network and results in the Curse of Dimensionality, which tends to require unpractical computation resources. In addition, since the FRLM is not specifically considered for EVs, the constraints from power distribution systems are not considered.

The work in [6] introduces another formulation based on the FRLM method and

calls it Capacitated-FRLM (CFRLM). In this study, the transportation network is expanded based on the algorithm introduced in [7] to consider the state of charge (SoC) at both ends of each trip. In this study, certain selected candidate paths are considered for each origin-destination (OD) pair, and the charging station placement problem is formulated as a mixed-integer linear programming problem. Nevertheless, this study does not consider the different traffic flow demands over time and the power loss terms, which can have a large impact on the locations of charging stations.

The work in [8] proposes a graph-based algorithm to find the optimal locations and size of the charging stations. Although the time-varying charging demand is considered in this study, the power network constraints such as power balance and power losses are not considered. This may lead to not choosing the optimal locations because power loss is an important factor to contribute.

On the other hand, several studies are mainly focused on the power system part of the charging station placement problem. In [9], the active power loss and the voltage deviation are considered as the main objective while the time-varying power demand and the RES are considered. The work in [10] also sets the active power flow loss and the annual maintenance costs as the main objective to be minimized, yet is also considers different sets of charging station locations and finds the one that can minimize the objective function. The work in [11] proposes a model based on CFRLM to find the optimum locations to place the charging stations and also proposes a strategy to expand the existing transportation and power network; however, the charging demand in this study is assumed as a steady state amount, which is not practical in real life situation.

As it is mentioned before, another approach to solving the siting and sizing problem is the NBO formulation. In this formulation, a set of nodes (charging/recharging demand) is normally selected/assumed to be covered by a certain number of stations with a certain coverage (driving) range. The main idea of this formulation is to locate charging stations in the network such that each charging station can satisfy the demand in its neighborhood. It means that the EVs of a network are put in a cluster based on their distance from the charging stations, and each charging station should satisfy the demands of EVs in that cluster. The set covering model, the maximal covering model, and the fixed charging model are some of the models that

are proposed based on the NBO formulation. The work in [12] uses this approach to find the optimum locations of the charging stations. In this study, the charging station placement problem is basically turned into the set covering problem. However, the power network characteristics are not considered, and it could lead to non-optimal charging station locations and sizing in power-traffic coupled networks.

Also, there are other algorithms aiming to solve this problem that consider different aspects of the problem, such as the battery SoC tracking model, tour-based model, etc. The battery SoC tracking model is introduced in [13]. This paper proposes a model to identify the optimal locations of refueling stations for road vehicles based on the characteristics of the road network and the demand for refueling. The authors also propose one heuristic algorithm to address large-scale instances of the problem based on a combination of clustering and a greedy procedure. The model is tested in a case study of a highway network in China. However, in this study, assumptions are simplified and limited data are used. Additionally, the study has a limited scope, which excludes other potential factors that might affect the effectiveness and efficiency of the transportation system.

In addition to the aforementioned research efforts, in Table 1.1, we provide a comprehensive overview of recently published papers, offering insights into various aspects of their studies. This comparative analysis allows us to identify key differentiators between these papers and our own research. By examining common factors typically considered in this field, we highlight the unique contributions and advancements of each publication.

Table 1.1: Overview of related research.

Ref	Year	Vehicle Types	Objectives	Power-traffic coupled	Traffic flow demand	Power-flow demand	User behavior	Model
[14]	2020	EVs	optimal number and sizing of charging piles and the maximum profit	–	✓	–	✓	–
[15]	2020	PEVs	minimize the expected planning cost	✓	✓	✓	–	Modified CFRL model
[16]	2021	SEV	minimum annual total cost	–	✓	–	✓	–
[17]	2021	PEV	minimize direct cost of FCS installation, its induced revenue, and long-term cost on the power grid	✓	✓	✓	–	Graph-based network approach
[18]	2022	BEVs	minimize the construction cost and total BEV travel cost	–	✓	–	✓	Bilevel model
[19]	2022	EVs	minimize total facility deployment costs, EV users travel times and charging expenses and maximize the revenue	–	✓	–	✓	–
[20]	2022	EVs	minimize the investment and operation costs	–	✓	✓	✓	carbon emission flow model
[21]	2022	EVs	minimize the total cost	✓	✓	✓	–	stochastic scenario-based model
[22]	2022	H2EVs	Minimize constructive cost with optimized PV utilization, voltage deviation, transmission loss, etc.	✓	✓	✓	–	Modified MCL model
[23]	2022	EVs	Maximize annual income of charging stations	–	–	–	✓	Charging Queuing Model
[24]	2023	EBs	minimize operation cost and maximize reserve service revenue	✓	✓	✓	–	spatial-temporal operation model
[25]	2023	EVs	Minimize voltage deviations, energy losses, and EVs owners dissatisfaction	–	–	✓	–	two-level optimization model
[26]	2023	EVs	minimize the mean extra time with a minimal sitting and sizing	–	✓	–	✓	graph of the road network
[27]	2023	BEVs	minimize the total electricity costs of all BEVs per interval	–	–	✓	✓	Grid-aware model
[28]	2023	EVs	minimize the operation cost with minimum extra user charges	✓	✓	✓	–	coupled power-transportation network model
[29]	2023	EBs	minimum cost design with optimal siting and sizing	–	✓	–	✓	mixed-integer nonlinear

1.2.2 Microgrids as a Solution for Self-Sustaining Charging Stations

As previously mentioned, establishing EV infrastructure significantly increases power demand, especially during peak hours, amplifying the criticality of power outages. The vast infrastructure of the United States' electric power system, responsible for delivering approximately 4184 TWh annually to millions, grapples with substantial disruptions resulting in multifaceted losses encompassing economic, social, and psychological impacts [30]. Studies conducted by EPRI, LBNL, and DOE estimate economic losses stemming from power outages to range between $30 billion and $400 billion per year [31, 32]. Furthermore, analysis from the Carnegie Mellon Electricity Industry Center underscores a notable uptick in blackout frequency, especially during peak daily and seasonal periods, attributing this surge notably to weather-related outages. Incidents have surged from 5-20 occurrences yearly in the 1990s to 50-100 annually in recent years [33].

Therefore, in response to the pressing challenges, there has been a growing emphasis on embracing RES as a viable solution. For example, Brazil and Costa Rica rely predominantly on RES for their primary energy needs. In Brazil, renewable energy makes up 85% of the energy supply, while in Costa Rica, it accounts for 90% [34]. Furthermore, numerous studies have forecasted a complete transition to RES by 2050. [35–37].

One promising approach involves the utilization of MGs, which first introduced in [38, 39] and considered CSs as one individual MG [40]. In the quest for a dependable integration of Distributed Energy Resources (DERs) like ESSs and manageable loads, the concept of a MG emerges as a unified system responsive to centralized control signals within the larger grid network. While there's ongoing discourse about the precise definition of MGs in technical circles, they can be visualized as an assemblage of loads, Distributed Generation (DG) units, and ESSs operating harmoniously to ensure a reliable electricity supply. These components interconnect with the primary power system at the distribution level, converging at a single Point of Common Coupling (PCC). Embracing MGs as the cornerstone for widespread distributed generation integration facilitates decentralized problem-solving, diminishing reliance on

an intricately coordinated central system and promoting the realization of the Smart Grid vision [41]. Figure 1.2 shows a typical topology for CSMG.

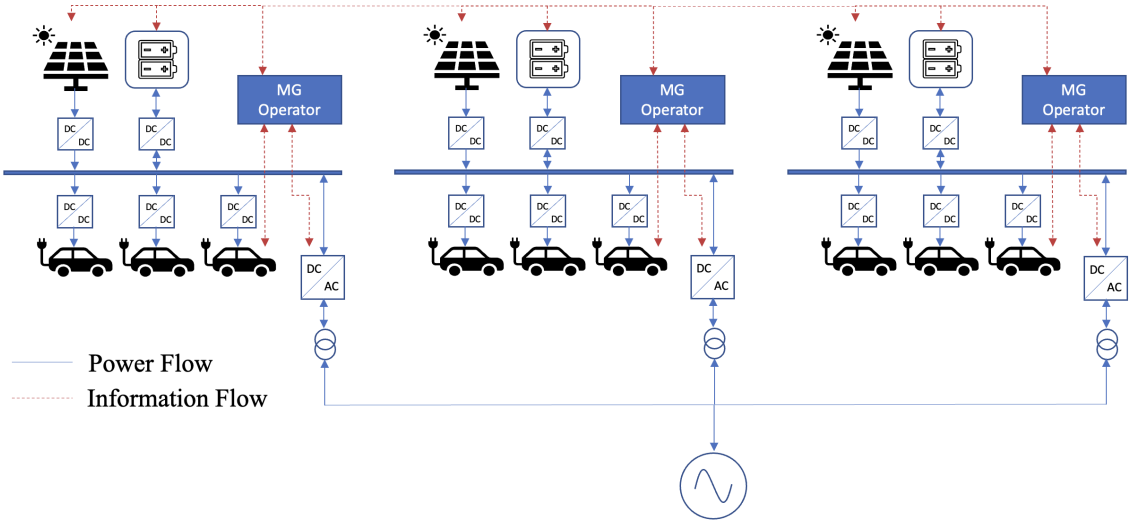

Figure 1.2: Charging Station Microgrid

Although the utilization of RES brings various advantages, it cannot serve as the sole energy source due to its intermittent nature. Consequently, MGs must maintain a stable energy supply, often by remaining connected to the main power grid or by equipping adequate energy storage. The operation of MGs comprises two distinct modes [42, 43]. The first mode is known as the *grid-connected mode*, in which an MG is capable of drawing energy from the main power grid. The second mode is referred to as the *islanded mode* or *stand alone mode,* during which the MG operates independently without relying on energy from the main grid. This islanded mode may come into play when the MG has a surplus of energy from renewable sources or when a blackout occurs in specific sections of the power network due to factors like feeder failures or damage to power lines.

Hence, owing to the sporadic nature of RES and the various uncertainties within MGs, the study of control strategies has emerged as a significant focus in recent years [44]. The aim is to cultivate a dependable and robust system capable of meeting energy demands consistently. Control strategies in MGs encompass multiple tiers, commencing from the micro-source level, which primarily revolves around distinct converter types (e.g., DC/DC and AC/DC), contingent upon the Distribution Gen-

erator (DG) units. At the pinnacle, we encounter the energy management aspect of MGs [45, 46]. This multifaceted control structure seeks to ensure a reliable power supply by efficiently orchestrating and optimizing various elements within MGs.

An inventive approach to power MGs involves peer-to-peer (P2P) energy trading among various MGs [47]. This method facilitates the exchange of surplus energy between MGs, effectively meeting each other's energy needs. Within the realm of energy coordination and P2P trading, distributed algorithms have been suggested. These algorithms involve individual prosumers maintaining a localized estimate of their energy profile and typically sharing this approximation directly with their connected neighbors [48–50].

As previously mentioned, the energy management level of MG controls encompasses four primary types of uncertainties, detailed below [51]:

1. Energy demand from each MG: This stands as the most evident uncertainty within the model. Despite the potential utilization of historical data for prediction, its variability can significantly disrupt system load balance.

2. Available renewable energy at each MG: The volatility of renewable energy has garnered significant attention in recent years. Various models, such as Maximum Power Point Tracking (MPPT) [52], are employed to manage these fluctuations. However, its intermittent nature renders it unreliable as a sole energy source.

3. Purchasing energy price from the main grid: Dynamic energy pricing constitutes another uncertain factor affecting MG operational costs. While different pricing policies exist, they are not the focal point of this study.

4. Blackout occurrences: The possibility of system parts being unable to directly access the main grid to purchase energy due to unforeseen incidents is a constant concern. Addressing these uncertainties is crucial for fostering a resilient system.

Numerous studies have been conducted with the primary objective of addressing the multifaceted uncertainties associated with energy systems. These studies endeavor to develop algorithms and employ various methodologies to enhance the optimization

of the entire system's operational costs. A prevalent approach in these investigations involves leveraging historical data of power demand and the availability of RES. Machine learning techniques are often harnessed to extrapolate future trends from this data [53]. For example, in [54], a combination of a Deep Recurrent Neural Network (DRNN) and Dynamic Programming (DP) was utilized to develop a nearly optimal real-time scheduling policy.

In addressing decision-making under uncertainty, numerous methodologies are deployed, each serving as a potential solution. Among these, Stochastic Optimization (SO) and Robust Optimization (RO) emerge as pivotal and extensively utilized approaches.

In the domain of energy management within single or multiple MGs, researchers have extensively explored stochastic optimization techniques to tackle the complexities arising from uncertainties. Studies such as [55–58] have delved into employing stochastic optimization to optimize energy distribution under various uncertain conditions. The fundamental principle behind stochastic optimization involves the generation of multiple hypothetical scenarios, each representing a potential outcome based on probability distributions characterizing uncertainties. By computing the expected outcomes or optimizing objectives across this array of scenarios, it aims to arrive at a robust decision [59]. However, a drawback that accompanies this method is the computational burden imposed by the necessity to evaluate a multitude of scenarios. Moreover, the reliance on pre-existing and accurately known probability distributions for each uncertainty poses practical challenges, making its implementation less feasible in real-world scenarios.

As mentioned before, another widely adopted methodology is RO. Unlike stochastic optimization, RO operates without requiring prior knowledge of probability distributions for uncertain parameters. Instead, it defines the range of fluctuations for these uncertainties by establishing an uncertain set. If the uncertain parameters remain within this predetermined set, RO typically generates feasible solutions [60, 61]. Studies such as [62–64] have employed RO to effectively manage the energy in MGs. However, a drawback of this approach is its inherent conservatism, as it operates on the premise of addressing the worst-case scenario for uncertainties, potentially leading to overly conservative solutions.

Beyond conventional methods, a diverse array of methodologies offers innovative approaches. Distributionally Robust Optimization (DRO) is a notable amalgamation of Stochastic Optimization (SO) and Robust Optimization (RO) principles [65–67]. In parallel, Model Predictive Control (MPC) adopts an iterative, horizon-based strategy, solving optimization problems continuously within a rolling framework [68]. Additionally, Deep Reinforcement Learning (DRL) undergoes offline training using historical data, facilitating its seamless real-time application for dispatch optimization [69–71].

Table 1.2: Overview of related research.

Ref	Year	MG Type	Uncertainties				Model
			RES	Load	Price	Fault	
[72]	2015	AC MG	✓	✓	✓		MPC
[73]	2017	AC MG	✓	✓			MPC
[74]	2017	AC MG	✓				MPC
[75]	2016	AC MG	✓	✓			SO
[76]	2020	AC MG	✓	✓	✓		MPC
[77]	2015	AC MG	✓	✓			RO
[78]	2016	AC MG	✓				RO
[58]	2021	AC MG	✓	✓			RO
[79]	2020	MMG				✓	SO, DRO
[80]	2015	MMG				✓	SO
[63]	2018	MMG	✓	✓	✓		RO
[61]	2017	MMG	✓	✓			RO
[65]	2016	MMG	✓				DRO

Another effective strategy for mitigating system uncertainties is through the imple-

mentation of online optimization techniques. This approach is particularly valuable in scenarios where inputs unfold sequentially, requiring algorithms to make decisions based solely on the information available at each step of the process. Online optimization offers a dynamic and adaptable framework that is well-suited to real-time decision-making. It enables systems to respond promptly to changing conditions, making it highly valuable in applications such as energy management, finance, and logistics. By continuously updating decisions as new information becomes available, online optimization algorithms can optimize system performance while accounting for evolving uncertainties.

1.3 Research Objectives

This study stands at the intersection of traffic and power networks, aiming to revolutionize the deployment of CSs within this integrated system. The primary goals are twofold: optimizing the physical placement of CSs and refining their energy management strategies by treating them as MGs equipped with ESS.

1. **Sizing and Placement Optimization:** The study delves into the intricate dynamics between traffic patterns, power demands, and user behavior to strategically determine the ideal locations and sizes of CSs. This involves formulating a comprehensive algorithmic approach, divided into three stages. The aim is to handle the complexities inherent in this problem by transforming non-convex optimization aspects into more manageable convex formulations. By doing so, the research endeavors to achieve optimal placement solutions that align with both traffic and power flow demands efficiently.

2. **Online Optimization Model for Energy Management:** Treating CSs as MGs, this research pioneers an innovative threshold-based online optimization model. This model is designed to navigate and effectively manage uncertainties inherent in the energy management of these stations. The mathematical underpinning aims to validate the optimality of these thresholds, showcasing their ability to adapt to real-world scenarios and simulated datasets. This approach seeks to ensure robust and adaptable energy management strategies, crucial in

ensuring the resilience and efficiency of the integrated traffic and power networks.

Through these objectives, this study seeks not only to redefine the physical landscape of CS deployment but also to revolutionize their functional role within the larger network, ensuring optimal energy utilization and robustness in the face of uncertainties.

1.4 Research Methodology

This study delves into a range of optimization methods to effectively pinpoint the ideal locations and sizes for the CSs operating within the network. Moreover, it orchestrates their collaboration to streamline operational costs.

To achieve these research objectives, the study progresses through a series of interconnected stages:

1. **Formulating an Extended Traffic Network:** Using a fresh approach proposed in this study, the formulation of an extended traffic network allows for expedited determination of the shortest routes between all pairs of nodes. This method surpasses well-known algorithms like Dijkstra's in terms of speed and efficiency.

2. **Iterative Three-Stage Optimization:** The study employs a three-stage optimization algorithm in an iterative manner. This method systematically identifies optimal locations and sizes for each CS. Crucially, it ensures that customer waiting times remain within predefined limits. Should the initial constraints not be met, the algorithm adapts by introducing new constraints and repeating the optimization process.

3. **Designing an Online Cooperation Algorithm:** The study crafts an online algorithm to facilitate collaboration among CSs functioning as MGs. This algorithm accounts for the uncertainties inherent in the system. It establishes two key thresholds: one for energy procurement and another for charging limits within each CS's ESSs. Furthermore, it evaluates the worst-case performance

through competitive-ratio analysis, providing a robust understanding of its efficacy.

4. **Benchmarking and Comparative Analysis:** To showcase the superiority of the proposed algorithm, the study compares it against existing threshold-based approaches. Leveraging the cooperation among MGs yields multifaceted benefits for the overall model. Furthermore, a comparative analysis between the results derived from our algorithm and those of an offline optimization approach demonstrates that our method closely approaches optimal performance under specific conditions.

These steps intricately weave together to form a comprehensive methodology that not only optimizes CS locations and sizes but also ensures efficient collaboration among them, thereby enhancing the network's overall performance and cost-effectiveness.

1.5 Thesis Organization

The rest of this thesis is structured into distinct chapters. Chapter 2 covers the integrated traffic and power networks, exploring the problem formulation of the CS siting and sizing problem. Moving forward, Chapter 3 delves into the proposed three-stage iterative algorithm for the CS siting and sizing problem, accompanied by a case study showcasing the model's performance. In Chapter 4, we present the problem formulation and the online optimization algorithm crafted specifically for managing energy in multiple MGs amid uncertainties. Finally, Chapter 5 serves as the conclusion, summarizing the thesis's unique contributions and discussing future prospects for enhancements and further work.

Chapter 2

Charging Station Problem Formulation

2.1 Integrated Networks

In this study, a coupling system consisting of transportation and power distribution networks is considered. These two networks are connected to each other on some points, which basically are the possible locations to place the charging stations. In this section, the description of these networks and the way they can interact with each other are presented. In particular, first, the introduction of our studied traffic network is followed by the proposal and proof of a new time-efficient formulation for finding the shortest path between every two nodes in the expanded graph. Second, the power network and AC power flow analysis, which are utilized in our study, are introduced. Lastly, the integration of these two networks is demonstrated. The notations which are used in Chapter 2 and 3 of this study can be found in Table 2.1.

2.1.1 Traffic Network

The transportation network graph is noted as a directed graph $\mathcal{G}_T(\mathcal{V}_T, \mathcal{E}_T)$ where $\mathcal{V}_T$ is the set of locations and $\mathcal{E}_T \subset \mathcal{V}_T \times \mathcal{V}_T$ is the set of all roads between different locations.

The connection matrix of a graph $\mathcal{G}_T$ with n nodes is defined as

$$C = [c_{ij}]_{n \times n}, \tag{2.1}$$

Table 2.1: Table of notations used in Chapter 2 and 3

Symbol	Definition	Symbol	Definition
$\mathcal{G}_T$	The transportation network graph	$\mathcal{G}_P$	The power network graph
$\hat{\mathcal{G}}_T$	The transportation network expanded graph	$\mathcal{V}_T$	Set of vertices of graph $\mathcal{G}_T$; indicates the potential charging station locations
$\mathcal{V}_P$	Set of vertices of graph $\mathcal{G}_P$; indicates the power buses	$\hat{\mathcal{V}}_T$	Set of vertices of graph $\hat{\mathcal{G}}_T$; which is equal to $\mathcal{V}_T \cup \mathcal{S} \cup \mathcal{T}$
$\mathcal{V}_I$	Set of vertices where the transportation graph and power graph are coupled	$\mathcal{E}_T$	Set of vertices of graph $\mathcal{G}_T$; indicates the roads between locations
$\mathcal{E}_P$	Set of vertices of graph $\mathcal{G}_P$; indicates the transmission lines between power buses	$\hat{\mathcal{E}}_T$	Set of vertices of graph $\hat{\mathcal{G}}_T$; indicates real and virtual roads
$\mathcal{T}$	Set of sink nodes of $\hat{\mathcal{G}}_T$	$\mathcal{S}$	Set of source nodes of $\hat{\mathcal{G}}_T$
$D_i(t)$	Cumulative departures from node i at time t	$d^{u,w}$	The length of edge from node u to node w
$f_i^{u,w}(t)$	The flow of commodity i on the edge from node u to node w at time t	d_{min}	The minimum total distance of EVs at all times within a day
$\theta_{ij}(t)$	The voltage phase angle difference between bus i and bus j	x_i	A binary variable that is equal to 1 if a charging station is placed at i and equal to 0 otherwise
$P_i^d(t), Q_i^d(t)$	The active and reactive power demand at bus i at time t	g_{ij}, b_{ij}	The conductance and susceptance of line between i and j of the power network
$P_i^g(t), Q_i^g(t)$	The generated active and reactive power of bus i at time t	$V_i(t)$	The voltage of bus i at time t
$\underline{V_i}, \overline{V_i}$	The minimum and maximum allowable voltage magnitude at bus i	$\underline{P_i^g}, \overline{P_i^g}$	The minimum and maximum allowable generated active power at bus i
$\underline{Q_i^g}, \overline{Q_i^g}$	The minimum and maximum allowable generated reactive power at bus i	y_i	An integer variable which indicates the number of charging units at node i and it is equal to 0 if $x_i = 0$
$\lambda_i(t)$	The arrival rate of EVs at node i at time t	μ	The service rate of an individual charging unit
W_i	The total waiting time of all EVs at node i	$A_i(t)$	Cumulative arrivals at node i at time t

in which

$$c_{ij} = \begin{cases} 1 & i = j, \\ 0 & i \neq j \text{ and there is no edge from } i \text{ to } j, \\ e_{ij} & i \neq j \text{ and edge } e_{ij} \text{ is from } i \text{ to } j, \end{cases}$$

where e_{ij} is basically the distance from node i to node j.

Assume the simple graph of Fig. 2.1 as an example of the traffic network which has 3 nodes and 5 edges. In this graph, $\mathcal{V}_T = \{X, Y, Z\}$ and $\mathcal{E}_T = \{e_1, e_2, e_3, e_4, e_5\}$.

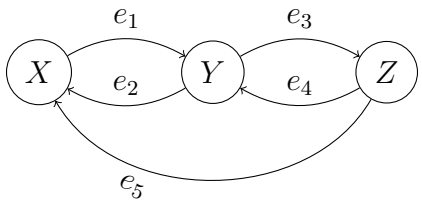

Figure 2.1: A simple example of graph expansion algorithm.

The connection matrix of this graph is:

$$C = \begin{array}{c} \\ X \\ Y \\ Z \end{array} \begin{array}{c} \begin{array}{ccc} X & Y & Z \end{array} \\ \begin{pmatrix} 1 & e_1 & 0 \\ e_2 & 1 & e_3 \\ e_5 & e_4 & 1 \end{pmatrix} \end{array}.$$

To find optimal locations of charging stations, we should analyze EVs' behavior in the traffic network. The graph expansion, which is described in [7], can be used in order to make this analysis much easier. By using this expanded graph, it is guaranteed that if a combination of the nodes meets all constraints, this combination is a feasible solution to the problem. Graph expansion consists of two simple steps: the first step is to add two virtual nodes for each node in the transportation network graph, and the second step is to add a virtual link between any pair of nodes whose shortest path length is below the driving range.

Step 1

Since each node could be an origin or the destination for EVs, a virtual *source node* and a virtual *sink node* are added to each node. For node i in the transportation network graph, e'_i is the edge from the virtual source node (S_i) to node i and its

length is $1 - SoC_o$, and e_i'' is the edge from node i to its virtual sink node (T_i) and its length is SoC_d. Here SoC_o and SoC_d are the State-of-Charge at the origin point and the destination point, respectively. The set of all virtual source and sink nodes are denoted by $\mathcal{S}$ and $\mathcal{T}$, respectively.

Considering these virtual nodes, the expanded graph $\hat{\mathcal{G}}_T(\hat{\mathcal{V}}_T, \hat{\mathcal{E}}_T)$ now has $3n$ nodes because $\hat{\mathcal{V}}_T = \mathcal{V}_T \cup \mathcal{S} \cup \mathcal{T}$. Thus, the connection matrix of expanded graph is introduced as:

$$\Sigma = [\sigma_{ij}]_{3n\times 3n} = \begin{array}{c} \\ \mathcal{V}_T \\ \mathcal{S} \\ \mathcal{T} \end{array} \begin{array}{c} \begin{array}{ccc} \mathcal{V}_T & \mathcal{S} & \mathcal{T} \end{array} \\ \begin{pmatrix} C_{n\times n} & 0 & C''_{n\times n} \\ C'_{n\times n} & I & 0 \\ 0 & 0 & I \end{pmatrix} \end{array}, \tag{2.2}$$

where I is an identity matrix. In (2.2), the source matrix C' and sink matrix C'' are block matrices written as

$$\begin{aligned} C' &= [c'_{ij}]_{n\times n}, \\ C'' &= [c''_{ij}]_{n\times n}, \end{aligned} \tag{2.3}$$

where

$$c'_{ij} = \begin{cases} 0 & i \neq j \\ e'_i & i = j \end{cases}, \quad c''_{ij} = \begin{cases} 0 & i \neq j \\ e''_i & i = j \end{cases}.$$

In the aforementioned simple example of Fig. 2.1, the set of virtual source nodes is $\mathcal{S} = \{S_X, S_Y, S_Z\}$, and the set of virtual sink nodes is $\mathcal{T} = \{T_X, T_Y, T_Z\}$. After adding the virtual source nodes and virtual sink nodes, this graph is turning to Fig. 2.2 which shows the first step of the graph expansion algorithm. C', C'' and Σ matrices are showed below:

$$C' = \begin{array}{c} \\ S_X \\ S_Y \\ S_Z \end{array} \begin{array}{c} \begin{array}{ccc} X & Y & Z \end{array} \\ \begin{pmatrix} e'_1 & 0 & 0 \\ 0 & e'_2 & 0 \\ 0 & 0 & e'_3 \end{pmatrix} \end{array}, \; C'' = \begin{array}{c} \\ X \\ Y \\ Z \end{array} \begin{array}{c} \begin{array}{ccc} T_X & T_Y & T_Z \end{array} \\ \begin{pmatrix} e''_1 & 0 & 0 \\ 0 & e''_2 & 0 \\ 0 & 0 & e''_3 \end{pmatrix} \end{array},$$

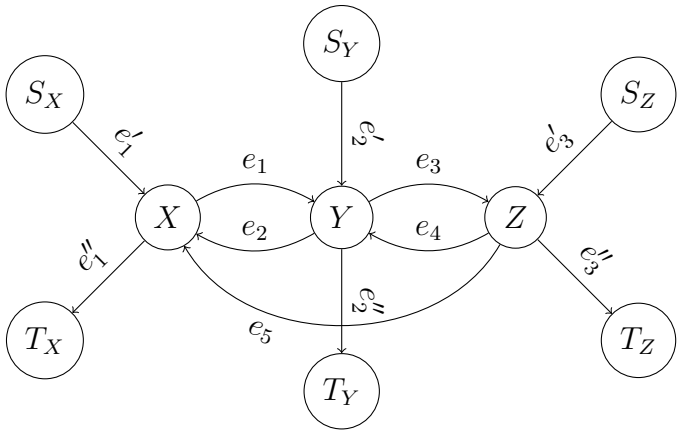

Figure 2.2: First step of the graph expansion algorithm.

$$\Sigma = \begin{array}{c} \\ X \\ Y \\ Z \\ S_X \\ S_Y \\ S_Z \\ T_X \\ T_Y \\ T_Z \end{array} \begin{array}{c} \begin{array}{ccccccccc} X & Y & Z & S_X & S_Y & S_Z & T_X & T_Y & T_Z \end{array} \\ \begin{pmatrix} 1 & e_1 & 0 & 0 & 0 & 0 & e_1'' & 0 & 0 \\ e_2 & 1 & e_3 & 0 & 0 & 0 & 0 & e_2'' & 0 \\ e_5 & e_4 & 1 & 0 & 0 & 0 & 0 & 0 & e_3'' \\ e_1' & 0 & 0 & 1 & 0 & 0 & 0 & 0 & 0 \\ 0 & e_2' & 0 & 0 & 1 & 0 & 0 & 0 & 0 \\ 0 & 0 & e_3' & 0 & 0 & 1 & 0 & 0 & 0 \\ 0 & 0 & 0 & 0 & 0 & 0 & 1 & 0 & 0 \\ 0 & 0 & 0 & 0 & 0 & 0 & 0 & 1 & 0 \\ 0 & 0 & 0 & 0 & 0 & 0 & 0 & 0 & 1 \end{pmatrix} \end{array}.$$

Step 2

Create a virtual link between any pair of nodes whose shortest path length is below the driving range. This ensures that if two nodes have a connection and each includes a charging station, there will always be a feasible path between them that can be traversed by an EV without exhausting the energy supply.

We develop a novel algorithm that efficiently determines the shortest path between all pairs of nodes simultaneously. This innovative approach has a time complexity of $\mathcal{O}(8n^4)$. As a comparison, the Dijkstra algorithm, which is a conventional method has the worst-case time complexity of $\mathcal{O}((3n)^4 \log(3n))$[81]. Thus, our algorithm is better

than the Dijkstra algorithm for finding the shortest paths in the network. Initially, we introduce a set of rules, followed by the subsequent proofs of Theorem 1 to 4, which establish the validity and correctness of our algorithm.

As [82] shows, if C is the connection matrix of graph $\mathcal{G}_T$, all paths in graph $\mathcal{G}_T$ can be got by computing matrix C^{n-1}, considering some rules. These rules are noted below:

$$1 + e_i \equiv 1, \tag{2.I}$$

$$e_i + e_i \equiv e_i, \tag{2.II}$$

$$e_i e_i \equiv e_i, \tag{2.III}$$

$$e_i + e_i e_j \equiv e_i(1 + e_j) \equiv e_i. \tag{2.IV}$$

Rule (2.I) stands out to make sure that there is not any self-loop in the graph, where self-loop is an edge that connects a vertex to itself. Rule (2.II) guarantees that there is not any duplicated path between the vertices, and Rule (2.III) ensures that a path does not include any loop. Rule (2.IV) is basically an extension of Rule 2.I.

Now by adding an additional rule, all paths of the graph $\hat{\mathcal{G}}_T$ can be obtained by calculating the matrix Σ^{n+1}. This rule is noted below:

$$e_i' e_i'' \equiv 0. \tag{2.V}$$

Rule (2.V) is added to account for the fact that idel cars, where drivers stay in the same spot and do not travel, are not considered in this work. In addition, each round trip is considered as 2 smaller parts, i.e., the origin and the destination of the trip cannot be the same.

The validity of our proposed formulation is established by proving Theorems 1, 2, and 4. Additionally, it is demonstrated in Theorem 3 that no loss is incurred in the overall analysis when the simplified version of the connection matrix for the expanded graph is employed.

Theorem 1 *If C is the connection matrix, $C^k + I = C^k, \forall k \in \mathbb{N}$.*

Proof. Each diagonal element of C^k matrix is in the form of $(1 + ...)$. Based on rule (i), every diagonal element of C^k is equal to 1. In addition, every diagonal

element of $C^k + I$ is in the form $(1 + ...)$, which is equal to 1 based on rule 2.I. So it is proved that $C^k + I = C^k, \forall k \in \mathbb{N}$. ■

Theorem 2 *k-th power of matrix* Σ *is in the form of*

$$\Sigma^k = \begin{bmatrix} C^k & 0 & C^{k-1}C'' \\ C'C^{k-1} & I & C'C^{k-2}C'' \\ 0 & 0 & I \end{bmatrix}. \tag{2.4}$$

Proof. Mathematical induction is employed to prove Theorem 2 in this study.

- **Base case:**

$$\Sigma^2 = \begin{bmatrix} C & 0 & C'' \\ C' & I & 0 \\ 0 & 0 & I \end{bmatrix} \begin{bmatrix} C & 0 & C'' \\ C' & I & 0 \\ 0 & 0 & I \end{bmatrix} = \begin{bmatrix} C^2 & 0 & CC'' + C'' \\ C'C + C' & I & C'C'' \\ 0 & 0 & I \end{bmatrix}$$

$$\xrightarrow{C'C''=0} \begin{bmatrix} C^2 & 0 & (C+I)C'' \\ C'(C+I) & I & 0 \\ 0 & 0 & I \end{bmatrix} = \begin{bmatrix} C^2 & 0 & CC'' \\ C'C & I & 0 \\ 0 & 0 & I \end{bmatrix}.$$

- **Induction step:**

$$\Sigma^m = \begin{bmatrix} C^m & 0 & C^{m-1}C'' \\ C'C^{m-1} & I & C'C^{m-2}C'' \\ 0 & 0 & I \end{bmatrix}$$

$$\Rightarrow \Sigma^{m+1} = \Sigma^m \Sigma$$

$$= \begin{bmatrix} C^m & 0 & C^{m-1}C'' \\ C'C^{m-1} & I & C'C^{m-2}C'' \\ 0 & 0 & I \end{bmatrix} \begin{bmatrix} C & 0 & C'' \\ C' & I & 0 \\ 0 & 0 & I \end{bmatrix}$$

$$= \begin{bmatrix} C^{m+1} & 0 & C^mC'' + C^{m-1}C'' \\ C'C^m + C' & I & C'C^{m-1}C'' + C'C^{m-2}C'' \\ 0 & 0 & I \end{bmatrix}$$

$$= \begin{bmatrix} C^{m+1} & 0 & (C+I)C^{m-1}C'' \\ C'(C^m + I) & I & C'C^{m-2}(C+I)C'' \\ 0 & 0 & I \end{bmatrix} = \begin{bmatrix} C^{m+1} & 0 & C^mC'' \\ C'C^m & I & C'C^{m-1}C'' \\ 0 & 0 & I \end{bmatrix}.$$

■

Theorem 3 *Σ matrix could be simplified as a $2n \times 2n$ matrix without loss of generality. The simplified Σ matrix is expressed as:*

$$\Sigma' = [\sigma_{ij}]_{2n\times 2n} = \begin{array}{c} \\ \mathcal{V}_T \\ \mathcal{S} \end{array} \begin{array}{c} \begin{array}{cc} \mathcal{V}_T & \mathcal{T} \end{array} \\ \begin{pmatrix} C & C'' \\ C' & 0 \end{pmatrix} \end{array} \tag{2.5}$$

Proof. Here it is shown that the k power of the original Σ matrix is equivalent to the k power of the simplified Σ. It means:

$$(\Sigma')^k_{2n\times 2n} = \begin{bmatrix} C^k & C^{k-1}C'' \\ C'C^{k-1} & C'C^{k-2}C'' \end{bmatrix}.$$

The mathematical induction is performed again:

- **Base case:**

$$\begin{aligned} (\Sigma')^2 &= \begin{bmatrix} C & C'' \\ C' & 0 \end{bmatrix} \begin{bmatrix} C & C'' \\ C' & 0 \end{bmatrix} \\ &= \begin{bmatrix} C^2 + C''C' & CC'' \\ C'C & C'C'' \end{bmatrix} \\ &\xrightarrow{C'C''=0} \begin{bmatrix} C^2 & CC'' \\ C'C & 0 \end{bmatrix}. \end{aligned}$$

- **Induction step:**

$$\begin{aligned} (\Sigma')^m &= \begin{bmatrix} C^m & C^{m-1}C'' \\ C'C^{m-1} & C'C^{m-2}C'' \end{bmatrix} \\ \Rightarrow (\Sigma')^{m+1} &= (\Sigma')^m\Sigma' \\ &= \begin{bmatrix} C^m & C^{m-1}C'' \\ C'C^{m-1} & C'C^{m-2}C'' \end{bmatrix} \begin{bmatrix} C & C'' \\ C' & 0 \end{bmatrix} \\ &= \begin{bmatrix} C^{m+1} + C^{m-1}C''C' & C^mC'' \\ C'C^m + C^{m-2}C''C' & C'C^{m-1}C'' \end{bmatrix} \\ &\xrightarrow{C'C''=0} \begin{bmatrix} C^{m+1} & C^mC'' \\ C'C^m & C'C^{m-1}C'' \end{bmatrix}. \end{aligned}$$

■

Theorem 4 *If $\mathcal{G}_T$ is a graph of n vertices, all paths of its expanded graph ($\hat{\mathcal{G}}_T$) can be calculated by obtaining P^{n+1}, where P is the simplified connection matrix of $\hat{\mathcal{G}}_T$.*

Proof. If C is the connection matrix of $\mathcal{G}_T$ with n vertices, then C^{n-1} can show all paths with at most $n-1$ edges. If a path has n edges, it is obvious that there is at least one loop in that path. Vertices of the expanded graph are in $\mathcal{V}_T$ or $\mathcal{S}$ or $\mathcal{T}$. In each path of graph $\hat{\mathcal{G}}_T$, there is at most 1 vertex in $\mathcal{S}$ because the in-degree of all vertices of $\mathcal{S}$ is 0. Similarly, since the out-degree of all vertices of $\mathcal{T}$ is 0, at most one of the vertices of $\mathcal{T}$ can be in each path. Thus, each path has at most $n+2$ vertices without any loop. So $(\Sigma')^{n+1}$ can completely consider all paths of graph $\hat{\mathcal{G}}_T$. ■

After obtaining all paths of the graph $\hat{\mathcal{G}}_T$, the shortest path matrix can be calculated from matrix $(\Sigma')^{n+1}$.[1] We denote matrix $(\Sigma')^{n+1}$ as matrix Σ'^s. Then the adjacency matrix of the expanded graph is calculated as equation (2.6):

$$\hat{A} = [\hat{a}_{ij}]_{2n\times 2n} \tag{2.6}$$

where:

$$\hat{a}_{ij} = \begin{cases} 0 & i = j, \\ 0 & i \neq j \text{ and } {\Sigma'^s}_{ij} > R, \\ 1 & \text{otherwise,} \end{cases}$$

where R is the driving range of EVs.

This adjacency matrix is constructed from the simplified version of the connection matrix and has size $2n \times 2n$. Thus, in order to make a corresponding graph from the adjacency matrix, it is necessary to convert it into the original $3n \times 3n$ form. Thus, the adjacency matrix of the expended graph could be expressed as equation (2.7):

$$A = \begin{bmatrix} \hat{A}_{11} & 0 & \hat{A}_{12} \\ \hat{A}_{21} & 0 & \hat{A}_{22} \\ 0 & 0 & 0 \end{bmatrix} \tag{2.7}$$

where $\hat{A}_{11}$, $\hat{A}_{12}$, $\hat{A}_{21}$ and $\hat{A}_{22}$ are $n \times n$ matrices, and are the upper-left block, upper-right block, bottom-left block, and bottom-right block of $\hat{A}$, respectively.

[1] Regarding calculation of matrix $(\Sigma')^{n+1}$, we need n matrix multiplications, and each matrix multiplication involves two $2n \times 2n$ matrices. Each matrix multiplication has a complexity of $\mathcal{O}((2n)^3)$. Thus, the overall complexity for calculation of matrix $(\Sigma')^{n+1}$ is $\mathcal{O}(n \cdot (2n)^3)$, which is $\mathcal{O}(8n^4)$.

The upper bound for the number of edges of expanded graph $\hat{\mathcal{G}}_T$ is $4n^2 - 2n$, where n is the number of vertices of graph $\mathcal{G}_T$. The exact number of edges depends on the length of each edge, SoC_o and SoC_d.

In the aforementioned example in Fig. 2.1, based on $(\Sigma')^4$ matrix, there are 2 paths from node Y to node T_X. The first one is $e_2 e_1''$ and the other one is $e_3 e_5 e_1''$. Thus, if the length of each edge is known, the shortest path between every 2 nodes could be calculated. In the above example let us assume $SoC_o = 55\%$ and $SoC_d = 30\%$. In addition, $e_1 = 30\%, e_2 = 40\%, e_3 = 60\%, e_4 = 50\%$ and $e_5 = 80\%$. Thus, the shortest path matrix corresponding to these numbers is:

$$\Sigma'^s = \begin{array}{c} \\ X \\ Y \\ Z \\ S_X \\ S_Y \\ S_Z \end{array} \begin{array}{c} \begin{array}{cccccc} X & Y & Z & T_X & T_Y & T_Z \end{array} \\ \begin{pmatrix} 1 & 60\% & 90\% & 30\% & 60\% & 120\% \\ 40\% & 1 & 60\% & 70\% & 30\% & 90\% \\ 80\% & 50\% & 1 & 110\% & 80\% & 30\% \\ 45\% & 75\% & 135\% & 0 & 105\% & 165\% \\ 85\% & 45\% & 105\% & 115\% & 0 & 135\% \\ 115\% & 95\% & 45\% & 145\% & 125\% & 0 \end{pmatrix} \end{array}$$

$$\Rightarrow A = \begin{array}{c} \\ X \\ Y \\ Z \\ S_X \\ S_Y \\ S_Z \\ T_X \\ T_Y \\ T_Z \end{array} \begin{array}{c} \begin{array}{ccccccccc} X & Y & Z & S_X & S_Y & S_Z & T_X & T_Y & T_Z \end{array} \\ \begin{pmatrix} 0 & 1 & 1 & 0 & 0 & 0 & 1 & 1 & 0 \\ 1 & 0 & 1 & 0 & 0 & 0 & 1 & 1 & 1 \\ 1 & 1 & 0 & 0 & 0 & 0 & 0 & 1 & 1 \\ 1 & 1 & 0 & 0 & 0 & 0 & 0 & 0 & 0 \\ 1 & 1 & 0 & 0 & 0 & 0 & 0 & 0 & 0 \\ 0 & 1 & 1 & 0 & 0 & 0 & 0 & 0 & 0 \\ 0 & 0 & 0 & 0 & 0 & 0 & 0 & 0 & 0 \\ 0 & 0 & 0 & 0 & 0 & 0 & 0 & 0 & 0 \\ 0 & 0 & 0 & 0 & 0 & 0 & 0 & 0 & 0 \end{pmatrix} \end{array}.$$

Thus, Fig. 2.3 shows the expanded graph of Fig 2.1. Dashed edges are the virtual edges that are added to the graph.

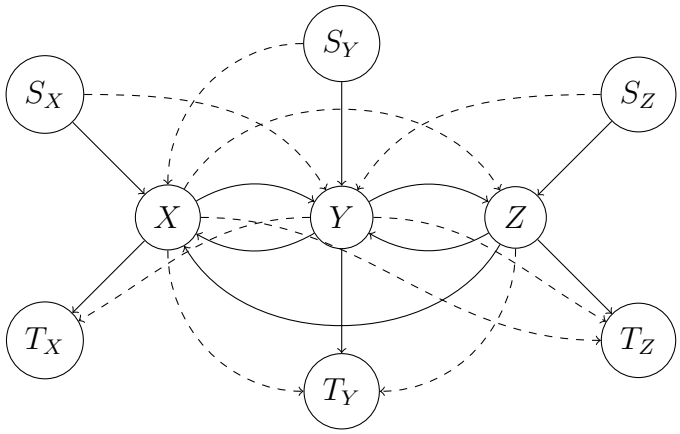

Figure 2.3: Second step of the graph expansion algorithm.

2.1.2 Power Network

The power distribution network is defined as an undirected graph $\mathcal{G}_P(\mathcal{V}_P, \mathcal{E}_P)$, where $\mathcal{V}_P$ is the set of all buses. Define $\bar{\mathcal{V}}_P = \mathcal{V}_P \backslash \{v_0\}$, where v_0 is the slack bus. $\mathcal{E}_P$ is the set of transmission lines between different buses. In this study, it is assumed that all buses but the slack bus are integrated with the traffic network nodes, i.e., $\bar{\mathcal{V}}_P \subseteq \mathcal{V}_T$. The power flow patterns will change as soon as a new power demand is added to the existing network. Thus, when a charging station connects to the distribution system, the power flow pattern will change significantly, and as a result, the transmission losses would be increased in the network[83]. Hence, the power losses should be considered in order to find the optimal charging station locations [84].

Based on the power flow analysis, it is known that:

$$\mathbf{I} = \mathbf{YV}, \tag{2.8}$$

where $\mathbf{Y}$ is the admittance matrix, $\mathbf{I}$ is the diagonal matrix of injection currents, and $\mathbf{V}$ is the diagonal matrix of bus voltages. In addition, the injection complex power to the network can be calculated as:

$$\mathbf{S} = \mathbf{VI}^* \times \vec{1} = \mathbf{VV}^*\mathbf{Y} \times \vec{1}. \tag{2.9}$$

Here $\vec{1}$ is a column vector with all elements being 1 and its size is same as the number of buses of the power network, $\mathbf{S}$ is the vector of apparent powers, and $(^*)$ is the conjugate transpose.

In order to find the active power loss of each line, it is necessary to first calculate the current of each line [85]. Let us assume there is a line with admittance $y_{mn} = g_{mn} + jb_{mn}$ between bus m with voltage $V_m\angle\theta_{mn}$ and bus n with voltage $V_n\angle\theta_0$ where $\theta_0 = 0$. Thus, the current on this line is:

$$\begin{aligned} I_{mn} &= (V_m\angle\theta_{mn} - V_n\angle\theta_0)g_{mn} \\ &= ((V_m\cos(\theta_{mn}) + jV_m\sin(\theta_{mn})) - V_n)g_{mn} \\ &= ((V_m\cos(\theta_{mn}) - V_n) + jV_m\sin(\theta_{mn}))g_{mn}. \end{aligned} \tag{2.10}$$

Since the active power is the real part of the apparent power, it is equal to

$$\begin{aligned} P^L_{mn} &= V_{mn}I^*_{mn} \\ &= ((V_m\cos(\theta_{mn}) - V_n) + jV_m\sin(\theta_{mn})) \\ &\times ((V_m\cos(\theta_{mn}) - V_n) - jV_m\sin(\theta_{mn}))g_{mn} \\ &= (V_m^2\cos^2(\theta_{mn}) + V_n^2 - 2V_mV_n\cos(\theta_{mn}) \\ &+ V_m^2\sin^2(\theta_{mn}))g_{mn} \\ &= (V_m^2 + V_n^2 - 2V_mV_n\cos(\theta_{mn}))g_{mn}. \end{aligned} \tag{2.11}$$

Hence, the total power loss can be calculated as

$$P^L = \sum_{(i,j)\in\mathcal{E}_P} P^L_{ij}. \tag{2.12}$$

The consideration of reactive power losses is omitted in order to keep the optimization problem simple. However, it can be incorporated into the objective function at a later stage.

In addition, when the bus voltage limits in the constraints are taken into account, it results in an unattractive voltage profile. To overcome this problem, an objective function that measures the deviation of load bus voltage can be set. For voltage profile improvement, the following objective function should be used [86]:

$$V^D = \sum_{i\in\mathcal{V}_P} |V_i - 1|. \tag{2.13}$$

2.1.3 Coupled Network

The power network and traffic network join together on some points and thus can form layered graphs [87]. These nodes are called *common nodes*. In other words, these

are the points that can be assumed as potential places for placing charging stations. These nodes are basically the intersections of the set of vertices of the traffic network and power network (equation (2.14)).

$$\mathcal{V}_I = \mathcal{V}_T \cap \mathcal{V}_P. \tag{2.14}$$

In these nodes, the power demand could change by the charging demand of EV flows of the edges connected to these nodes. Since the charging demands are only considered active power loads, they only affect the active power demands. This demand is based on the number of EVs that request to charge at each time and also the length of edge that they come from because the EVs which travel longer edges have higher power demands. It is worth mentioning that the consumption rate of EVs has a significant effect on the power demand for EVs. Since it is assumed that all EVs are identical in this study, the consumption rate γ_c for all EVs are the same. For node $u \in \mathcal{V}_I$, the active power demand at time t is

$$P_u^d(t) = p_u^d(t) + \gamma_c \sum_{i=1}^{K} \sum_{w \in \mathcal{V}_T} d^{u,w} f_i^{w,u}(t), \tag{2.15}$$

where K is the number of commodities. Here $P_u^d(t)$ is the total active power demand at bus u, and $p_u^d(t)$ is the demand from the grid. For the nodes $u \notin \mathcal{V}_I$, the active and reactive power demands only come from the grid. In other words, the following two equations show the active and reactive power demands:

$$P_u^d(t) = p_u^d(t), \tag{2.16}$$

$$Q_u^d(t) = q_u^d(t). \tag{2.17}$$

2.2 Optimization Formulation

The objective of charging station siting and sizing problem is to minimize the overall cost, considering the planning of the charging station costs, power loss costs, and social welfare costs. In this study, an iterative algorithm is employed to find the optimum solution for charging stations' locations and the number of charging units at each station. The most important factors for finding the location of a charging station are how this location impacts the path that EV owners need to choose and

how the power distribution pattern changes by applying this additional load at some locations, especially in peak hours. In addition, the number of spots at each location is only affected by the allowable waiting time at each station, and other factors do not have a significant impact on the number of required spots. As far as the authors are aware, other studies have taken all factors into account altogether, and it can cause some problems. In this study, all EVs can flow arbitrarily in the system, as long as their traveled path is within a threshold.

2.2.1 Optimization Assumptions

In this part, all the assumptions that are made in order to make the model simpler are stated.

- The charging process is performed at a constant rate, specifically focusing on constant current charging for the EVs while omitting the constant voltage charging part of the process [88].
- It is assumed that the speed of vehicles are constant over a day on every roads. In other words, the traffic does not affect the charging station choice from EVs.
- It is assumed that there is enough space at each charging station for EVs to wait in order to receive service. In other words, the waiting line does not have any impact on the traffic flows.
- The land cost is constant over all the possible locations of placing the charging stations.
- When EVs reach the charging station, they charge their battery up to the maximum possible. In other words, the SoC is 100% as they leave the charging station.
- EVs are getting service in a first-come first-serve discipline. It means that the only contributing parameter for the order of receiving service is the time they arrive at the charging station.
- All EVs and all charging units are identical.

- The driving range of EVs do not change over time of study and the battery degradation is relaxed in order to make the problem simpler.

- It is assumed that each node $v \in \mathcal{V}_I$ could be a possible location for the placement of charging station. Other contributing factors to find the best locations of charging station (such as the traffic constraints, different land costs and the possibility of constructing a charging station at locations from construction point of view) are omitted in order to make the problem simpler.

2.2.2 Problem Formulation

Objective function

As it is mentioned before, the objective function of this problem consists of different terms and can be written as

$$\min\{C_1^I + C_1^S + C_1^E + C_2^I + C_2^S\}. \tag{2.18}$$

Each term in this equation corresponds to one of the costs that are mentioned before.

1. Charging station installation costs:

$$C_1^I = C_1 \sum_{i \in \mathcal{V}_P} x_i, \tag{2.19}$$

   where C_1 is the cost of installing a charging station, and x_i (a binary variable) is equal to 1 if there is a charging station at node i; or equal to zero otherwise.

2. Social welfare cost:

$$C_1^S = C_2 \left[\left[\sum_{i=1}^{K} \sum_{(u,w) \in \mathcal{E}_T} d^{u,w} \int f_i^{u,w}(t) dt \right] - d_{min} \right], \tag{2.20}$$

   where C_2 is the cost of additional driving distance that EVs should travel in order to make their trip without running out of charge. K is the number of commodities. Each commodity K_i is noted as a set of three such $K_i(S_i, T_i, F_i(t))$. Here S_i and T_i are the source and the sink nodes of the i-th commodity, respectively, and $F_i(t)$ is the flow demand function from S_i to T_i over time. K is the total number of commodities in the network, and $d^{u,w}$ is the distance of

edge (u, w). $f_i^{u,w}(t)$ is the flow of commodity i on edge (u, w), and d_{min} is the minimum total distance that EVs travel during a day. This term shows the cost of increased milage caused by placing charging stations in certain locations.

3. Power loss costs:

$$\begin{aligned} C_1^E =& C_3 \sum_{(i,j)\in\mathcal{E}_P} \int [V_i^2(t) + V_j^t(t) \\ & - 2V_i(t)V_j(t)\cos(\theta_{ij}(t))]dt \\ & + C_4 \sum_{i\in\mathcal{V}_P} \int |V_i(t) - 1|\, dt \end{aligned} \tag{2.21}$$

where C_3 and C_4 are the cost of power loss and voltage deviation.

4. Charging units additional costs:

$$C_2^I = C_5 \sum_{i\in\{j\in\mathcal{V}_I | x_j=1\}} y_i, \tag{2.22}$$

where C_5 is the cost of additional land use, required equipment, and installation, and y_i (an integer variable) represents the number of charging units in a charging station.

5. Waiting time costs:

$$C_2^S = C_6 \sum_{i\in\{j\in\mathcal{V}_I | x_j=1\}} W_i, \tag{2.23}$$

where C_6 is the time cost that EVs need to wait in the queue in order to get service, and W_i is the total waiting time of EVs in the queue in a day at node i.

Waiting time is a function of the arrival rate ($\lambda_i(t)$), service rate ($\mu_i(t)$), and the number of charging units (y_i). In this study, it is assumed that the service rate is constant over time. Fig. 2.4 shows the cumulative charging request over time ($A_i(t)$). Thus, the relation between $A_i(t)$ and $\lambda_i(t)$ is:

$$\frac{dA_i(t)}{dt} = \lambda_i(t), \tag{2.24}$$

$$\frac{dD_i(t)}{dt} = \mu, \tag{2.25}$$

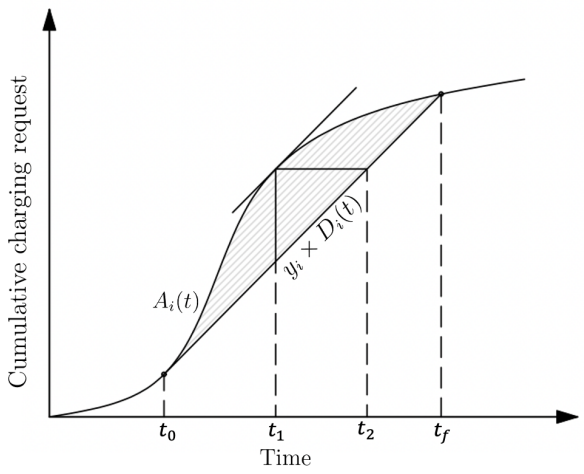

Figure 2.4: Cumulative arrival and departure figure.

$$W_i = \int_{t_0}^{t_f} (A_i(t) - D_i(t))dt, \tag{2.26}$$

where t_0 is the time that the queue starts growing. In other words, it is a time when the arrival rate gets larger than the service rate. Thus, on this point, we have

$$\begin{cases} \lambda_i(t_0) = y_i \times \mu \\ A_i(t_0) = y_i \times D_i(t_0) \end{cases}. \tag{2.27}$$

In addition, t_f is a time when the queue vanishes, and after that, there is no wait time in the queue. It means

$$A_i(t_f) = y_i \times D_i(t_f). \tag{2.28}$$

At each location, the cumulative charging request is equal to the sum of all cumulative flows that are injected to the charging station placed at that location. In other words,

$$A_i(t) = \sum_{j=1}^{K} \sum_{w \in \mathcal{V}_T} \int^{t_{i,w}} f_j^{w,i} dt, \tag{2.29}$$

where $t_{i,w}$ is the time needed to reach node i from node w.

Constraints

The constraints of the first-stage optimization problem are listed in this section. Each of these constraints is related to a term of the objective function.

$$\sum_{w\in\mathcal{V}_T}\int f_i^{u,w}(t)dt - \sum_{w\in\mathcal{V}_T}\int f_i^{w,u}(t)dt = \begin{cases} \int F_i(t)dt & u\in\mathcal{S}, \\ -\int F_i(t)dt & u\notin\mathcal{S}, \\ 0 & \text{otherwise}, \end{cases} \quad ,\forall u\in\mathcal{V}_T. \tag{2.30}$$

This constraint is related to the multi-commodity term (equation (2.20)). This term is simply to make sure that all the flow demand of commodity K_i reaches from its source node to its sink node and that there is no flow remaining in other nodes.

$$0 \le f_i^{u,w}(t) = x_w f_i^{u,w}(t) \quad ,\forall i\in\{1,\dots,K\}, \forall w\in\mathcal{V}_T. \tag{2.31}$$

Constraint (2.31) makes sure that if an edge is in a route, it is possible to take that edge without running out of energy in the middle of that edge. In other words, this constraint checks the feasibility of a selected route. This constraint is related to the locations of the selected nodes as charging stations (equation (2.19)).

$$P_i^g(t) - P_i^d(t) = V_i(t)\sum_{j\in\mathcal{V}_P} V_j(t)(g_{ij}\cos(\theta_{ij}(t)) + b_{ij}\sin(\theta_{ij}(t))) \quad ,\forall i\in\mathcal{V}_P, \tag{2.32}$$

$$Q_i^g(t) - Q_i^d(t) = V_i(t)\sum_{j\in\mathcal{V}_P} V_j(t)(g_{ij}\sin(\theta_{ij}(t)) + b_{ij}\cos(\theta_{ij}(t))) \quad ,\forall i\in\mathcal{V}_P, \tag{2.33}$$

$$\overline{V_i} \ge V_i(t) \ge \underline{V_i} \quad ,\forall i\in\mathcal{V}_P, \tag{2.34}$$

$$\overline{P_i^g} \ge P_i^g(t) \ge \underline{P_i^g} \quad ,\forall i\in\mathcal{V}_P, \tag{2.35}$$

$$\overline{Q_i^g} \ge Q_i^g(t) \ge \underline{Q_i^g} \quad ,\forall i\in\mathcal{V}_P. \tag{2.36}$$

Equations (2.32) to (2.36) are the constraints of the power flow in the network. Equations (2.32) and (2.33) are the power balance equations, and equations (2.34) to (2.36)

are the limits of the voltage, active power and reactive power, respectively. Here P_i^g and Q_i^g are the generated active and reactive power, and P_i^d and Q_i^d are the demand active and reactive power.

$$y_i \leq \overline{y_i}, \qquad \forall i \in \{j \in \mathcal{V}_I | x_j = 1\}. \tag{2.37}$$

This constraint shows that the number of charging units at each charging station should not exceed the limit. Due to the traffic problems that a large charging station can cause, it is not possible to have a charging station with unlimited units.

$$W_i^{max} \leq \overline{W_i}, \qquad \forall i \in \{j \in \mathcal{V}_I | x_j = 1\}. \tag{2.38}$$

where W_i^{max} is the maximum wait time and according to Fig. 2.4, is equal to

$$W_i^{max} = t_2 - t_1 = \frac{(A_i(t) - y_i D_i(t))}{y_i \mu}. \tag{2.39}$$

This is the maximum wait time of all EVs using charging station i during the day.

Chapter 3

Charging Station Optimization Algorithm

3.1 Optimization Algorithm

Our iterative algorithm, which is first introduced in this study, can address the issues regarding the complexity of the optimization. In the flow chart of Fig. 3.1, the optimization's procedure is explained.

The algorithm operates by relaxing constraint 2.38 and splitting the objective function and constraints into two distinct groups. The initial set involves equations 2.19, 2.20, and 2.21 as its objective function, and equations 2.30 through 2.36 as its constraints. This segment focuses solely on determining the optimal positions of CSs within the network. The subsequent group encompasses 2.22 and 2.23 as the objective function, with 2.37 serving as the constraint. Here, the aim is to address the required number of charging units at each charging station. Given that the shared variables between these groups are solely the traffic flow and CS locations, and considering the relaxation of constraint 2.38, an additional stage becomes necessary to verify compliance with constraint 2.38. If it's not met, a new constraint is added, and the process iterates. Each stage of the optimization problem can be summarized as follows:

First Stage: In this stage, the optimal locations of the charging stations are determined in a manner that ensures every vehicle can complete its trips without experiencing a depletion of charge. In order to obtain the optimum set of locations, it is necessary to consider the fixed costs associated with the installation

of a charging station, irrespective of the number of charging units. Furthermore, the power loss in the network throughout the day, considering the power demand pattern of the existing network, as well as the additional demand resulting from the implementation of the charging stations, and the welfare costs arising from not situating the charging stations along the optimal route of the travelers, need to be taken into account. In this section, the objective function and constraints are defined in turn.

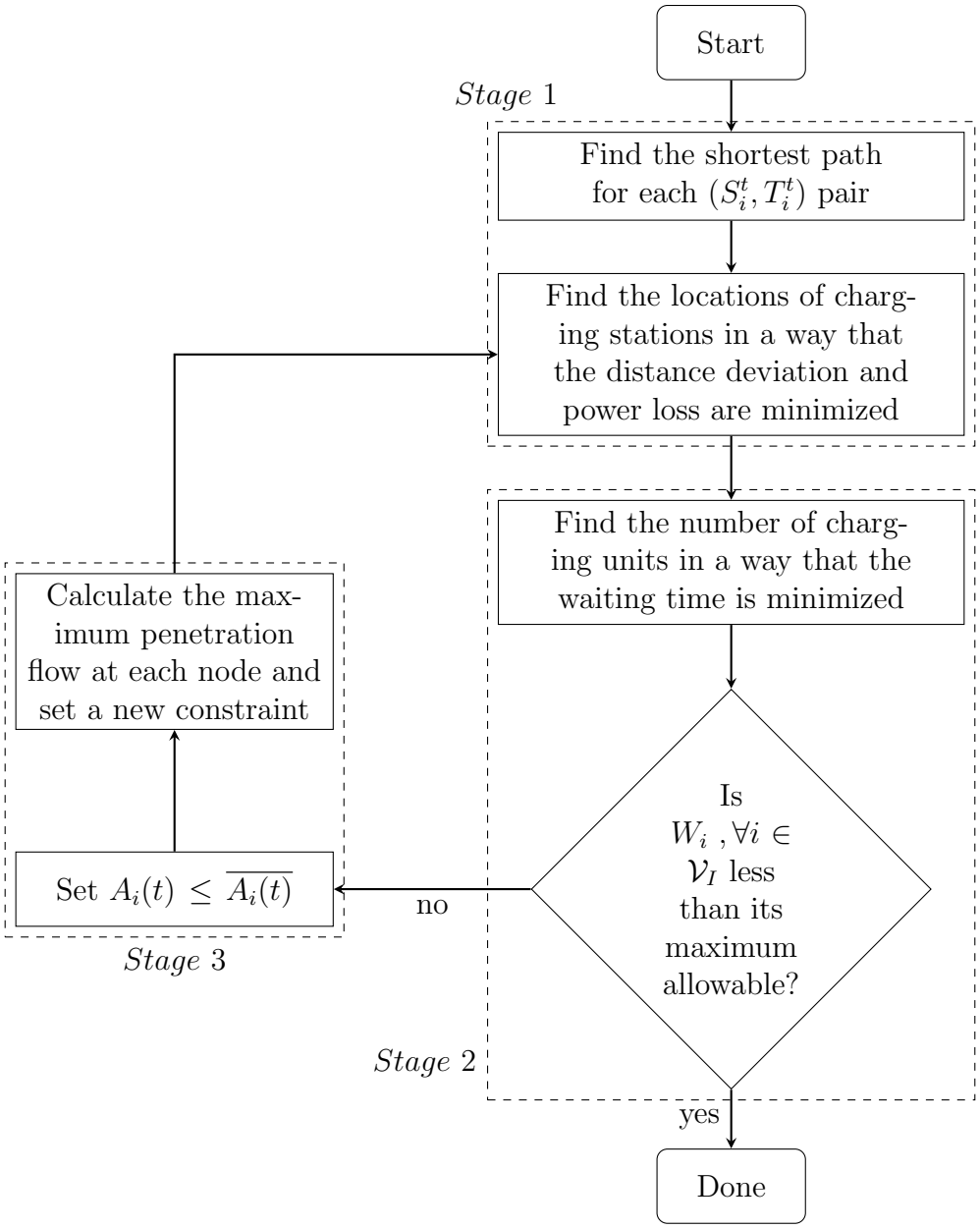

Figure 3.1: Optimization flow chart.

Second Stage: In this stage, the number of optimal charging units at each charging station is calculated, considering the maximum waiting time in the queue and also the maximum allowable number of charging units at each station.

Third Stage: In this stage, the maximum waiting time is checked to determine if it exceeds its limit. If this is more than the allowable waiting time ($\overline{W_i}$), the locations of the charging stations need to be reconsidered. It means returning

to stage 1, considering a new constraint. This constraint is:

$$A_i(t) \leq \overline{A_i(t)}. \tag{3.1}$$

While acknowledging the challenge of precisely analyzing the overall approach's complexity due to the combination of various algorithms and specific problem characteristics, we address the time-consuming aspect, the integer programming part, which traditionally has an exponential complexity of $\mathcal{O}(2^{2k})$ (where k is the number of integer variables in $\mathcal{V}_I$). Our multi-stage algorithm significantly reduces the number of integer variables at each iteration, from k to l ($l \leq k$), resulting in a reduced complexity of $\mathcal{O}(2^k + 2^l)$. Moreover, the division of the problem into stages helps ease constraints, leading to a more efficient algorithm that utilizes l integers and l continuous constraints instead of $2k$ integer constraints.

The first stage of the optimization problem contains continuous and integer variables (x) and linear and non-linear equations. Thus, this part of the problem forms a Mixed Integer Non-Linear Programming (MINLP) problem, which is in general NP-hard complex. In addition, since there are non-convex constraints and objective functions, solving the problem is more difficult and computationally expensive. Also, the number of traffic flow variables in the multi-commodity term is $9 \times n^4$ where n is the number of transportation nodes. In order to reduce the complexity of the problem, some of the non-convex constraints are relaxed and the number of variables is reduced, as detailed in this section.

3.1.1 Convergence of the Optimization Stages

We have three optimization stages. If optimization stage 1 or 2 does not give a solution, it means our research problem is not feasible (for example, due to inappropriate settings), and thus, our algorithm is terminated. If optimization stage 1 and 2 give solutions, we proceed to optimization stage 3 and check the maximal wait time constraints. If all the constraints are met, then our obtained solution in optimization stage 1 and 2 will be our final solution of our research problem; otherwise, we add constraint(s) to one or more node i and then we go back to stage 1 to repeat the procedure. If we still have solutions in stage 1 and 2, then we again proceed to stage 3, and add constraint(s) and go back to stage 1 if necessary. Please note that if we

add a new constraint for node i in stage 3 of an iteration, we will not need to add a new constraint for node i in later iterations. This means that the total number of added new constraints in all iterations is bounded by n (the total number of nodes). Thus, our algorithm will have at most n iterations, which means that our algorithm is guaranteed to converge.

3.1.2 Non-Convex Relaxation

In the first stage of the optimization formulation, constraints (2.31) - (2.33) are non-convex, and the cost function (2.21) includes non-convex terms. In [89], a second-order cone programming (SOCP) formulation for optimal power flow analysis is proposed for the radial networks, which fits our studied network. The radial networks are basically a tree graph. It means that each bus has a specific parent. Thus, $|\mathcal{E}_P| = |\mathcal{V}_P| - 1$. In this formulation, new variables are defined such that

$$u_i = \frac{V_i^2}{\sqrt{2}}, \tag{3.2}$$

$$R_{ij} = V_i V_j \cos(\theta_{ij}), \tag{3.3}$$

$$I_{ij} = V_i V_j \sin(\theta_{ij}). \tag{3.4}$$

In this way, equation (2.21) will change to

$$C_1^E = C_3 \sum_{(i,j)\in\mathcal{E}_P} \int \left(\sqrt{2}\left(u_i(t) + u_j(t)\right) - 2R_{ij}(t)\right) dt. \tag{3.5}$$

And constrain (2.32) and (2.33) can be rewritten as

$$P_i^g(t) - P_i^d(t) = \sqrt{2}u_i(t) \sum_{j\in\mathcal{V}_P} g_{ij} + \sum_{j\in\mathcal{V}_P} \left(g_{ij}R_{ij}(t) + b_{ij}I_{ij}(t)\right), \tag{3.6}$$

$$Q_i^g(t) - Q_i^d(t) = \sqrt{2}u_i(t) \sum_{j\in\mathcal{V}_P} b_{ij} + \sum_{j\in\mathcal{V}_P} \left(g_{ij}I_{ij}(t) - b_{ij}R_{ij}(t)\right). \tag{3.7}$$

All of the equations (3.5) to (3.7) are linear. So they are convex as well. However, since two variables (V and θ) are replaced with three new variables (u, R and I), another constraint is required to render this new formulation solvable. Equation (3.8) is a new constraint that should be added to the previous formulation to make it solvable.

$$2u_i(t)u_j(t) = R_{ij}^2(t) + I_{ij}^2(t). \tag{3.8}$$

Equation (3.8) is also non-convex. In [89], it is shown that the optimal power flow (OPF) can be obtained using the following second-order cone programming.

$$\max \quad \sum_{(i,j)\in\mathcal{E}_P} R_{ij} \tag{3.9}$$

$$\text{s.t.} \quad (2.35) \text{ and } (2.36),$$

$$2u_i u_j \geq R_{ij}^2 + I_{ij}^2, \tag{3.10}$$

$$R_{ij} \geq 0, \forall (i,j) \in \mathcal{E}_P. \tag{3.11}$$

Thus, by adding equation (3.9) to the objective function of stage 1 and equations (3.5) to (3.8), (3.10), and (3.11) to the existing formulation, the OPF part can be made convex. In addition, constraint (2.31) is also non-convex. The equality constraint can be changed to an inequality constraint by considering an upper bound for the in-flow of each location, thereby making it convex. In other words, equation (2.31) can be rewritten as

$$0 \leq f_i^{u,w} \leq x_w f_{max} \quad , \forall i \in \{1, \ldots, K\}, \forall w \in \mathcal{V}_T, \tag{3.12}$$

where f_{max} is a constant value at all nodes. By using this formulation instead of the previous one, the stage 1 of the optimization algorithm turns to a mixed integer second-order cone programming [24].

3.1.3 Reduce the Number of Variables

For each pair of origin and destination, there is a $3n \times 3n$ matrix of variables, which shows the commodity flow on each edge. Although many of the elements of this matrix are zero, there are significant amounts of non-zero variables remaining that make the calculation time-consuming. In order to reduce the number of non-zero variables, the paths which have a length of more than $\gamma d_{min}^{u,v}$ from the origin to the destination are omitted. Here γ is a constant value, and $d_{min}^{u,v}$ is the length of the minimum path from u to v. In order to find these paths between any two nodes, the algorithm of section II.A can be used. If matrix A is raised to the power of $n+1$, all the possible paths between every two nodes can be easily found, and for each origin-destination pair, a set can be defined

$$\mathbb{E}_{ij} = \{(u,w) | (u,w) \in \mathcal{P}_{ij} \ \& \ len(\mathcal{P}_{ij}) \leq \gamma d_{min}^{i,j}\}, \tag{3.13}$$

where $\mathcal{P}_{ij}$ is a path from i to j and $len(\cdot)$ means length of a path. Thus, the set $\mathbb{E}_{ij}$ is a set of all edges that are in at least one of the paths from i to j with a length less than or equal to $\gamma d_{min}^{i,j}$.

3.2 Case Study

In this study, a 25-node transportation network integrated with IEEE 33-bus system is used. Fig. 3.2 shows the topology of these two networks. The data of the 33-bus system can be found in [90]. This power network consists of one generation bus and 32 load buses.

3.2.1 System Settings

It is assumed that the hourly power demand at each node follows equation (3.14) and (3.15):

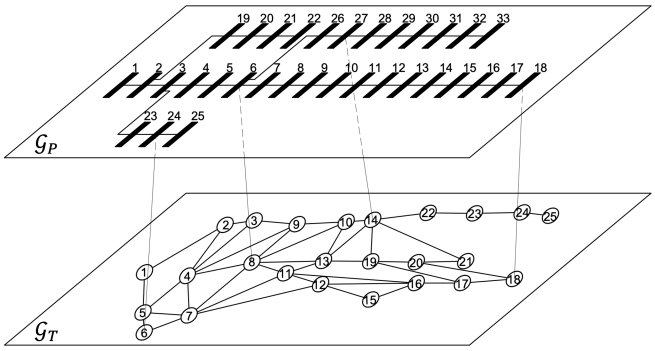

Figure 3.2: Power network and traffic network.

$$p_u^d(t) = \alpha_p(t) p_u^d + \beta_p(t) \quad \forall u \in \mathcal{V}_P, \tag{3.14}$$

$$q_u^d(t) = \alpha_q(t) q_u^d + \beta_q(t) \quad \forall u \in \mathcal{V}_P, \tag{3.15}$$

where p_u^d (q_u^d) is the total active (reactive) base power demand of bus u. $\alpha_p(t), \alpha_q(t), \beta_p(t)$ and $\beta_q(t)$ are the same for all buses in the network. A distribution of 3000 vehicles in the network at peak hours is randomly performed. It is assumed that the flow demand for each commodity follows the equation (3.16).

$$F_i^t = \alpha_T^t F_i, \tag{3.16}$$

where F_i is the flow demand at the pick hours, and α_T^t is a coefficient that changes over time. As [91] shows, the traffic flow changes over time and has two peaks, one around 9 AM and the other around 5 PM. Thus, it is assumed that α_T^t follows the same pattern as the traffic flow demands over time.

The maximum allowable number of charging units is considered as $\overline{y_i} = 100, \forall i \in \mathcal{V}_T$, and the maximum allowable waiting time is set as $W_i^{max} = 20$ min, $\forall i \in \mathcal{V}_T$. The service rate is also set to $\mu = 3$ vehicles/hour. The driving range is set as 300 km, and the fuel consumption rate is set as 0.14 kWh/km. The construction cost of a charging station is set as $\$163,000$ with 10 years of effective life and it is assumed that the land use cost is constant in different locations of the network. In addition, the cost of adding a charging station is set as $\$23,500$. The cost of waiting in the queue to get service is set as \$5/min and the cost of power loss is set as \$0.105/kWh. These inputs are set based on the inputs of [6]. The SoC at the origin and destination points are set as 40%. It means that each EV has at least 40% charge when it starts its trip or ends it. In addition, it is assumed that all EVs and all charging units are identical. Table II summarizes the setting of the base case scenario of the optimization problem.

Algorithm 1 Pseudocode of proposed three-stage optimization algorithm

Input: $\mathcal{G}_T, \mathcal{G}_P, R, p_i^d(t), q_i^d(t), g_{ij}, b_{ij}, \mu, \overline{y_i}, \overline{W_i}, f_{max}$
Initialization: Obtain graph $\hat{\mathcal{G}}_T$ based on graph $\mathcal{G}_T$ and R.
while $c \neq 0$ **do**
    $x_i \leftarrow \arg\min\{C_1^I + C_1^S + C_1^E\},\ \forall i \in \mathcal{V}_I$
    $A_i(t) \leftarrow x_i$
    $y_i \leftarrow \arg\min\{C_2^I + C_2^S\},\ \forall i \in \mathcal{V}_I$
    $c \leftarrow 0$
    for $i = 1$ to $|\mathcal{V}_I|$ **do**
        if $W_i^{max} > \overline{W_i}$ **then**
            $A_i(t) \leq \overline{A_i(t)}$ and $c \leftarrow c + 1$
        end if
    end for
end while
return x_i and y_i $\forall i \in \mathcal{V}_I$

In addition, it is assumed that the number of EVs that need to use the charging station does not affect the traffic flow and that the traffic flow speed on each road is constant over time. Also, this speed is the same for all roads; thus, in this way, the only effective parameter that makes EVs choose their path is the length of that path.

Table 3.1: System settings

Symbol	notion	Value
$\overline{y_i}$	maximum allowable number of charging units	100
W_i^{max}	maximum allowable waiting time	20 min
μ	service rate	3 Veh/hr
R	driving range	300 km
γ_c	fuel consumption rate	0.14 kWh/km
$C1$	cost of installing a charging station	\$163,000
$C2$	cost of additional driving distance	\$0.03/km
$C3$	cost of power loss	\$0.105/kWh
$C4$	cost of voltage deviation	\$1050
$C5$	cost of adding a charging station	\$23,500
$C6$	cost of waiting in the queue	\$5/min
SoC_o	battery SoC at the origin points	40%
SoC_d	battery SoC at the destination points	40%

3.2.2 Optimization Formulation

Since the size of $\mathcal{V}_T$ is 25, it means that the number of nodes in the expanded graph of this network is $3 \times 25 = 75$. As mentioned before, in order to reduce the number of decision variables related to transportation, only the paths with a length of $\gamma d_{min}^{u,w}$ or less are considered. In this study, γ is assumed as 1.5. In this way, the number of flow-related decision variables dropped 88%. In addition, this problem consists of $|\mathcal{V}_I|$ binary decision variables (which refers to x_i) and the same number of integer variables (which refers to y_i). Finally, there are $3 \times (|\mathcal{V}_P| - 1)$ variables related to the power network. Algorithm 1 is the pseudocode of the implemented algorithm for this optimization problem. The Gurobi[1] optimizer in the Python environment is utilized to solve the optimization problem on an 8-core computer equipped with an

[1]https://www.gurobi.com/

Intel Core i7 (11th generation) processor. Each iteration of the optimization problem takes about 10 minutes on average, and in our test scenarios, no case takes more than 5 iterations.

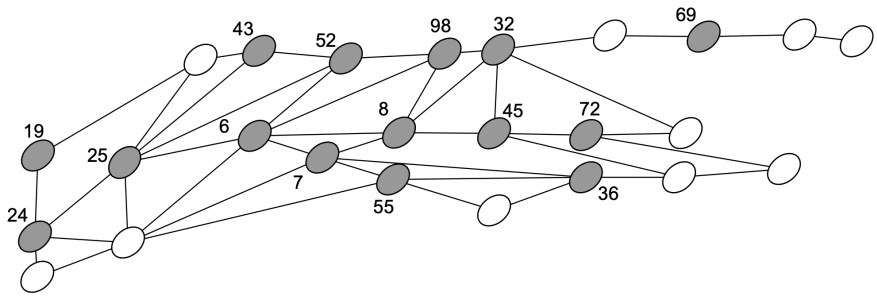

Figure 3.3: An example of locations and sizes of the charging stations after optimization. The numbers indicate the number of charging units of charging stations.

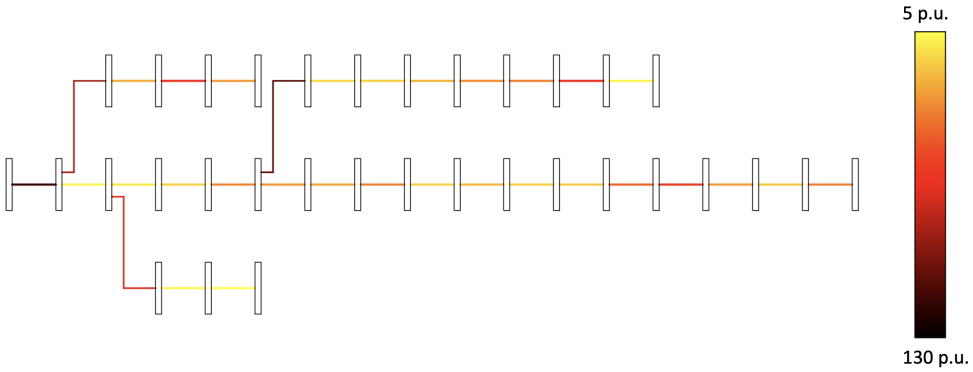

Figure 3.4: Power losses on the transmission lines.

Fig. 3.3 shows how the charging stations are distributed in the traffic network graph, and the number beside each station shows the number of charging units in that station. In addition, Fig. 3.4 shows the active power loss in each line in this case. The results of our experiments demonstrate that the active power loss cost increases 2.31 times when the charging stations are placed in the network, and this shows the importance of considering the active power loss in this optimization problem.

3.2.3 Driving Range

In order to ascertain the effect of the driving range, different driving ranges of EVs are considered. Table 3.2 presents a selection of battery models that are currently popular

in the market [92], [93]. The driving range can affect the optimization problem in different ways. First of all, the expanded graph would be changed by the changes in the driving range because when we want to construct matrix $\hat{A}$, more edges will satisfy the condition $\gamma_{ij}^{s} < R$. Thus, the number of candidate paths changes and it makes more options for the EVs to choose their paths. In addition, higher driving range means that the number of EVs that need to charge their batteries is reduced because more EVs can complete its trip without running out of charge. Fig. 3.5 shows how the charging stations change under the driving range from 300 km to 500 km. As this figure suggests, the number of charging stations decreases when the driving range increases. The total cost would be reduced too.

Table 3.2: Environmental Protection Agency estimates range of selected commercial EV models

Make,model	**Battery capacity (kWh)**	**Total Range (km)**
Nissan, Leaf	40	240
BMW, i4	83.9	444
Mercedes, EQS	120	521
Tesla, Model Y	82	531
Tesla, Model 3	75	576
Volkswagen, ID4	82	468
Hyundai, ioniq 5	77	487

3.2.4 State-of-Charge

In addition, another factor that can have a significant impact on the number and the locations of the charging stations is the SoC at the origin and the destination point. This can affect both the power network and the traffic network. Since in the expanded graph, the virtual source nodes and sink nodes are considered based on the SoC in the origin and the destination, the traffic network would be affected. In addition, the number of EVs required to charge their batteries would be increased when the SoC_d increases or the SoC_o decreases. Fig. 3.6 shows the total cost of

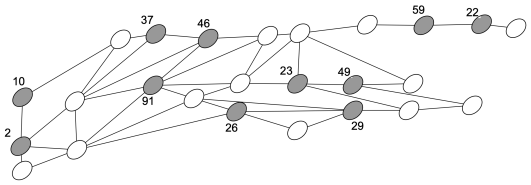

(a) Driving range 350 km

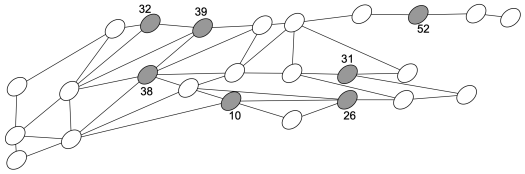

(b) Driving range 400 km

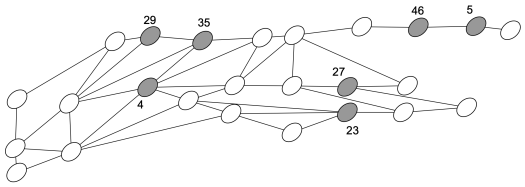

(c) Driving range 450 km

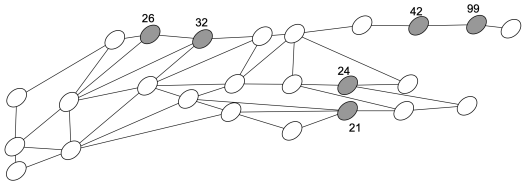

(d) Driving range 500 km

Figure 3.5: Optimal locations and size of the charging stations with different driving ranges. The numbers indicate the number of charging units of charging stations.

the optimization problem with respect to the changes in the SoC_o and the SoC_d. As this figure suggests, the minimum investment cost is achieved when the SoC_o is 90% and the SoC_d is 10%. It means that the EV can start its trip with an almost full battery and end with an almost empty one. It is worth mentioning that in the figure, the points with an investment cost of 1000 are essentially infeasible. However, for aesthetic purposes, they are included in the graph. Also, since it is assumed that it is impossible to place the charging station at all nodes, the scenario in which $SoC_o = 100\%$ and $SoC_d = 0\%$ is also infeasible.

3.2.5 Waiting Time

Other important factors that should be considered are the effect of maximum allowable waiting time and charging rate. These two factors only have an impact on the second stage of the optimization problem. They do not have a direct impact on the traffic network. However, this can have an indirect impact on the locations of the charging stations because the constraint of the third stage depends on the maximum allowable waiting time, and this can have a noticeable impact on the first stage of the optimization. In addition, the charging rate basically depends on the charging technology of chargers that are used in the charging stations. Although a

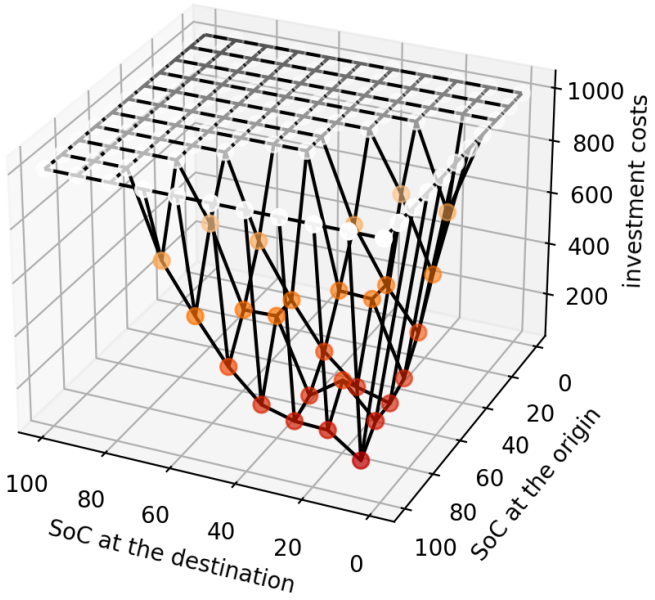

Figure 3.6: SoC effect on the investment costs.

higher charging rate can be beneficial in many aspects, there are some drawbacks as well. Higher charging rates can lead to increased demand and transformer overloading, which can reduce the lifespan of grid infrastructure. Additionally, the EV fast charging can cause voltage drops and fluctuations, which can affect the stability of the power grid. In addition, a higher charging rate would reduce the waiting time for EVs in the charging stations. Different scenarios are considered in which the only changing factors from the base scenario are the maximum allowable waiting time and the charging rate. This is done to observe the effects of these parameters. It is worth mentioning that in this study, a penalty for the unsatisfied demand is not considered, resulting in some cases being infeasible. It means that there is no solution that can satisfy all the constraints. The power balance constraints are the most sensitive constraints of our formulation. The results of the optimization problem show that when the waiting time is reduced to 5 minutes, it is impossible to place the charging stations unless the maximum allowable charging units is set to at least 500 units at each station. In addition, when the charging rate is reduced to 1 vehicle/hour, the investment cost increases 2.26 times. On the other hand, as the charging rate increases to 12 vehicles/hour, the investment cost decreases by 20%. The results show that the maximum number of charging units at each station has the least effect on

the locations of the charging station. However, it can make the problem infeasible. It means that when this factor reaches the feasibility threshold, it does not have much effect on the results. The results show that when the maximum number of charging units is less than 25, the problem is unsolvable unless the number of vehicles in the system is less than 1500.

3.2.6 Discussions and Recommendations

The charging station planner and customer perspectives provide different insights into the factors that affect the efficiency of charging infrastructure for EVs. It is essential to consider both perspectives to optimize the infrastructure for cost-effectiveness and convenience.

- Driving Range: Regarding driving range, the charging station planner should consider the balance between reducing the number of charging stations required and the total investment cost with the increased charging time that comes with higher driving ranges. On customers' side, higher driving ranges provide more flexibility and convenience, allowing for longer trips without frequent charging stops.

- State-of-Charge: The state-of-charge factor requires the charging station planner to balance the number and locations of charging stations required with the investment cost while considering the traffic and power networks' impact. From the customers' side, high starting SoC and low ending SoC levels can maximize driving range and reduce the need for frequent charging stops, but planning around charging station availability may be necessary.

- Waiting Time: The waiting time factor requires the charging station planner to strike a balance between minimizing waiting time for EV customers and ensuring the charging network can handle the load. From the customers' perspective, selecting charging stations carefully to avoid long wait time during peak usage periods while choosing shorter waiting time and higher charging rates can increase convenience and reduce trip time.

Table 3.3 summarizes these recommendations. Overall, optimizing charging infrastructure for EVs requires considering all these factors together. It is necessary to minimize investment cost, reduce the pressure on the power network, and provide efficient charging solutions for EV owners.

Table 3.3: Recommendations

Factors	**Influence**	**Recommendations**
Driving Range	Less charging facilities are needed	Developing the battery technology to increase the driving range of EVs
State-of-Charge	More EVs can complete their trip without charging needs	Making the home charging available
Waiting time	More charging units are needed	Using the fast charging units in the charging stations

Chapter 4

Cooperative Microgrid Management System: Online Optimization Algorithm

4.1 Problem Formulation

As outlined in the introductory chapter, one promising approach to addressing the high load demand in CSs involves the use of Charging Station Microgrids (CSMGs). In this framework, each CS is equipped with its own RES and ESS, with the EV charging demand managed as an unpredictable load. Within this section, we delve deeply into a model centered around implementing energy storage management. Our primary goal is to curtail operational costs, all while accommodating the uncertainties inherent in this model. Our exploration begins with a comprehensive look at the offline setting, where all relevant information is readily available in advance. Subsequently, we introduce the crux of this chapter: our groundbreaking online algorithm. This algorithm stands as our principal contribution, specifically designed to navigate real-time scenarios, adapting to dynamic changes and uncertainties in the system.

4.1.1 Offline Setting

In Figure 4.1, the coordination of three MGs is depicted as an example of Multi-MicroGrid (MMG) energy management [94]. In this system, each MG has access to its individual renewable energy sources (RES) and is equipped with an Energy Storage System (ESS) to store the energy for later use. MGs can also purchase energy from the main grid, which follows an unknown dynamic pricing, namely $p(t)$. Without

loss of generality, although the exact price at each time is unknown, it is possible to assume that the price is bounded, i.e., $m \leq p(t) \leq M$. This price is set based on the demand of users, which is beyond the scope of this study.

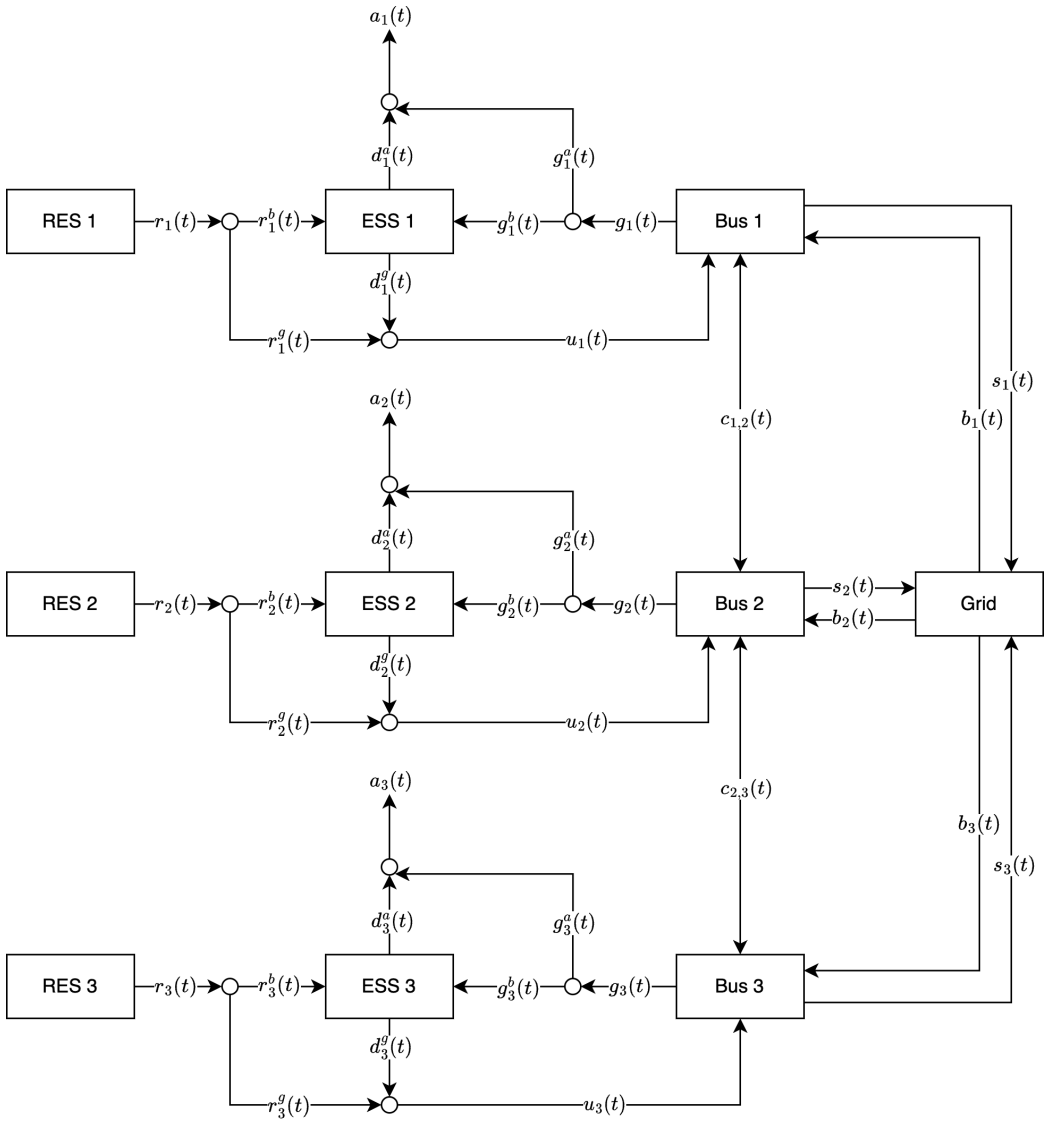

Figure 4.1: Cooperative MMGs example

Furthermore, MGs can even monetize their surplus energy generated from RES by selling it back to the main grid. This becomes particularly relevant when energy storage systems reach their capacity limits, necessitating an outlet for the excess energy produced by the RES. However, it is hard to know when is the right time of buying the energy, selling the energy, storing the energy or sharing it due to the uncertainties of the system related to the energy demand from the customers side,

the price of the energy, and the amount of available energy from RES. Thus, it is assumed that MGs can share their surplus energy with other MGs in order to reduce the purchasing cost from the main grid. However, it is presumed that this is not a cost-free action. MGs must pay P' as a unit sharing price in this procedure, which is less than $p(t)$ ($p' \leq p(t)$). Furthermore, MGs can sell their surplus energy to the main grid to make a profit. The unused renewable energy can be sold to the main grid with the unit price of p''. It is believed that this price is always less than the purchasing price from the grid, and this indeed makes sense because otherwise, MGs can just buy energy from the grid and sell it again to main power grid and make a profit, which is impractical from the perspective of the main power grid. In fact, assume there are two MGs that one of them needs X units of energy, and the other one has X unit surplus energy. We want to make sure that MGs prefer to share their surplus energy instead of selling and purchasing energy. Thus,

$$\begin{aligned} & p(t)X - p''X \geq p'X \Rightarrow p(t) \geq p' + p'' \\ & \xrightarrow{\min_t p(t)=m} p' + p'' \leq m \end{aligned} \tag{4.1}$$

We can assume that $p' + p'' = m$. In this way, we can always ensure that sharing energy among MGs is more profitable for the whole system compared to purchasing. Thus, we defined α such that $p' = m(1-\alpha)$ and $p'' = m\alpha$.

Let $\mathcal{I}$ be the set I different CSs, while $\mathcal{T}$ represents the discretized time horizon, ranging from 0 to T. Table 4.1 outlines the specific notations employed in this study for clarity and reference.

In the following section, we present the offline-optimization formulation designed to minimize overall operational costs. These costs consist of three key components: purchasing energy directly from the main grid, sharing energy among MGs, and revenue from selling surplus energy back to the main grid. Notably, this optimization model simplifies by excluding considerations of battery degradation costs associated with charging and discharging.

The optimization formulation of this problem is formulated as:

Table 4.1: Table of notations used in Chapter 4

Symbol	Definition	Symbol	Definition
$r_i(t)$	Renewable energy of MG i at time t	η_c/η_d	Charging/Discharging efficiency of batteries
$r_i^b(t)$	Renewable energy of MG i to charge battery at time t	μ_c	Maximum charging rate of batteries
$r_i^g(t)$	Renewable energy of MG i to share with other MGs at time t	μ_d	Maximum discharging rate of batteries
$d_i^a(t)$	Energy from battery of MG i to full-fill demand at time t	$p(t)$	Purchasing energy price from the main grid at time t
$d_i^g(t)$	Energy from battery of MG i to share with other MGs at time t	p'	Sharing energy price from one MG to other MGs
$g_i^a(t)$	Energy from main grid to MG i to full-fill demand at time t	p''	Selling energy price to the main grid
$g_i^b(t)$	Energy from main grid to MG i to charge battery at time t	$x_i(t)$	Binary variable: 1 if MG i connects the main grid at time t, 0 otherwise
$c_{i,j}(t)$	Shared energy from MG i to j at time t	$a_i(t)$	Unsatisfied Demand of MG i at time t
$u_i(t)$	Penetrated energy from MG i to the system at time t	B	Maximum energy level of batteries
$E_i(t)$	Energy storage level of MG i at time t	B_0	Energy level at initial time horizon
$b_i(t)$	Purchased energy of MG i from the main grid at time t	B_T	Energy level at final time horizon
$s_i(t)$	Sold energy from MG i to the main grid at time t		

$$\min \sum_{t=1}^{T}\sum_{i=1}^{I}\left[p(t)b_i(t) + \sum_{j\neq i}^{I} p' c_{i,j}(t) - p'' s_i(t)\right] \tag{4.2}$$

$$\text{s.t. } g_i^a(t) + d_i^a(t) = a_i(t), \qquad \forall i \in \mathcal{I} \tag{4.3}$$

$$r_i^b(t) + r_i^g(t) \leq r_i(t), \qquad \forall i \in \mathcal{I} \tag{4.4}$$

$$g_i^a(t) + g_i^b(t) = g_i(t), \qquad \forall i \in \mathcal{I} \tag{4.5}$$

$$d_i^g(t) + r_i^g(t) = u_i(t), \qquad \forall i \in \mathcal{I} \tag{4.6}$$

$$g_i(t) + \sum_j c_{i,j}(t) + x_i(t)s_i(t) = u_i(t) + \sum_j c_{j,i}(t) + x_i(t)b_i(t), \qquad \forall i,j \in \mathcal{I} \tag{4.7}$$

$$c_{i,j}(t)c_{j,i}(t) = 0, \qquad \forall i,j \in \mathcal{I} \tag{4.8}$$

$$u_i(t)g_i(t) = 0, \qquad \forall i,j \in \mathcal{I} \tag{4.9}$$

$$r_i^b(t) + g_i^b(t) \leq \mu_c, \qquad \forall i \in \mathcal{I} \tag{4.10}$$

$$d_i^a(t) + d_i^g(t) \leq \mu_d, \qquad \forall i \in \mathcal{I} \tag{4.11}$$

$$E_i(t+1) = E_i(t) + \eta_c\left(r_i^b(t) + g_i^b(t)\right) - \eta_d\left(d_i^a(t) + d_i^g(t)\right), \qquad \forall i \in \mathcal{I} \tag{4.12}$$

$$0 \leq E_i(t) \leq B, \qquad \forall i \in \mathcal{I} \tag{4.13}$$

$$E_i(0) = B_0, \qquad \forall i \in \mathcal{I} \tag{4.14}$$

$$E_i(T) = B_T, \qquad \forall i \in \mathcal{I} \tag{4.15}$$

$$r_i^b(t), r_i^g(t), g_i^a(t), g_i^b(t), d_i^a(t), d_i^g(t), c_{i,j}(t), s_i(t), b_i(t) \geq 0$$

The constraints (4.3) to (4.7) within this formulation ensure that the power flowing in and out of individual nodes remains balanced. Specifically, these constraints maintain equilibrium between the incoming and outgoing power at each signal node. Constraint (4.8) serves to enforce unidirectional energy sharing, allowing energy transfer in one direction only at any given time. This restriction prevents simultaneous bidirectional energy exchange between nodes. Furthermore, constraints (4.10) and (4.11) are integral in regulating the charging and discharging rates, preventing these actions from surpassing their designated limits. These limitations are crucial in maintaining the stability and operational boundaries of the system. Finally, constraints (4.12) to

(4.15) are dedicated to upholding power balance within the battery across different time intervals. These constraints play a pivotal role in ensuring that the battery operates within prescribed power thresholds, guaranteeing its optimal functioning while adhering to predefined energy parameters.

Moreover, this offline optimization is a convex problem, because the only nonlinear constraints are constraints (4.8) and (4.9), which are quadratic and convex. Therefore, there are multiple options and solvers to solve these type of optimization problems. In this study, we used Gurobi to solve the convex programming problem of the off-line setting.

4.1.2 Online Optimization Algorithm

In the online optimization setting, we assume that there is no prior information about the power demand, available renewable energy, the occurrence of the fault, and the electricity price. However, it seems to be impossible to design a good online algorithm to solve this problem. In order to make this problem solvable, we can use some assumptions without losing any generality. These assumptions are stated as follows:

- The electricity price is unknown. But we can assume that the electricity price is fluctuated between m and M. In other words, $m \leq p(t) \leq M$

- The proportion between available renewable energy and demand over time, as highlighted by [95], exhibits higher predictability compared to the precise values at each time step. Denoted as ρ_i, this ratio is defined as $\rho_i = \frac{\sum_{t=1}^{T} a_i(t)}{\sum_{t=1}^{T} r_i(t)} \frac{\eta_d}{\eta_c}$, assuming $0 \leq \rho_i \leq 1$.

- At each time, there is at least one MG that remains connected to the main grid, which can be expressed as $\sum_i x_i(t) \geq 1, \forall t \in T$. In other words, it is ensured that all MGs cannot be in islanded mode simultaneously. This assumption is made to guarantee the possibility of meeting the energy demand of all MGs at any given time. Additionally, it is assumed that the blackout duration is known in advance and is represented as $\frac{\sum_t x_i(t)}{T} = k_i$.

In this online optimization problem, the inputs consist of sequences representing demand, market prices, renewable energy supplies, and fault occurrences. The decision variables for our problem are denoted as $\mathbf{D} = (r^b(t), r^g(t), g^a(t), g^b(t), d^a(t), d^g(t), s(t), l(t), c(t))_{t=1}^T$, and the inputs are represented by $\mathbf{I} = (a(t), p(t), r(t), x(t))_{t=1}^T$. However, $\mathbf{I}$ is not known in advance and is revealed over time, placing this problem in the setting of online optimization.

Let us assume $\mathrm{OPT}(\sigma)$ represents the optimal solution in an offline setting, signifying the objective function's value when all information is known in advance in instance σ. The goal is to design an algorithm that can perform as close as possible to the OPT solution. To evaluate the online learning algorithm, various metrics can be used, such as *regret* and *competitive ratio*. In this study, we employ the competitive ratio (CR) as our metric [96]. CR is defined as the worst-case ratio between the cost of the online algorithm and that of an offline optimal solution. Let $\mathrm{ALG}(\sigma)$ be the output of the online optimization algorithm. Then, CR is the maximum competitive ratio over all possible instances.

$$\mathrm{CR} = \max_{\sigma} \frac{\mathrm{ALG}(\sigma)}{\mathrm{OPT}(\sigma)}$$

To develop an algorithm for the energy management of the Multi-MicroGrid (MMG) system, we have designed a threshold-based online optimization approach. Two distinct thresholds need to be defined for this purpose.

The first threshold, denoted as θ, represents the purchasing price threshold. When the energy price falls below this threshold, it is more cost-effective to procure energy from the main grid. When the energy price exceeds θ, MGs prioritize using the stored energy in their ESS rather than purchasing energy from the main grid. It is intuitive to understand that if θ is set too high, there's a risk of missing lower charging prices. Conversely, if set too low, the ability to find sufficiently low prices for recharging batteries is reduced, compelling MGs to procure energy at higher costs to meet their demand.

The second threshold, denoted as $\hat{B}$, pertains to the storage capacity of each MG. The design of this threshold requires careful consideration. If it is set too low, it may lead MGs to purchase energy during periods of high prices. Conversely, if set too high, MGs may miss opportunities to charge their storage systems at lower prices.

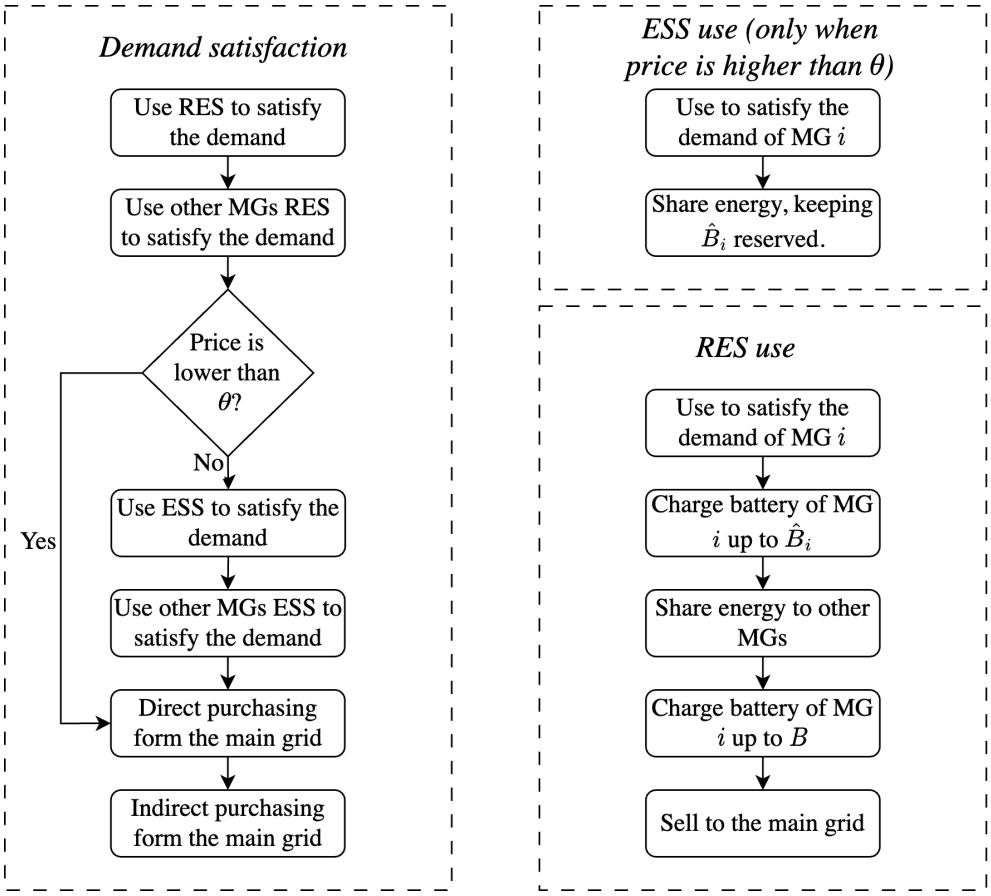

Figure 4.2: Algorithm 2 summary

If an MG is not directly connected to the main grid, it can still maintain an indirect connection. Let $\beta \geq 1$ be the factor representing indirect buying/selling of energy to/from the main grid. In this way, MG i can procure energy from the main grid at the unit price of $\beta p(t)$.It is reasonable to prioritize certain MGs for receiving shared energy from other MGs, especially those not directly connected to the main grid, as they face higher purchasing prices.

The Multi-Online algorithm outlined in Algorithm 2 can be summarized in Figure 4.2. Note that in this study, we define $[\cdot]^+ = \max\{0, \cdot\}$.

Algorithm 2 Multi-Online algorithm

$\mathcal{P}(t) = \{j | x_j(t) = 0\}$ ▷ Set of MGs that are disconnected
for $i \in \mathcal{I}$ **do** ▷ Use RE to charge the storage up to $\hat{B}_i$
  $r_i^b(t) \leftarrow \min\left\{\mu_c, \frac{\hat{B}_i - E_i(t-1)}{\eta_c}, r_i(t)\right\}$
  for $j \in \mathcal{P}(t)$ **do** ▷ Use RE to satisfy disconnected MGs demand
    $c_{i,j}^{r,a}(t) \leftarrow \min\left\{a_j(t), \left[r_i(t) - r_i^b(t) - \sum_j c_{i,j}^{r,a}(t)\right]^+\right\}$
    $a_j(t) \leftarrow a_j(t) - c_{i,j}^{r,a}(t)$
  end for
  for $j \in \mathcal{I}/\mathcal{P}(t)$ **do** ▷ Use RE to satisfy connected MGs demand
    $c_{i,j}^{r,a}(t) \leftarrow \min\left\{a_j(t), \left[r_i(t) - r_i^b(t) - \sum_j c_{i,j}^{r,a}(t)\right]^+\right\}$
    $a_j(t) \leftarrow a_j(t) - c_{i,j}^{r,a}(t)$
  end for ▷ Use RE to charge the storage up to B
  $r_i^b(t) \leftarrow r_i^b(t) + \min\left\{\mu_c - r_i^b(t), \frac{B - E_i(t-1)}{\eta_c} - r_i^b(t), \left[r_i(t) - r_i^b(t) - \sum_j c_{i,j}^{r,a}(t)\right]^+\right\}$
end for
if $p(t) \leq \theta$ **then**
  for $i \in \mathcal{I}$ **do**
    $b_i(t) \leftarrow x_i a_i(t)$ ▷ Purchase energy from the grid
    for $j \in \mathcal{P}(t)$ **do** ▷ Purchase energy for other MGs
      $b_{i,j}(t) \leftarrow x_i(t) a_j(t)$
      $a_j(t) \leftarrow a_j(t) - b_{i,j}(t)$
      $b_i(t) \leftarrow b_i(t) + b_{i,j}(t)$
    end for
  end for
  for $i \in \mathcal{I}$ **do**
    $g_i^b(t) \leftarrow x_i(t) \min\left\{\mu_c - r_i^b(t), \left[\frac{\hat{B}_i - E_i(t-1)}{\eta_c} - r_i^b(t)\right]^+\right\}$ ▷ Fill upto $\hat{B}_i$
    $b_i(t) \leftarrow b_i(t) + g_i(t)$
    $s_i(t) \leftarrow \left[r_i(t) - r_i^b(t) - \sum_j c_{i,j}^{r,a}(t)\right]^+$ ▷ Sell energy to the grid
    $d_i^a(t) \leftarrow 0$
    $d_i^g(t) \leftarrow 0$
    $r_i^g(t) \leftarrow \left[r_i(t) - r_i^b(t)\right]^+$
    for $j \in \mathcal{I}$ **do**
      $c_{i,j} \leftarrow c_{i,j}^{r,a}$
    end for
  end for
else
  for $i \in \mathcal{I}$ **do** ▷ Use SE to satisfy the demand
    $d_i^a(t) \leftarrow \min\left\{\mu_d, a_i(t), \frac{E_i(t-1)}{\eta_d}\right\}$
    $a_i(t) \leftarrow a_i(t) - d_i^a(t)$
  end for

for $i \in \mathcal{I}$ **do**
  for $j \in \mathcal{P}(t)$ **do** ▷ Use SE to satisfy disconnected MGs demand
    $c_{i,j}^{d,a} \leftarrow \min\left\{a_j(t), \mu_d - d_i^a(t), \left[\frac{E_i(t-1)-\hat{B}_i}{\eta_d} - d_i^a(t)\right]^+\right\}$
    $a_j(t) \leftarrow a_j(t) - c_{i,j}^{d,a}$
  end for
  for $j \in \mathcal{I}/\mathcal{P}(t)$ **do** ▷ Use SE to satisfy connected MGs demand
    $c_{i,j}^{d,a} \leftarrow \min\left\{a_j(t), \mu_d - d_i^a(t), \left[\frac{E_i(t-1)-\hat{B}_i}{\eta_d} - d_i^a(t)\right]^+\right\}$
    $a_j(t) \leftarrow a_j(t) - c_{i,j}^{d,a}$
  end for
end for
for $i \in \mathcal{I}$ **do**
  $b_i(t) \leftarrow x_i a_i(t)$ ▷ Purchase energy from the grid
  for $j \in \mathcal{P}(t)$ **do** ▷ Purchase energy for other MGs
    $b_{i,j}(t) \leftarrow x_i(t) a_j(t)$
    $a_j(t) \leftarrow a_j(t) - b_{i,j}(t)$
    $b_i(t) \leftarrow b_i(t) + b_{i,j}(t)$
  end for
end for
for $i \in \mathcal{I}$ **do**
  $g_i^b(t) \leftarrow 0$
  $s_i(t) \leftarrow \left[r_i(t) - r_i^b(t) - \sum_j c_{i,j}^{r,a}(t)\right]^+$ ▷ Sell energy to the grid
  $d_i^g(t) \leftarrow \sum_j c_{i,j}^{d,a}$
  $r_i^g(t) \leftarrow \left[r_i(t) - r_i^b(t)\right]^+$
  for $j \in \mathcal{I}$ **do**
    $c_{i,j} \leftarrow c_{i,j}^{r,a} + c_{i,j}^{r,b}$
  end for
end for
end if

Now we need to design θ and $\hat{B}$ and then calculate the competitive ratio of our algorithm. In order to calculate these parameters, we can use the results of ref [95] to have some intuition. In this case, if $\alpha = 0$, $I = 1$ and $\sum_t x_i(t) = T$, then the problem is reduced to the problem [95] tried to solve. In addition, if we assume that $I = 1$, $\sum_t x_i(t) = T$, $\rho = 0$, $\eta_c = \eta_d = 1$, and $\mu_c = \mu_d = \infty$, then the results of this problem are the same as the One-way trading problem [97].

However, our problem differs in several aspects. Firstly, there are multiple MGs in the system. Additionally, an MG may be unable to acquire the required energy from

the grid due to the blackout of certain system segments. Sharing energy with other MGs and selling excess renewable energy back to the grid are further distinctions between our problem and the previously mentioned one. Nonetheless, some insights can be gleaned from the work in [95]. For example, when ρ approaches 1, it implies that most of the demand can be met by RES; thus, necessitating minimal battery charging. Conversely, if ρ is too small, it indicates that the majority of the demand must be satisfied using stored energy in the ESS.

In our problem, since it is possible that some MGs may be in the islanded mode, $\hat{B}$ should be related to k_i as well. Because if the MG is in the islanded mode most of the time, then it prefers to charge its battery more aggressively when it is possible. It also has less desire to share its energy with other MGs since it may force it to purchase energy in the high price hours. Additionally, the amount of renewable energy is another factor that can affect $\hat{B}$. If MG can satisfy its own demand by its produced energy from RES, then the interest in charging the ESS by purchasing energy is less. Therefore, $\hat{B}$ is also related to ρ_i.

$$\hat{B}_i = B(1 - k_i\rho_i)$$

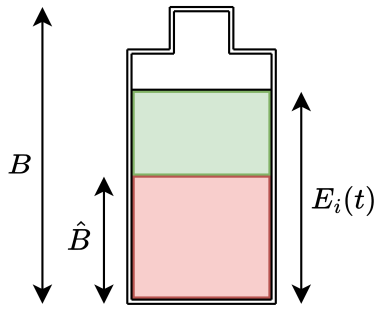

Figure 4.3: Illustrating B, $\hat{B}$, and $E(t)$ dynamics

In this context, if k_i is close to zero, it indicates that the connection of MG i with the main grid is mostly not established. Therefore, MG i must significantly charge its battery whenever possible. On the other hand, if ρ_i is too high, it implies that MG i is likely able to meet its energy demand solely from its own RES; thus, requiring less charging.

4.1.3 Competitive Analysis

Theorem 5 *Let $\hat{B}_i = B(1-k_i\rho_i)$ for all $i \in \mathcal{I}$ with the terminal condition of $E_i(T) = B$ for all $i \in \mathcal{I}$ and the assumption that $M\beta \geq \frac{\eta_d}{\eta_c}\alpha m$, the competitive ratio of Algorithm 2 is*

$$CR = \max_i \max \Bigg\{ \frac{\theta_i^1 \frac{\eta_d}{\eta_c}(1-k_i\rho_i) + k_i\rho_i(M\beta - \alpha\frac{\eta_d}{\eta_c}m)(1-\rho_i) - (\rho_i - k_i\rho_i)\frac{\eta_d}{\eta_c}\alpha m}{m(1-\rho_i)}, \tag{4.16}$$

$$\frac{\theta_i^1 \frac{\eta_d}{\eta_c}\rho_i(1-k_i\rho_i) + (M\beta - \alpha k_i\rho_i\frac{\eta_d}{\eta_c}m)(1-\rho_i) - (\rho_i - k_i\rho_i)\frac{\eta_d}{\eta_c}\alpha m}{\theta_i^1 \frac{\eta_d}{\eta_c}(1-\rho_i)}, \tag{4.17}$$

$$\frac{\theta_i^2 \frac{\eta_d}{\eta_c}(1-k_i\rho_i) + k_i\rho_i(M\beta - \alpha\frac{\eta_d}{\eta_c}m) - (\rho_i - k_i\rho_i)\frac{\eta_d}{\eta_c}\alpha m}{(1-\alpha\rho_i\frac{\eta_d}{\eta_c})m}, \tag{4.18}$$

$$\frac{M\beta - \alpha k_i\rho_i\frac{\eta_d}{\eta_c}m - (\rho_i - k_i\rho_i)\frac{\eta_d}{\eta_c}\alpha m}{\theta_i^2\frac{\eta_d}{\eta_c} - \rho_i\alpha\frac{\eta_d}{\eta_c}m} \Bigg\} \tag{4.19}$$

where θ_i^1 is the answer of equality of equations 4.16 and 4.17, and θ_i^2 is the answer of equality of equations 4.18 and 4.19. Also, θ is the maximizer of CR.

Proof. See Appendix A for the proof. ■

Remark 6 *Based on Theorem 5, we can have mulitple observations.*

1. *The product of α, ρ, and $\frac{\eta_d}{\eta_c}$ cannot exceed 1. This limitation arises from the negativity of Equation 4.18 in such instances, rendering it an impossibility. Practically, it has been observed that when $\frac{\eta_d}{\eta_c}\alpha\rho \geq 1$, the optimization problem becomes unbounded. This scenario implies that in the optimization process, the sale of energy becomes significantly more profitable than satisfying the demand. Consequently, Microgrids (MGs) prioritize selling all their renewable energy instead of meeting the demand, leading to an infeasible solution for the optimization problem.*

2. *By incrementing α from 0 to 1, the competitive ratio initially declines, then ascends. During the declining phase, $\theta_i = \theta_i^1$, and transitioning to $\theta_i = \theta_i^2$ during the ascending phase. Intuitively, as α increases, the online algorithm*

approximates the offline solution more closely until a certain threshold. However, as the selling of energy becomes more lucrative than meeting demands, the offline algorithm significantly outperforms the online approach. This divergence occurs because the offline algorithm has foresight into future prices and demands. Consequently, it can leverage this information advantageously. Figure 4.4 demonstrates how the competitive ratio varies concerning different α values.

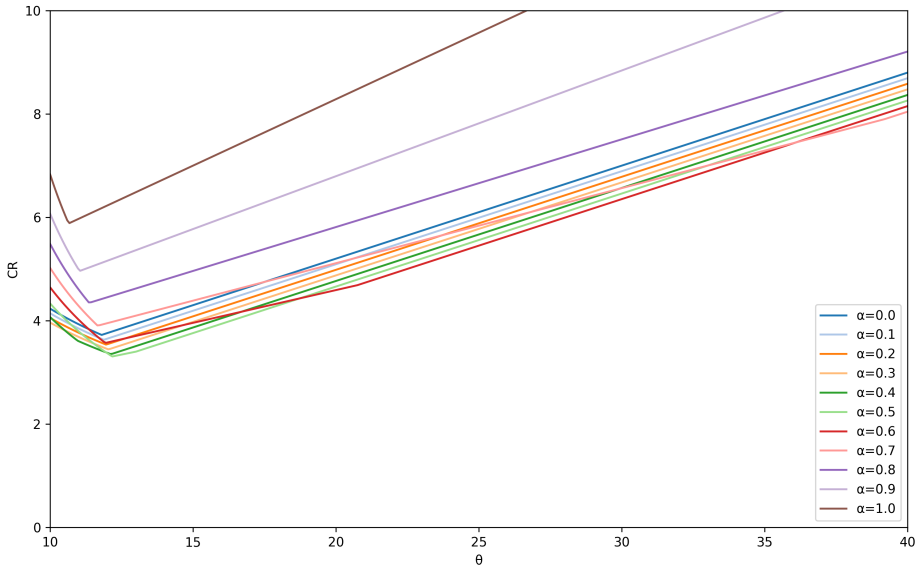

Figure 4.4: Changes of the competitive ratio with respect to α

3. *When $\alpha = 0$, the worst-case scenario of our online algorithm for multiple MGs aligns with that of the Single MG online algorithm. This equivalence arises from the fact that a zero selling price implies that selling does not contribute any profit to the MG management system.*

4. *When $k = 1$, it implies that $\rho = k\rho$, or in other words, MGs are consistently connected to the main grid. As k decreases, the competitive ratio first decreases θ concomitantly decreases. This is a logical conclusion, indicating that with a less stable connection of the MG to the main grid, the algorithm becomes more inclined to accept higher prices for charging its ESS from the main grid. Figure 4.5 illustrates the variations in competitive ratio with changing k when $\alpha = 0.5$.*

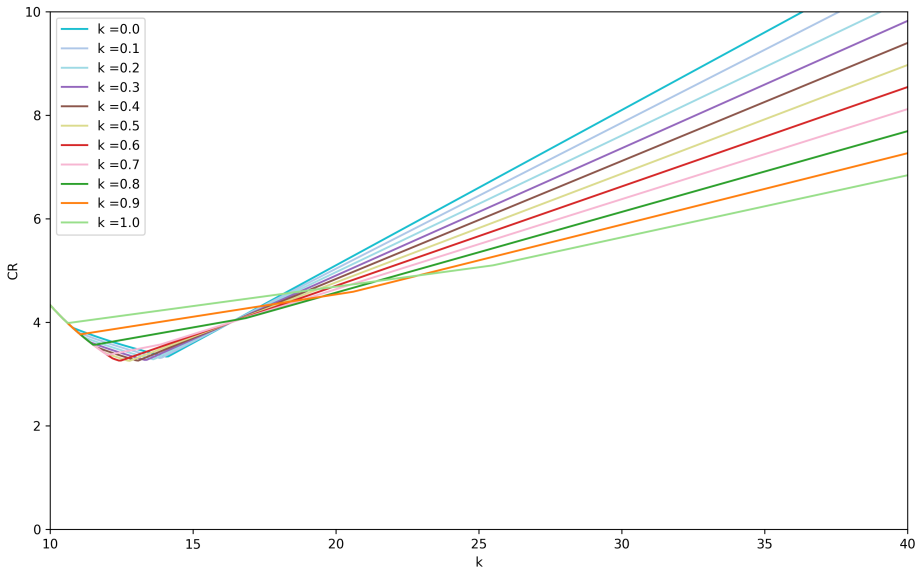

Figure 4.5: Changes of the competitive ratio with respect to k

4.2 Case study

In this section, we delve into two distinct case studies, demonstrating the superior performance of our model compared to existing models in cooperative MG operations. The initial case involves the creation of data to address unknown inputs within the problem. This primary case comprises several subcases, each elucidated in comprehensive detail later on.

Moving to the second case, we utilize real-world data, conducting a comparative analysis between our algorithm and established algorithms already in use. This comparison serves to underscore the efficacy and advantages of our approach when applied to practical scenarios, emphasizing its superiority over existing methods.

4.2.1 Randomized Dataset

In this segment of our case study, we generated a randomized dataset to gauge our model's performance. Establishing $\eta_c = 0.95$ and $\eta_d = 1.05$, we standardized the battery storage across all MGs at 20 MWh with an initial half-charge. Our assessment spanned 2 days, structured in 20-minute increments ($T = 2 \times 24 \times 3$). Within this framework, we randomly generated renewable energy data spanning 40 MWh and

demand requests from 0 to 50 MWh. Additionally, we created random energy prices ranging between 10 and 40 $/KWh.

We analyzed our model using the algorithm referenced in [95] alongside an offline algorithm to benchmark its performance. This evaluation was iterated 50 times to fortify the simulation's robustness. Figure 4.6 showcases our model's performance within a 95% confidence interval. Setting $\alpha = 0.8$, the figure distinctly illustrates our algorithm's superiority over existing online algorithms, which in turn outperformed established models like the Lyapunov stochastic optimization algorithm proposed in [98]. Notably, augmenting the number of MGs accentuated the performance disparity between our model and existing ones.

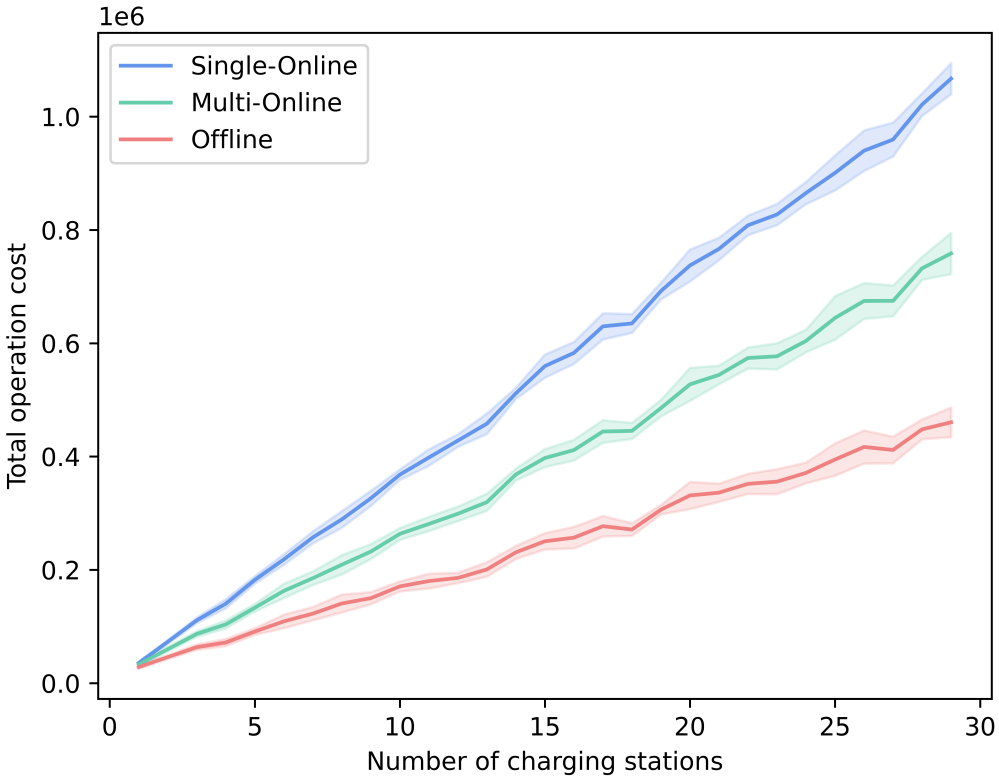

Figure 4.6: Algorithm performance comparison

Figure 4.7 shows how much energy microgrids share. It is clear that as more microgrids join, the shared energy increases. Additionaly, the offline algorithm, which knows future information, shares more energy compare to the multi-online algorithm,

which makes sense.

Also, when there are more charging stations, the difference between the Multi-Online and offline algorithms grows. This happens because the offline one plans better with future data, while the Multi-Online reacts in real time, causing a larger gap in shared energy between the two.

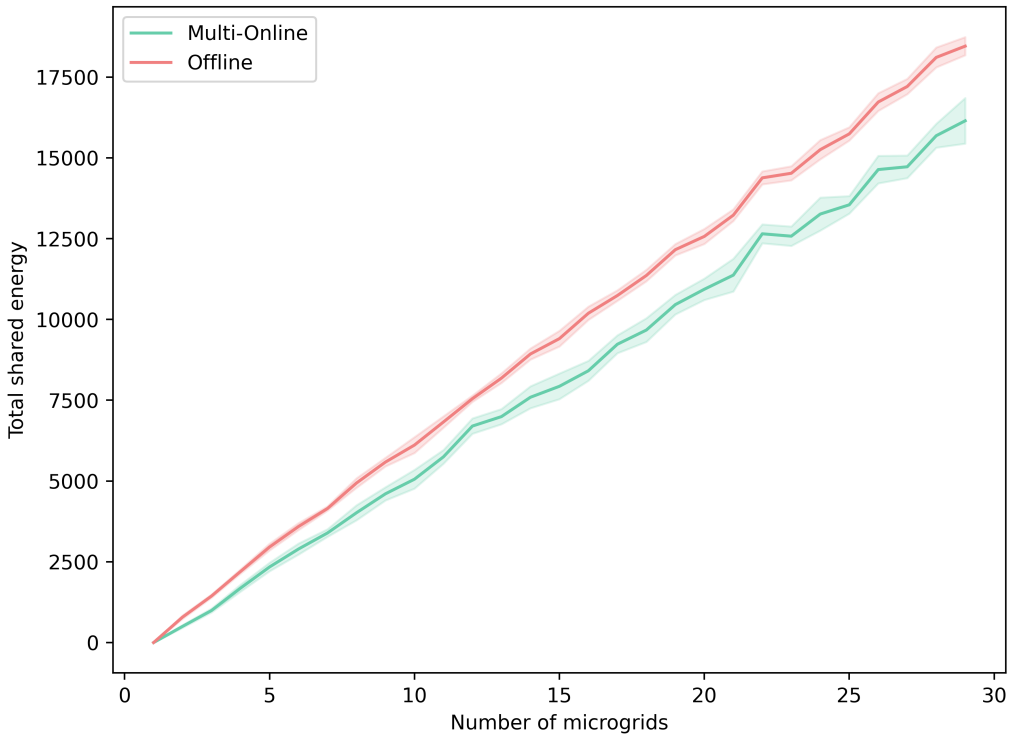

Figure 4.7: Shared energy comparison

In Figure 4.8, we've observed the behavior of 10 MGs in the system while adjusting the parameter α from 0 to 1. This exploration aims to uncover how changes in α influence the performance of the algorithms utilized. The insights gleaned from this figure shed light on how these algorithms respond to varying α values.

Remarkably, the Single-Online Algorithm remains steadfast in its behavior irrespective of changes in α. This consistency aligns with the algorithm's inherent design, where the absence of energy selling capabilities results in a consistent performance regardless of α variations.

Conversely, both the Multi-Online Algorithm and the offline algorithm display a fascinating trend of improved performance as α increases. This trend stems from these algorithms' ability to sell energy. With higher α values, the potential for selling energy grows, leading to a noticeable reduction in the total incurred cost. This observed pattern underscores a direct link between the ability to sell energy and the subsequent cost reduction, playing a pivotal role in enhancing the performance of the Multi-Online and offline algorithms.

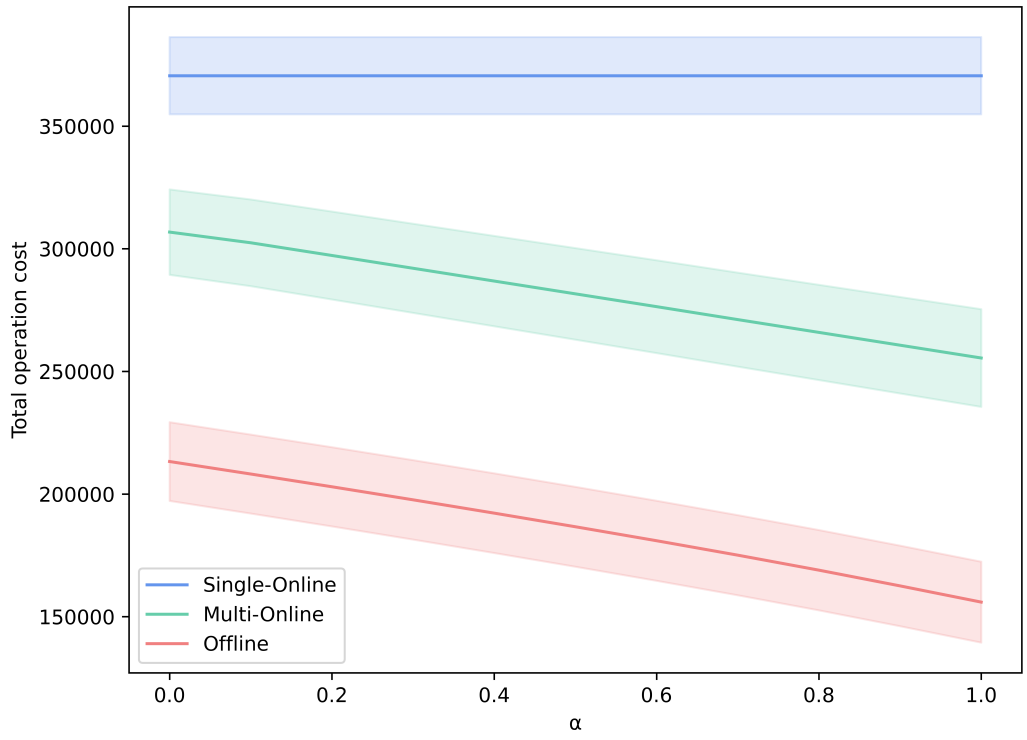

Figure 4.8: Algorithm performance comparison

In another test, we played around with the $B/\max(a)$ ratio from 1 to 20 in a 10 MG system to see how our algorithm behaves. Our algorithm always has a set limit ($\hat{B}$) for buying energy, but the offline one doesn't have this restriction. Figure 4.9 shows how the operational cost changes with different $B/\max(a)$ ratios.

Both algorithms make costs go down as the ratio goes up. But notice something interesting: the cost reduction in the Multi-Online algorithm slows down as the ratio

gets higher. This happens because buying more energy stops making sense when the microgrids already meet their needs using renewables and stored power.

On the flip side, the offline algorithm has an edge. It cleverly buys energy when prices are low and sells it at higher prices, always reducing operational costs. This smart strategy can even lead to negative costs, meaning it could make a profit. This advantage comes from the offline algorithm being able to predict and use price changes, a trick not available to real-time algorithms like the Multi-Online.

This difference highlights how the offline algorithm's savvy planning, especially with price shifts, not only cuts costs but also opens the door to potential profits.

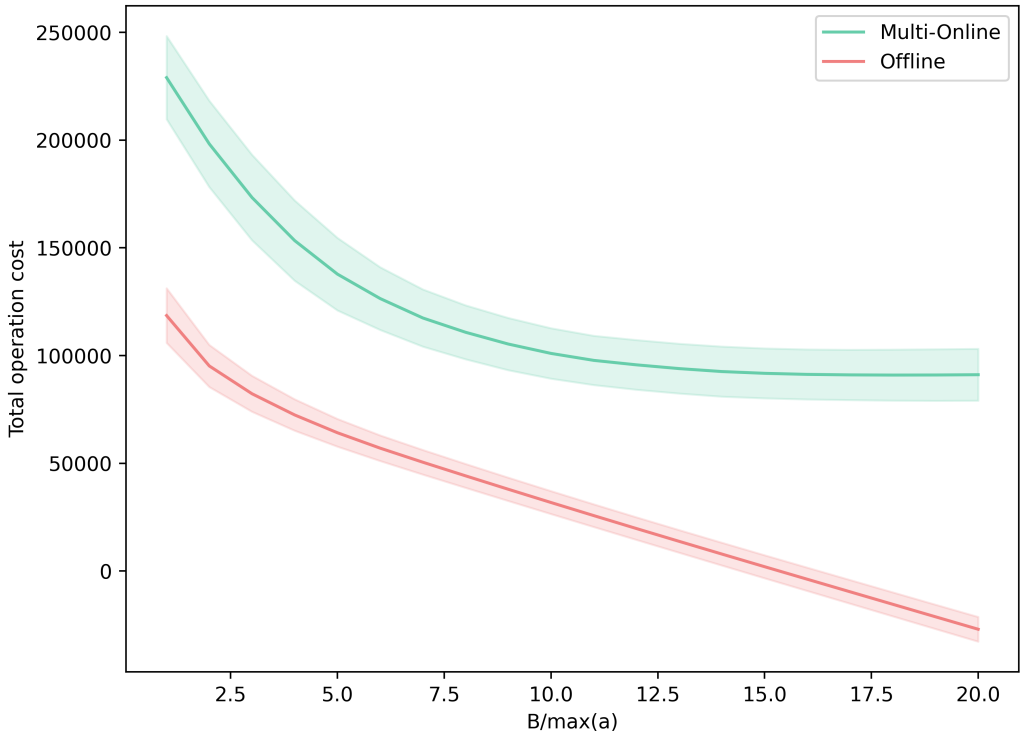

Figure 4.9: $B/\max(a)$ ratio changes impact

4.2.2 Real-World Dataset

In this section, we embarked on evaluating our model's performance using real-world datasets. These datasets encompass hourly records of both renewable energy production and demand across ten distinct locations within the USA's California province,

spanning from September 10, 2023, to September 30, 2023 [99]. Figure 4.10 visually represents these ten locations. While these locations might not conventionally be classified as microgrids, their ability to independently generate energy via RES and potential for interconnection led us to consider them as analogous to microgrids. Consequently, we employed scaled data derived from these ten locations to simulate our model's behavior. This approach allowed us to adapt and apply our model within the context of these diverse yet interrelated energy production sites.

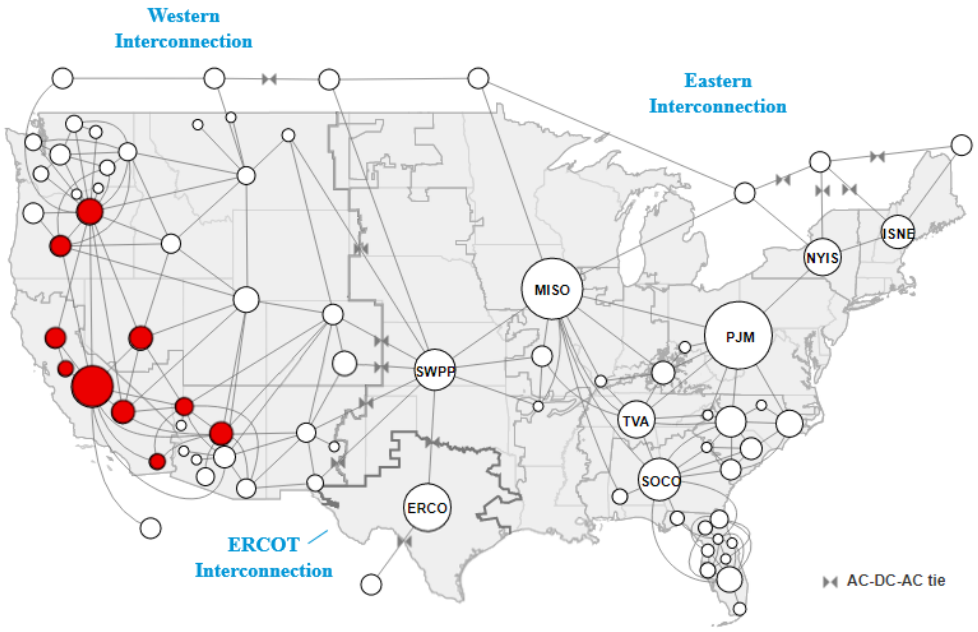

Figure 4.10: locations of the used points as the dataset

Additionally, we integrated hourly energy price data within the same time frame. This dataset originates from the UK's energy pricing policies but mirrors the pricing structures observed in California. Illustrated in Figure 4.11, this comprehensive depiction showcases the fluctuations in demand, renewable energy generation, and energy pricing over a span of 20 days. Notably, each day exhibits nearly two distinct peaks in demand, underscoring the dual high-demand periods.

Furthermore, it is pertinent to highlight the diverse sources contributing to renewable energy generation, primarily stemming from photovoltaic (PV) panels, wind turbines, or a combination of both. This variance in energy sources is reflected in the figure, where certain locations exhibit pronounced, sharp spikes in generated energy,

while others display more gradual, subtle peaks. Such fluctuations underscore the heterogeneous nature of renewable energy production across these sites, influenced by the prevailing environmental conditions and energy generation technologies in use.

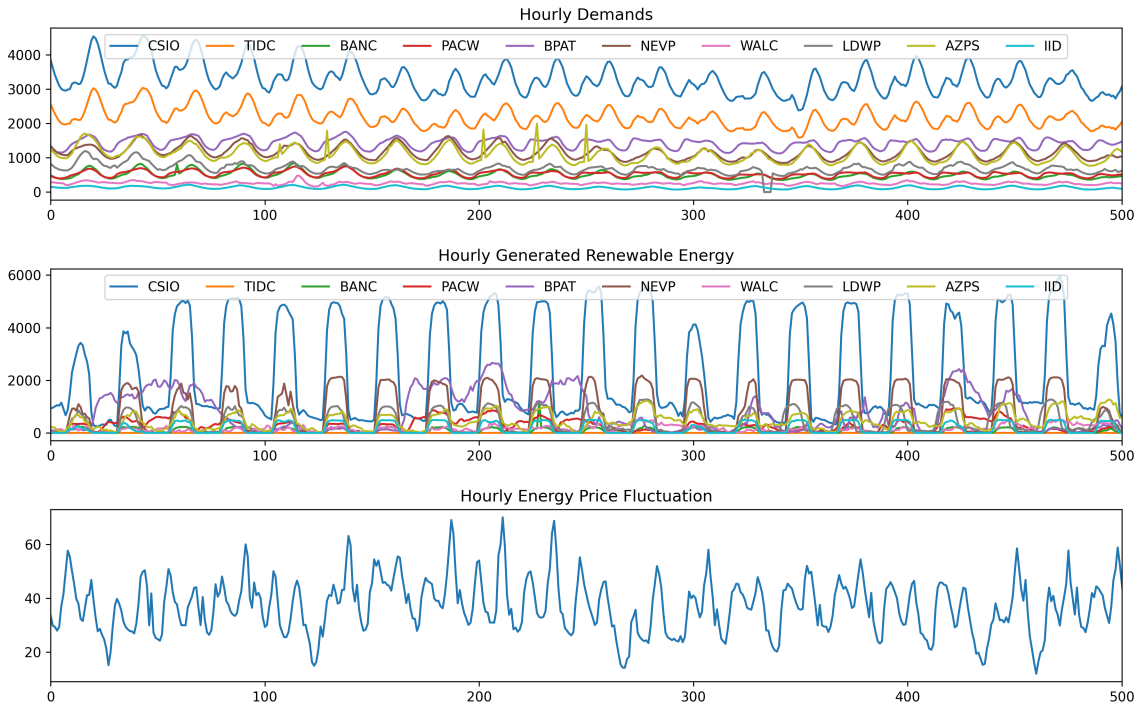

Figure 4.11: Dataset of the Hourly demand, Hourly generated RES and energy price

Our simulation highlights that our algorithm performs better than the Single-Online algorithm in terms of total cost. Notably, the simulation results reveal that our algorithm exhibits significantly lower total battery charging and discharging compared to both the Single-Online and offline algorithms. This aspect is crucial considering battery degradation, although not accounted for in this study, could pose a significant concern.

Figure 4.12 presents changes in the average State of Charge (SoC) of batteries across all 10 MGs, along with the average energy purchasing behavior of these MGs. The figure indicates that the offline algorithm aggressively manages charging and discharging, leveraging its advantage of possessing all information beforehand. This algorithm aims to profit by buying energy when the price is low and using it when the price is higher.

Moreover, the energy purchasing trends demonstrate that the Multi-Online algorithm consistently procures less energy compared to other algorithms. This occurs because in the Multi-Online algorithm, MGs collaborate, sharing surplus energy among themselves instead of solely relying on purchases from the main grid.

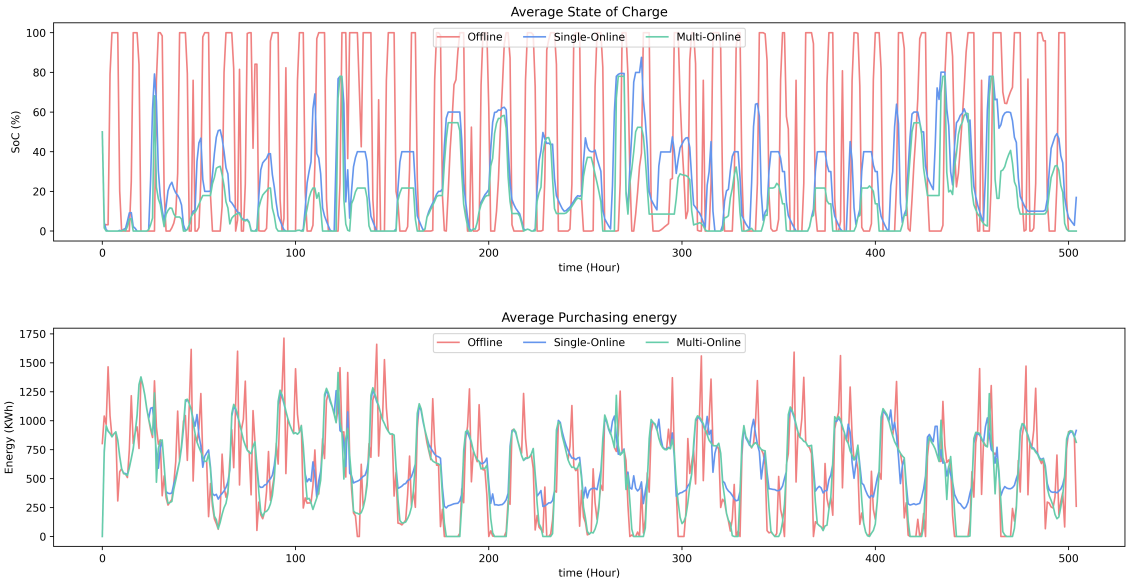

Figure 4.12: Comparison of the state of charge of ESSs and the amount of purchased energy

Moreover, Figure 4.13 provides insights into the average sharing and selling of energy across these 10 MGs. These figures hint at a notable observation: considering that the total demand consistently falls below the renewable energy generated by these MGs (refer to Figure 4.11), selling energy is not a viable option for MGs. Instead, they prioritize sharing surplus energy among themselves to collectively meet the demands of all MGs.

This figure underscores a significant point: the performance of the Multi-Online algorithm closely aligns with that of the offline algorithm. This alignment signifies the robust performance of our model, demonstrating its efficiency in managing energy sharing among MGs.

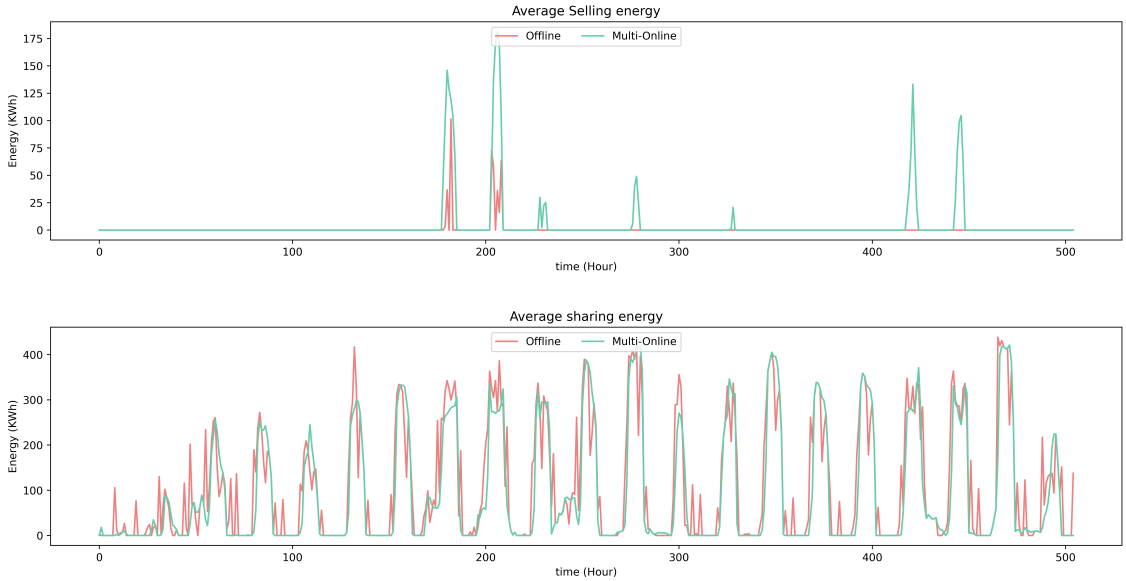

Figure 4.13: Comparison of the amount of sold and shared energy profiles

In our recent experiment, we explored how MGs would function when disconnected from the main grid. This investigation involved four distinct scenarios, each representing different average k_i values: 0.2, 0.5, 0.8, and 1. Figure 4.14 portrays the outcomes obtained from these simulations.

The findings from this figure strongly indicate that as the k value decreases, there is a noticeable reduction in the amount of purchased energy. This decline suggests that MGs face limitations in directly accessing energy from the main grid to charging their batteries. Instead, they rely more on indirect methods, likely involving energy exchanges among MGs within the network.

Moreover, the figure highlights an intriguing trend: as k decreases, the significance of energy sharing among MGs becomes more pronounced. This underscores the vital role of cooperation among these MG systems, particularly in blackout scenarios. Even without advanced future information, these systems demonstrate an impressive capability to manage and distribute energy effectively during disconnection from the main grid.

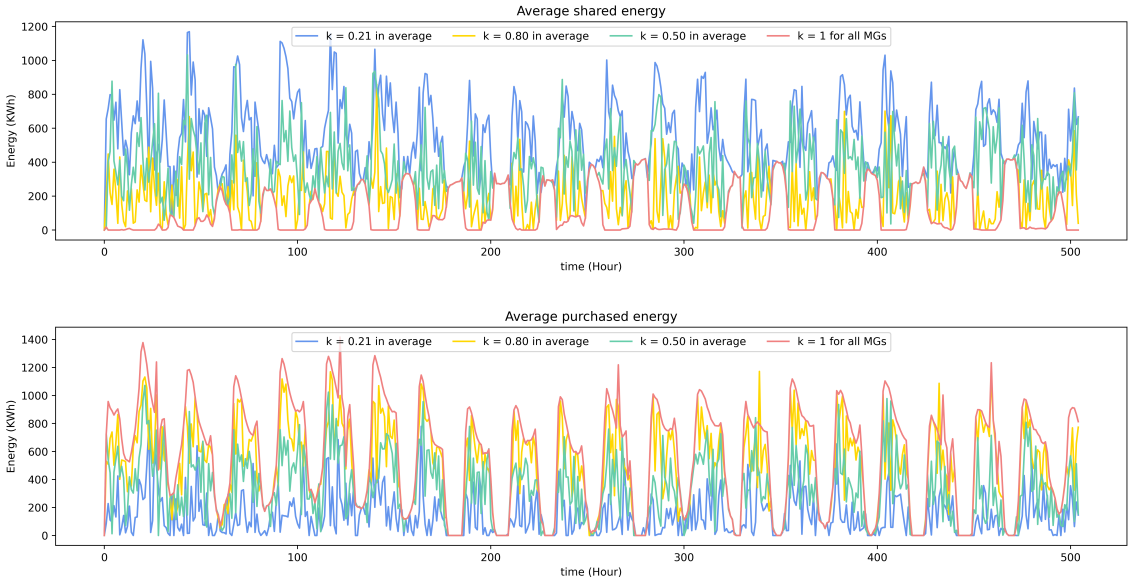

Figure 4.14: Effect of the blackout on the amount of shared and purchased energy

4.3 Discussion

This chapter's findings present an innovative approach to cooperative MG management through a threshold-based online optimization algorithm. This discussion section reflects on the implications, limitations, and potential future directions based on the results obtained.

4.3.1 Effectiveness of the Threshold-based Approach

The threshold-based online optimization technique has demonstrated notable effectiveness in managing the dynamic and unpredictable nature of energy resources within MGs. By setting predefined thresholds for energy generation and consumption, the system can make real-time decisions that optimize energy distribution and storage. This method allows for a more responsive and adaptable energy management system compared to traditional static strategies. However, the study also highlights the need for fine-tuning these thresholds based on changing grid conditions and energy demands to ensure optimal performance continually.

4.3.2 Integration with Renewable Energy Sources

A significant aspect of the study was its focus on integrating renewable energy sources into the MG management system. The algorithm's ability to accommodate the variability and unpredictability of renewable energy sources, such as solar and wind, is critical for modern energy systems that aim to be sustainable and reduce reliance on fossil fuels. Future iterations of the study could explore more sophisticated prediction models for renewable energy outputs to further enhance the algorithm's performance and reliability.

4.3.3 Implications for Energy Efficiency and Sustainability

The proposed online optimization algorithm has important implications for energy efficiency and sustainability. By optimizing the use and distribution of energy within MG, the system can reduce waste and ensure that energy production closely matches consumption patterns. This not only leads to cost savings but also contributes to the overall sustainability of the energy system by minimizing unnecessary energy generation and the associated environmental impact.

4.3.4 Limitations and Challenges

While the study's results are promising, it is important to acknowledge the limitations and challenges faced. One of the key challenges is the need for accurate and timely data to inform the optimization algorithm. Delays or inaccuracies in data can lead to suboptimal decisions and reduced system performance. Additionally, the study's scope may be limited to specific types of MGs or geographic areas, and further research is needed to validate the algorithm's applicability across various contexts and scales.

4.3.5 Future Research Directions

The study opens several avenues for future research:

1. **Dynamic Threshold Adjustment**: Investigating methods for dynamically adjusting thresholds in response to real-time data and predictive analytics could enhance the algorithm's adaptability and performance.

2. **Economic and Policy Implications**: Further research could explore the economic benefits and policy implications of widespread adoption of such online optimization algorithms in MGS, including potential incentives and regulatory frameworks.

3. **Scalability and Robustness**: Testing the algorithm's scalability and robustness across a wider range of microgrid configurations and external conditions will be important to understand its broader applicability.

4. **Advanced Forecasting Techniques**: Integrating advanced forecasting techniques for renewable energy outputs and consumer demand can improve the predictive capabilities of the system and lead to more efficient energy management.

Chapter 5

Conclusion

5.1 Research Summary and Conclusion

In the chapter 1 and 2 of this study, an iterative optimization algorithm is developed to find optimal sites for charging stations and the optimal number of charging units at each station:

1. The proposal of a comprehensive extended-graph-based formulation to capture the composite EVs' behavior in transportation and power networks enables the optimization of infrastructure investment costs and service quality simultaneously.

2. The proposed iterative algorithm comprises three stages and can effectively address the optimization requirements from both the planner and customer sides. The algorithm calculates the optimal locations of charging stations, the number of charging units at each station, and examines the maximum waiting time obtained to ensure customer satisfaction.

3. Important factors, such as driving range, SoC, and waiting time, are investigated in the case study based on a 25-node transportation network integrated with IEEE 33-bus system. The numerical results demonstrate that both the availability of home charging and the driving range play important roles in investment cost (positive correlation), while a higher charging rate can greatly improve the service quality within a limited waiting time.

Overall, the work contributes to addressing the critical question of the optimal

deployment of EV charging stations in power-traffic coupled networks and provides an efficient algorithmic solution to this problem.

Additionally, in chapter 3, we introduced and scrutinized an online algorithm tailored for multiple cooperative microgrids aimed at effectively sharing energy to meet collective demands. Our approach comprehensively accounted for various uncertainties inherent in microgrid energy management: the fluctuations in energy demand, renewable energy generation, electricity pricing, and the occurrence of blackouts.

Furthermore, we devised a threshold-based algorithm with two optimal thresholds, mathematically substantiating their optimality within our proposed framework. Furthermore, we extensively assessed our model's performance across diverse scenarios, comparing it against both the offline algorithm and individual non-collaborative microgrids. Our evaluation encompassed two distinct case studies: one generated randomly and the other derived from real-world data.

The outcomes derived from our simulations unequivocally showcase the superior performance of our model compared to non-collaborative microgrids, often approaching optimality across various scenarios. These findings underscore the efficacy of our approach in fostering collaboration among microgrids, paving the way for efficient and robust energy management systems.

5.2 Research Contributions

1. Graph-Based Formulation Extension: Our study employs a novel graph algebraic algorithm to enhance traffic network graphs. Unlike traditional expanding graph methods, our approach introduces theoretical advancements outlined in Theorem 2-4. These advancements effectively reduce the size of the expanded graph. Additionally, we devise an algorithm utilizing this reduced-size expanded graph, enabling the computation of shortest paths between any node pair with significantly lower computational burden compared to the Dijkstra algorithm.

2. Holistic Optimization: Existing methods, as depicted in Table I, often overlook four critical factors in the identification and sizing of charging stations: the power-traffic coupled network, traffic flow demand, power-flow demand, and user behavior. To bridge this gap, we integrate all four factors into our problem

formulation, resulting in a more comprehensive and challenging problem to solve. To address this complexity, we propose a three-stage iterative algorithm. [1]

3. Efficient Computational Framework: Within the first and second stages of our iterative algorithm, we optimize the process by relaxing specific constraints. Our engineering-driven methodology merges branch and bound with interior methods, yielding nearly optimal solutions. This approach significantly reduces algorithmic complexity, consequently minimizing overall running time.

4. Addressing Microgrid Uncertainties: This study delves into various uncertainties impacting microgrids. Its objective is to fortify microgrids, enhancing their reliability by effectively managing these uncertainties.

5. P2P Energy Trading Analysis: We explore the scenario of peer-to-peer energy trading and introduce an innovative online algorithm. Additionally, we provide theoretical evidence demonstrating the assured performance of this algorithm.

6. Real-World Validation: Utilizing authentic data in our analysis, we demonstrate the superior performance of our algorithm compared to existing online algorithms. Remarkably, even in scenarios without system blackouts, our findings showcase the algorithm's effectiveness.

5.3 Future Works

In our study, we acknowledge certain limiting assumptions and commit to addressing them in future research endeavors. One such assumption involves our reliance on prior knowledge of EV travel time and an assumption that all EVs require a full battery charge. However, these factors are often unknown and uncertain in practical settings, potentially not aligning with real-life scenarios. To confront this challenge, we propose the utilization of a stochastic online optimization framework. This framework aims to incorporate uncertainties associated with EV travel time and power

[1] While iterative algorithms are not new in literature, our approach introduces unique value. In the third stage, we derive a new set of constraints. These constraints refine the optimization variables from stage one in subsequent implementations, alongside simplifying certain constraints to expedite our iterative algorithm.

demand. Additionally, exploring the interplay between user behavior and the siting and sizing of charging stations presents an intriguing and crucial aspect. We aspire for our work to serve as an initial step, paving the way for investigations into such coupled problems.

Another prospective avenue involves leveraging predictions to enhance performance, specifically within the realm of learning augmented algorithms. Typically, a learning augmented algorithm operates on an input ($\mathcal{I}$,$\mathcal{A}$), where $\mathcal{I}$ represents a problem instance, and $\mathcal{A}$ denotes advice—a prediction concerning a specific property of the optimal solution. The nature of the problem instance and prediction varies based on the algorithm. Such algorithms typically adhere to two key properties, Consistency and Robustness. Consistency in learning augmented algorithms is demonstrated when accurate predictions align with well-performing models, while robustness ensures bounded worst-case performance, even in scenarios with inaccurate predictions [100].

Bibliography

[1] Z. Ma, D. S. Callaway, and I. A. Hiskens, "Decentralized charging control of large populations of plug-in electric vehicles," *IEEE Transactions on control systems technology*, vol. 21, no. 1, pp. 67–78, 2011.

[2] O. Van Vliet, A. S. Brouwer, T. Kuramochi, M. van Den Broek, and A. Faaij, "Energy use, cost and CO_2 emissions of electric cars," *Journal of power sources*, vol. 196, no. 4, pp. 2298–2310, 2011.

[3] M. Kchaou-Boujelben, "Charging station location problem: A comprehensive review on models and solution approaches," *Transportation Research Part C: Emerging Technologies*, vol. 132, p. 103 376, 2021.

[4] F. Zinnari, S. Strada, M. Tanelli, S. Formentin, and S. M. Savaresi, "Electrification potential of fuel-based vehicles and optimal placing of charging infrastructure: A large-scale vehicle-telematics approach," *IEEE Transactions on Transportation Electrification*, vol. 8, no. 1, pp. 466–479, 2021.

[5] M. Kuby and S. Lim, "The flow-refueling location problem for alternative-fuel vehicles," *Socio-Economic Planning Sciences*, vol. 39, no. 2, pp. 125–145, 2005.

[6] H. Zhang, S. J. Moura, Z. Hu, and Y. Song, "PEV fast-charging station siting and sizing on coupled transportation and power networks," *IEEE Transactions on Smart Grid*, vol. 9, no. 4, pp. 2595–2605, 2016.

[7] S. MirHassani and R. Ebrazi, "A flexible reformulation of the refueling station location problem," *Transportation Science*, vol. 47, no. 4, pp. 617–628, 2013.

[8] H. Parastvand, V. Moghaddam, O. Bass, M. A. Masoum, A. Chapman, and S. Lachowicz, "A graph automorphic approach for placement and sizing of charging stations in ev network considering traffic," *IEEE Transactions on Smart Grid*, vol. 11, no. 5, pp. 4190–4200, 2020.

[9] M. H. Moradi, M. Abedini, S. R. Tousi, and S. M. Hosseinian, "Optimal siting and sizing of renewable energy sources and charging stations simultaneously based on differential evolution algorithm," *International Journal of Electrical Power & Energy Systems*, vol. 73, pp. 1015–1024, 2015.

[10] A. Zeinalzadeh, Y. Mohammadi, and M. H. Moradi, "Optimal multi objective placement and sizing of multiple DGs and shunt capacitor banks simultaneously considering load uncertainty via mopso approach," *International Journal of Electrical Power & Energy Systems*, vol. 67, pp. 336–349, 2015.

[11] X. Wang, M. Shahidehpour, C. Jiang, and Z. Li, "Coordinated planning strategy for electric vehicle charging stations and coupled traffic-electric networks," *IEEE Transactions on Power Systems*, vol. 34, no. 1, pp. 268–279, 2018.

[12] D. Hu, J. Zhang, and Z.-W. Liu, "Charging stations expansion planning under government policy driven based on bayesian regularization backpropagation learning," *Neurocomputing*, vol. 416, pp. 47–58, 2020.

[13] Y.-W. Wang and C.-C. Lin, "Locating road-vehicle refueling stations," *Transportation Research Part E: Logistics and Transportation Review*, vol. 45, no. 5, pp. 821–829, 2009.

[14] X. Gan, H. Zhang, G. Hang, Z. Qin, and H. Jin, "Fast-charging station deployment considering elastic demand," *IEEE Transactions on Transportation Electrification*, vol. 6, no. 1, pp. 158–169, 2020.

[15] B. Zhou, G. Chen, T. Huang, Q. Song, and Y. Yuan, "Planning pev fast-charging stations using data-driven distributionally robust optimization approach based on ϕ-divergence," *IEEE Transactions on Transportation Electrification*, vol. 6, no. 1, pp. 170–180, 2020.

[16] N. Wang, C. Wang, Y. Niu, M. Yang, and Y. Yu, "A two-stage charging facilities planning method for electric vehicle sharing systems," *IEEE Transactions on Industry Applications*, vol. 57, no. 1, pp. 149–157, 2020.

[17] D. Mao, J. Tan, and J. Wang, "Location planning of pev fast charging station: An integrated approach under traffic and power grid requirements," *IEEE Transactions on Intelligent Transportation Systems*, vol. 22, no. 1, pp. 483–492, 2020.

[18] T.-Y. Zhang, Y. Yang, Y.-T. Zhu, E.-J. Yao, and K.-Q. Wu, "Deploying public charging stations for battery electric vehicles on the expressway network based on dynamic charging demand," *IEEE Transactions on Transportation Electrification*, vol. 8, no. 2, pp. 2531–2548, 2022.

[19] A. Mirheli and L. Hajibabai, "Hierarchical optimization of charging infrastructure design and facility utilization," *IEEE Transactions on Intelligent Transportation Systems*, vol. 23, no. 9, pp. 15 574–15 587, 2022.

[20] T. Wu, X. Wei, X. Zhang, G. Wang, J. Qiu, and S. Xia, "Carbon-oriented expansion planning of integrated electricity-natural gas systems with ev fast-charging stations," *IEEE Transactions on Transportation Electrification*, vol. 8, no. 2, pp. 2797–2809, 2022.

[21] A. Fathollahi, S. Y. Derakhshandeh, A. Ghiasian, and M. A. Masoum, "Optimal siting and sizing of wireless ev charging infrastructures considering traffic network and power distribution system," *IEEE Access*, vol. 10, pp. 117 105–117 117, 2022.

[22] Y. Li *et al.*, "Coupled multinetwork constrained planning of energy supplying facilities for hybrid hydrogen-electric vehicles," *IEEE Transactions on Industry Applications*, vol. 58, no. 2, pp. 2848–2862, 2021.

[23] M. Zhang, S. Lou, Y. Wu, Y. Wang, and R. Chen, "Research on charging station planning method considering electric vehicle charging queuing," in *2022 IEEE 3rd China International Youth Conference on Electrical Engineering (CIYCEE)*, IEEE, 2022, pp. 1–5.

[24] L. Kong, H. Zhang, W. Li, H. Bai, and N. Dai, "Spatial-temporal scheduling of electric bus fleet in power-transportation coupled network," *IEEE Transactions on Transportation Electrification*, 2022 (Early Access).

[25] A. Ali, M. F. Shaaban, A. S. Awad, M. A. Azzouz, M. Lehtonen, and K. Mahmoud, "Multi-objective allocation of ev charging stations and ress in distribution systems considering advanced control schemes," *IEEE Transactions on Vehicular Technology*, vol. 72, no. 3, pp. 3146–3160, 2022.

[26] S. Schoenberg, D. S. Buse, and F. Dressler, "Siting and sizing charging infrastructure for electric vehicles with coordinated recharging," *IEEE Transactions on Intelligent Vehicles*, vol. 8, no. 2, pp. 1425–1438, 2022.

[27] J. D. Peper, J. Schmeing, and U. Häger, "Spatio-temporal electric vehicle charging optimization considering distribution grid constraints and flexible electricity prices," in *2023 19th International Conference on the European Energy Market (EEM)*, IEEE, 2023, pp. 1–6.

[28] C. Shao, K. Li, X. Li, Z. Hu, M. Shahidehpour, and X. Wang, "A decentralized bi-level decomposition method for optimal operation of electric vehicles in coupled urban transportation and power distribution systems," *IEEE Transactions on Transportation Electrification*, 2023 (Early Access).

[29] G. Ferro, R. Minciardi, L. Parodi, and M. Robba, "Optimal location and line assignment for electric bus charging stations," *IEEE Systems Journal*, 2023.

[30] A. Castillo, "Risk analysis and management in power outage and restoration: A literature survey," *Electric Power Systems Research*, vol. 107, pp. 9–15, 2014.

[31] K. H. LaCommare and J. H. Eto, "Understanding the cost of power interruptions to us electricity consumers," Lawrence Berkeley National Lab.(LBNL), Berkeley, CA (United States), Tech. Rep., 2004.

[32] G. Rouse and J. Kelly, "Electricity reliability: Problems, progress, and policy solutions," *Galvin electricity initiative*, vol. 28, pp. 17–20, 2011.

[33] P. Hines, J. Apt, and S. Talukdar, "Large blackouts in north america: Historical trends and policy implications," *Energy Policy*, vol. 37, no. 12, pp. 5249–5259, 2009.

[34] D. Gibb *et al.*, "Renewables 2022 global status report+ renewable energy data in perspective+ press releases+ regional fact sheets+ country fact sheets," 2022.

[35] N. Reyseliani and W. W. Purwanto, "Pathway towards 100% renewable energy in indonesia power system by 2050," *Renewable Energy*, vol. 176, pp. 305–321, 2021.

[36] M. Ram, J. C. Osorio-Aravena, A. Aghahosseini, D. Bogdanov, and C. Breyer, "Job creation during a climate compliant global energy transition across the power, heat, transport, and desalination sectors by 2050," *Energy*, vol. 238, p. 121 690, 2022.

[37] L. Al-Ghussain, A. M. Abubaker, and A. D. Ahmad, "Superposition of renewable-energy supply from multiple sites maximizes demand-matching: Towards 100% renewable grids in 2050," *Applied Energy*, vol. 284, p. 116 402, 2021.

[38] B. Lasseter, "Microgrids [distributed power generation]," in *2001 IEEE power engineering society winter meeting. Conference proceedings (Cat. No. 01CH37194)*, IEEE, vol. 1, 2001, pp. 146–149.

[39] R. H. Lasseter, "Microgrids," in *2002 IEEE power engineering society winter meeting. Conference proceedings (Cat. No. 02CH37309)*, IEEE, vol. 1, 2002, pp. 305–308.

[40] D. Savio Abraham *et al.*, "Electric vehicles charging stations' architectures, criteria, power converters, and control strategies in microgrids," *Electronics*, vol. 10, no. 16, p. 1895, 2021.

[41] D. E. Olivares *et al.*, "Trends in microgrid control," *IEEE Transactions on smart grid*, vol. 5, no. 4, pp. 1905–1919, 2014.

[42] H. Karimi, H. Nikkhajoei, and R. Iravani, "Control of an electronically-coupled distributed resource unit subsequent to an islanding event," *IEEE Transactions on Power Delivery*, vol. 23, no. 1, pp. 493–501, 2007.

[43] F. Katiraei, M. R. Iravani, and P. W. Lehn, "Micro-grid autonomous operation during and subsequent to islanding process," *IEEE Transactions on power delivery*, vol. 20, no. 1, pp. 248–257, 2005.

[44] Y. R. Li, F. Nejabatkhah, and H. Tian, *Smart Hybrid AC/DC Microgrids: Power Management, Energy Management, and Power Quality Control*. John Wiley & Sons, 2022.

[45] Z. Jiang and X. Yu, "Hybrid dc-and ac-linked microgrids: Towards integration of distributed energy resources," in *2008 IEEE Energy 2030 Conference*, IEEE, 2008, pp. 1–8.

[46] E. Unamuno and J. A. Barrena, "Hybrid ac/dc microgrids—part i: Review and classification of topologies," *Renewable and Sustainable Energy Reviews*, vol. 52, pp. 1251–1259, 2015.

[47] E. A. Soto, L. B. Bosman, E. Wollega, and W. D. Leon-Salas, "Peer-to-peer energy trading: A review of the literature," *Applied Energy*, vol. 283, p. 116 268, 2021.

[48] D. Gregoratti and J. Matamoros, "Distributed energy trading: The multiple-microgrid case," *iEEE Transactions on industrial Electronics*, vol. 62, no. 4, pp. 2551–2559, 2014.

[49] N. Liu, J. Wang, and L. Wang, "Distributed energy management for interconnected operation of combined heat and power-based microgrids with demand response," *Journal of Modern Power Systems and Clean Energy*, vol. 5, no. 3, pp. 478–488, 2017.

[50] Y. Zhou, S. Ci, H. Li, and Y. Yang, "A new framework for peer-to-peer energy sharing and coordination in the energy internet," in *2017 IEEE International Conference on Communications (ICC)*, IEEE, 2017, pp. 1–6.

[51] G. Ma, J. Li, and X.-P. Zhang, "A review on optimal energy management of multimicrogrid system considering uncertainties," *IEEE Access*, vol. 10, pp. 77 081–77 098, 2022.

[52] S. Motahhir, A. El Hammoumi, and A. El Ghzizal, "The most used mppt algorithms: Review and the suitable low-cost embedded board for each algorithm," *Journal of cleaner production*, vol. 246, p. 118 983, 2020.

[53] F. Hafiz, M. Awal, A. R. de Queiroz, and I. Husain, "Real-time stochastic optimization of energy storage management using deep learning-based forecasts for residential pv applications," *IEEE Transactions on Industry Applications*, vol. 56, no. 3, pp. 2216–2226, 2020.

[54] P. Zeng, H. Li, H. He, and S. Li, "Dynamic energy management of a microgrid using approximate dynamic programming and deep recurrent neural network learning," *IEEE Transactions on Smart Grid*, vol. 10, no. 4, pp. 4435–4445, 2018.

[55] W. Su, J. Wang, and J. Roh, "Stochastic energy scheduling in microgrids with intermittent renewable energy resources," *IEEE Transactions on Smart grid*, vol. 5, no. 4, pp. 1876–1883, 2013.

[56] Z. Lyu, L. Zheng, and X. Yang, "Dual-layer optimized grid-connected operation strategy of electro-thermal multi-microgrid system considering the uncertainty of renewable energy sources," *Journal of Renewable and Sustainable Energy*, vol. 13, no. 6, 2021.

[57] X. Hu and T. Liu, "Co-optimisation for distribution networks with multi-microgrids based on a two-stage optimisation model with dynamic electricity pricing," *IET Generation, Transmission & Distribution*, vol. 11, no. 9, pp. 2251–2259, 2017.

[58] J. Yang and C. Su, "Robust optimization of microgrid based on renewable distributed power generation and load demand uncertainty," *Energy*, vol. 223, p. 120 043, 2021.

[59] H. Robbins and S. Monro, "A stochastic approximation method," *The annals of mathematical statistics*, pp. 400–407, 1951.

[60] B. Tan, H. Chen, X. Zheng, and J. Huang, "Two-stage robust optimization dispatch for multiple microgrids with electric vehicle loads based on a novel data-driven uncertainty set," *International Journal of Electrical Power & Energy Systems*, vol. 134, p. 107 359, 2022.

[61] G. Zhu, J. Lin, Z. Luo, S. Dai, L. Qin, C. Liu, *et al.*, "Review of robust optimization for generation scheduling in power systems," 2017.

[62] A. Hussain, V.-H. Bui, and H.-M. Kim, "Robust optimization-based scheduling of multi-microgrids considering uncertainties," *Energies*, vol. 9, no. 4, p. 278, 2016.

[63] H. Qiu, B. Zhao, W. Gu, and R. Bo, "Bi-level two-stage robust optimal scheduling for ac/dc hybrid multi-microgrids," *IEEE Transactions on Smart Grid*, vol. 9, no. 5, pp. 5455–5466, 2018.

[64] I. Gomes, R. Melicio, and V. Mendes, "A novel microgrid support management system based on stochastic mixed-integer linear programming," *Energy*, vol. 223, p. 120 030, 2021.

[65] W. Wei, F. Liu, and S. Mei, "Distributionally robust co-optimization of energy and reserve dispatch," *IEEE Transactions on Sustainable Energy*, vol. 7, no. 1, pp. 289–300, 2015.

[66] W. Huang, W. Zheng, and D. J. Hill, "Distributionally robust optimal power flow in multi-microgrids with decomposition and guaranteed convergence," *IEEE Transactions on Smart Grid*, vol. 12, no. 1, pp. 43–55, 2020.

[67] F. Alismail, P. Xiong, and C. Singh, "Optimal wind farm allocation in multi-area power systems using distributionally robust optimization approach," *IEEE Transactions on Power Systems*, vol. 33, no. 1, pp. 536–544, 2017.

[68] Y. Zhang, F. Meng, R. Wang, B. Kazemtabrizi, and J. Shi, "Uncertainty-resistant stochastic mpc approach for optimal operation of chp microgrid," *Energy*, vol. 179, pp. 1265–1278, 2019.

[69] B. Zhang *et al.*, "Dynamic energy conversion and management strategy for an integrated electricity and natural gas system with renewable energy: Deep reinforcement learning approach," *Energy conversion and management*, vol. 220, p. 113 063, 2020.

[70] L. Wen, K. Zhou, J. Li, and S. Wang, "Modified deep learning and reinforcement learning for an incentive-based demand response model," *Energy*, vol. 205, p. 118 019, 2020.

[71] C. Guo, X. Wang, Y. Zheng, and F. Zhang, "Real-time optimal energy management of microgrid with uncertainties based on deep reinforcement learning," *Energy*, vol. 238, p. 121 873, 2022.

[72] Y. Zhang, T. Zhang, R. Wang, Y. Liu, and B. Guo, "Optimal operation of a smart residential microgrid based on model predictive control by considering uncertainties and storage impacts," *Solar Energy*, vol. 122, pp. 1052–1065, 2015.

[73] Y. Zheng, S. Li, and R. Tan, "Distributed model predictive control for on-connected microgrid power management," *IEEE Transactions on Control Systems Technology*, vol. 26, no. 3, pp. 1028–1039, 2017.

[74] S. R. Cominesi, M. Farina, L. Giulioni, B. Picasso, and R. Scattolini, "A two-layer stochastic model predictive control scheme for microgrids," *IEEE Transactions on Control Systems Technology*, vol. 26, no. 1, pp. 1–13, 2017.

[75] M.-C. Hu, S.-Y. Lu, and Y.-H. Chen, "Stochastic programming and market equilibrium analysis of microgrids energy management systems," *Energy*, vol. 113, pp. 662–670, 2016.

[76] M. Elkazaz, M. Sumner, and D. Thomas, "Energy management system for hybrid pv-wind-battery microgrid using convex programming, model predictive and rolling horizon predictive control with experimental validation," *International Journal of Electrical Power & Energy Systems*, vol. 115, p. 105 483, 2020.

[77] E. Kuznetsova, C. Ruiz, Y.-F. Li, and E. Zio, "Analysis of robust optimization for decentralized microgrid energy management under uncertainty," *International Journal of Electrical Power & Energy Systems*, vol. 64, pp. 815–832, 2015.

[78] H. Zhang, D. Yue, and X. Xie, "Robust optimization for dynamic economic dispatch under wind power uncertainty with different levels of uncertainty budget," *IEEE Access*, vol. 4, pp. 7633–7644, 2016.

[79] S. Babaei, R. Jiang, and C. Zhao, "Distributionally robust distribution network configuration under random contingency," *IEEE Transactions on Power Systems*, vol. 35, no. 5, pp. 3332–3341, 2020.

[80] A. Arab, A. Khodaei, S. K. Khator, K. Ding, V. A. Emesih, and Z. Han, "Stochastic pre-hurricane restoration planning for electric power systems infrastructure," *IEEE Transactions on Smart Grid*, vol. 6, no. 2, pp. 1046–1054, 2015.

[81] T. H. Cormen, C. E. Leiserson, R. L. Rivest, and C. Stein, *Introduction to algorithms*. MIT press, 2022.

[82] B. Zhang and D. Qiu, *Sneak circuits of power electronic converters*. John wiley & sons, 2015.

[83] G. Wang, Z. Xu, F. Wen, and K. P. Wong, "Traffic-constrained multiobjective planning of electric-vehicle charging stations," *IEEE Transactions on Power Delivery*, vol. 28, no. 4, pp. 2363–2372, 2013.

[84] L. F. Grisales-Noreña, D. Gonzalez Montoya, and C. A. Ramos-Paja, "Optimal sizing and location of distributed generators based on PBIL and PSO techniques," *Energies*, vol. 11, no. 4, p. 1018, 2018.

[85] J. J. Grainger and W. D. Stevenson, *Power Systems: Analysis and Design*. McGraw-Hill, 1994.

[86] A Khorsandi, S. Hosseinian, and A Ghazanfari, "Modified artificial bee colony algorithm based on fuzzy multi-objective technique for optimal power flow problem," *Electric Power Systems Research*, vol. 95, pp. 206–213, 2013.

[87] Y. Li, J. Kuprat, Y. Li, and M. Liserre, "Graph-theory-based derivation, modeling, and control of power converter systems," *IEEE journal of emerging and selected topics in power electronics*, vol. 10, no. 6, pp. 6557–6571, 2022.

[88] Y. Zhang, S. Ren, Z. Y. Dong, Y. Xu, K. Meng, and Y. Zheng, "Optimal placement of battery energy storage in distribution networks considering conservation voltage reduction and stochastic load composition," *IET Generation, Transmission & Distribution*, vol. 11, no. 15, pp. 3862–3870, 2017.

[89] R. A. Jabr, "Radial distribution load flow using conic programming," *IEEE transactions on power systems*, vol. 21, no. 3, pp. 1458–1459, 2006.

[90] V. Vita, "Development of a decision-making algorithm for the optimum size and placement of distributed generation units in distribution networks," *Energies*, vol. 10, no. 9, p. 1433, 2017.

[91] F. M. Andersen, H. K. Jacobsen, and P. A. Gunkel, "Hourly charging profiles for electric vehicles and their effect on the aggregated consumption profile in denmark," *International Journal of Electrical Power & Energy Systems*, vol. 130, p. 106 900, 2021.

[92] B. Vaidya and H. T. Mouftah, "Smart electric vehicle charging management for smart cities," *IET Smart Cities*, vol. 2, no. 1, pp. 4–13, 2020.

[93] Bloomberg, *EV highway range: This data might surprise you*, Accessed on March 27, 2023, 2023. [Online]. Available: https://www.bloomberg.com/news/articles/2023-03-01/ev-highway-range-this-data-might-surprise-you.

[94] S. C.-K. Chau, J. Xu, W. Bow, and K. Elbassioni, "Peer-to-peer energy sharing: Effective cost-sharing mechanisms and social efficiency," in *Proceedings of the Tenth ACM International Conference on Future Energy Systems*, 2019, pp. 215–225.

[95] C.-K. Chau, G. Zhang, and M. Chen, "Cost minimizing online algorithms for energy storage management with worst-case guarantee," *IEEE Transactions on Smart Grid*, vol. 7, no. 6, pp. 2691–2702, 2016.

[96] A. Borodin and R. El-Yaniv, *Online computation and competitive analysis*. cambridge university press, 2005.

[97] R. El-Yaniv, A. Fiat, R. M. Karp, and G. Turpin, "Optimal search and one-way trading online algorithms," *Algorithmica*, vol. 30, pp. 101–139, 2001.

[98] R. Urgaonkar, B. Urgaonkar, M. J. Neely, and A. Sivasubramaniam, "Optimal power cost management using stored energy in data centers," in *Proceedings of the ACM SIGMETRICS joint international conference on Measurement and modeling of computer systems*, 2011, pp. 221–232.

[99] *Electricity grid monitor*, Accessed on Nov 2023, U.S. Energy Information Administration. [Online]. Available: https://www.eia.gov/electricity/gridmonitor/dashboard/custom/pending.

[100] M. Mitzenmacher and S. Vassilvitskii, "Algorithms with predictions," *Communications of the ACM*, vol. 65, no. 7, pp. 33–35, 2022.

Appendix A: Proof of Theorem 5

Theorem 7 *Let $\hat{B}_i = B(1-k_i\rho_i)$ for all $i \in \mathcal{I}$ with the terminal condition of $E_i(T) = B$ for all $i \in \mathcal{I}$ and the assumption that $M\beta \geq \frac{\eta_d}{\eta_c}\alpha m$, the competitive ratio of Algorithm 2 is*

$$CR = \max_i \max \Bigg\{ \frac{\theta_i^1 \frac{\eta_d}{\eta_c}(1-k_i\rho_i) + k_i\rho_i(M\beta - \alpha\frac{\eta_d}{\eta_c}m)(1-\rho_i) - (\rho_i - k_i\rho_i)\frac{\eta_d}{\eta_c}\alpha m}{m(1-\rho_i)}, \tag{A.1}$$

$$\frac{\theta_i^1 \frac{\eta_d}{\eta_c}\rho_i(1-k_i\rho_i) + (M\beta - \alpha k_i\rho_i\frac{\eta_d}{\eta_c}m)(1-\rho_i) - (\rho_i - k_i\rho_i)\frac{\eta_d}{\eta_c}\alpha m}{\theta_i^1 \frac{\eta_d}{\eta_c}(1-\rho_i)}, \tag{A.2}$$

$$\frac{\theta_i^2 \frac{\eta_d}{\eta_c}(1-k_i\rho_i) + k_i\rho_i(M\beta - \alpha\frac{\eta_d}{\eta_c}m) - (\rho_i - k_i\rho_i)\frac{\eta_d}{\eta_c}\alpha m}{(1-\alpha\rho_i\frac{\eta_d}{\eta_c})m}, \tag{A.3}$$

$$\frac{M\beta - \alpha k_i\rho_i\frac{\eta_d}{\eta_c}m - (\rho_i - k_i\rho_i)\frac{\eta_d}{\eta_c}\alpha m}{\theta_i^2\frac{\eta_d}{\eta_c} - \rho_i\alpha\frac{\eta_d}{\eta_c}m} \Bigg\} \tag{A.4}$$

where θ_i^1 is the answer of equality of equations A.1 and A.2, and θ_i^2 is the answer of equality of equations A.3 and A.4. Also, θ is the maximizer of CR.

Proof. Demand sequence a_t indexed by $t = 1$ to T is referred to as a one-shot demand when there exists a solitary time slot t_{nz} within the range of 1 to T such that:

$$a_t = \begin{cases} 0 & \text{if } t \neq t_{nz} \\ \bar{a} & \text{if } t = t_{nz} \end{cases}$$

Utilizing the decomposition of one-shot demands, as discussed in [95], offers an alternative to the demand profile. Considering our scenario involving multiple MGs, the introduced one-shot decomposition here deviates slightly from the definition in the referenced literature. It is formally expressed as:

$$\textbf{1sDecompose}\left[\left((a_i(t))_{t=1}^{T}\right)_{i=1}^{I}\right] = \left((t_s^n, t_{nz}^n, \bar{a}_i^n)_{n=1}^{N_i}\right)_{i=1}^{I}$$

In this formulation, N_i signifies the count of decomposed one-shot demands for MG i. The variable t_{nz}^n denotes the time slot of the non-zero demand, while $\bar{a}_i^n$ represents the peak demand for the n-th one-shot demand. Additionally, t_s^n ($\leq t_{nz}^n$) stands for the minimum starting time slot for the n-th one-shot demand. The decomposition adheres to the following constraints:

1. Reconstruction of $a_i(t)$ using the one-shot demands is given by:

$$a_i(t) = \sum_{n:t_{nz}^n = t} \bar{a}_i^n \quad \forall t \in \mathcal{T}$$

2. There exists a non-decreasing order between starting time slots and non-zero demand time slots:

$$t_s^n \leq t_s^{n+1} \quad \text{and} \quad t_{nz}^n \leq t_{nz}^{n+1} \quad \forall t \in \mathcal{T}$$

3. Define $\mathcal{D}_i$ as the set of one-shot demands with nonzero durations: $\mathcal{D}_i = \{n \mid t_s^n < t_{nz}^n\}$. Further, let $\mathcal{D}_i^n$ represent the subset within $\mathcal{D}_i$ where the peak demands fall within $[t_s^n, t_{nz}^n]$. For $n \in \mathcal{D}_i$, the condition is:

$$\sum_{l \in \mathcal{D}_i^n} \bar{a}^l \leq \frac{B}{\eta_d}$$

   This ensures that accommodating other one-shot demands in $[t_s^n, t_{nz}^n]$ using energy storage reserves enough capacity for the n-th one-shot demand.

The core rationale behind employing one-shot decomposition lies within storage management, where each time step facilitates a transfer of up to $\frac{B}{\eta_d}$. This delineates that any offline optimization decisions can be individually executed for each one-shot demand. For instance, if the optimal offline decision involves purchasing energy during a demand-free period, the purchase amount remains confined to $\frac{B}{\eta_d}$. Consequently,

the cumulative impact of applying an offline algorithm to each one-shot demand mirrors applying the same algorithm to the entire demand of each MG. The pivotal consideration centers on the sequence of occurrence for one-shot demands. With the involvement of multiple MGs, it becomes imperative to arrange one-shot demands sequentially, ensuring that the initiation time of each subsequent one-shot demand is greater than or equal to the non-zero time of the preceding one-shot demand.

Here in figure A.1 an example of decomposition of one-shot demands of two MGs are considered. In addition, the ordering of these one-shot decompositions are mentioned as well.

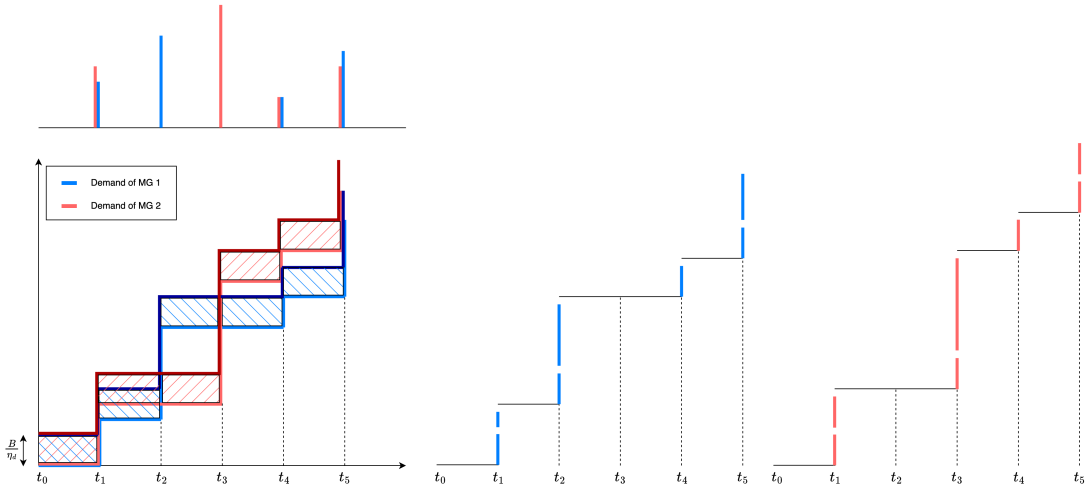

Figure A.1: One-shot decomposition

Now we can say that

$$\mathcal{A}_{\text{ofl}}\left[(a_i(t))_{i=1}^{I}\right] = \sum_{i=1}^{I}\sum_{n=1}^{N_i}\mathcal{A}_{\text{ofl}}\left[(t_s^n, t_{nz}^n, \bar{a}_i^n)\right]$$

Next, we need to perform the same analysis for our proposed algorithm. Given that each one-shot demand has a demand request denoted as $\bar{a}$, and considering that online algorithms operate when each demand is received, we can observe that $\hat{B}_i = \bar{a}_i(1-k_i\rho_i)$ can also represent the outcomes of the online algorithm on the entire demand. In the context of Constraint No. 3, we can conceptualize it as follows: we partition the battery capacity into $\bar{a}^n$ portions, where $\sum l :\in \mathcal{D}_i^n \bar{a}^l \leq \frac{B}{\eta_d}$.

Therefore, we can rewrite the competitive ratio as:

$$\mathrm{CR} = \max \frac{\mathcal{A}_{\text{alg}}\left[(a_i(t))_{i=1}^{I}\right]}{\mathcal{A}_{\text{ofl}}\left[(a_i(t))_{i=1}^{I}\right]} = \frac{\sum_{i=1}^{I}\sum_{n=1}^{N_i}\mathcal{A}\left[(t_s^n, t_{nz}^n, \bar{a}_i^n)\right]}{\sum_{i=1}^{I}\sum_{n=1}^{N_i}\mathcal{A}\left[(t_s^n, t_{nz}^n, \bar{a}_i^n)\right]}$$

Now let assume the unconstrained case where μ_c, μ_d could be higher than B. There are different cases based on the amount of renewable energy that can be satisfied by the renewable energy, and the energy price. Consider that if MGs had the ability to share energy among themselves, the combined cost of both $\mathcal{A}_{\text{alg}}$ and $\mathcal{A}_{\text{opt}}$ would decrease. However, the ratio between these costs would be lower compared to when energy sharing isn't an option. Consequently, the adversary will consistently opt for scenarios where energy sharing is not feasible.

Case 1. $p(t) \geq \theta_i$ for all $t \in [t_s^n, t_{nz}^n]$. In this case, the algorithm will not charge the storage from the grid. However, it is possible to charge it using the renewable energy. Let $\gamma_n^i \bar{a}_i^n$ be the amount of renewable energy that is available for one-shot demand of $\bar{a_i^n}$ from time t_s^n to t_{nz}^n. Based on the amount of γ_i^n there are different scenarios that can happen:

Case 1.1. $\boldsymbol{\frac{\eta_c}{\eta_d}\gamma_i^n \leq 1}$: In this case, the algorithm will charge $\gamma_i^n \hat{a}_i^n$ completely in the storage. Thus in the worst case, MG has to purchase the the rest from the grid. This is exactly the case in the offline setting.

$$\mathrm{Cost}\left[\mathcal{A}_{\text{alg}}\right] \leq (1 - \gamma_i^n \frac{\eta_c}{\eta_d})\bar{a}_i^n M\beta$$
$$\mathrm{Cost}\left[\mathcal{A}_{\text{ofl}}\right] \geq (1 - \gamma_i^n \frac{\eta_c}{\eta_d})\bar{a}_i^n \theta_i \frac{\eta_d}{\eta_c}$$

Case 1.2. $\boldsymbol{1 \leq \frac{\eta_c}{\eta_d}\gamma_i^n}$: In this case, since the adversary will select the cases that no sharing is possible, our algorithm and the optimal solution will work similarly. They both charge the battery completely and will sell the excessive energy to the grid with the price of αm. Thus in this case, the

costs are:

$$\text{Cost}\left[\mathcal{A}_{\text{alg}}\right] \leq (\frac{\eta_d}{\eta_c} - \gamma_i^n)\bar{a}_i^m \alpha m$$
$$\text{Cost}\left[\mathcal{A}_{\text{ofl}}\right] \geq (\frac{\eta_d}{\eta_c} - \gamma_i^n)\bar{a}_i^m \alpha m$$

Case 2. In this case, it is assumed that $p(t) \leq \theta_i$for some $t \in [t_s^n, t_{nz}^n]$. In this case, the algorithm will purchase energy from the main grid to charge its battery upto $\bar{a}_i^n(1 - k_i\rho_i)$. Same as Case 1. based on the amount of γ_i^n there are some possible scenarios. Here, in the worst-case scenario of online setting, MG charge its battery upto $\bar{a}_i^n(1 - k_i\rho_i)$ by purchasing energy from the grid first, and therefore there is not storage to store the renewable energy in it. there are only two scenarios:

Case 2.1. $\boldsymbol{\frac{\eta_c}{\eta_d}\gamma_i^n \leq \rho_i k_i \leq 1}$: In this case, the the worst scenario of online setting would buy energy from the grid with the price of θ_i at first and then has to satisfy its demand with the price of $M\beta$. However, the offline setting could purchase energy at the at the minimum cost in the best-case.

$$\text{Cost}\left[\mathcal{A}_{\text{alg}}\right] \leq (1 - k_i\rho_i)\bar{a}_i^n\theta_i\frac{\eta_d}{\eta_c} + (k_i\rho_i - \gamma_i^n\frac{\eta_c}{\eta_d})\bar{a}_i^n M\beta$$
$$\text{Cost}\left[\mathcal{A}_{\text{ofl}}\right] \geq (1 - \gamma_i^n\frac{\eta_c}{\eta_d})\bar{a}_i^n m$$

Case 2.2. $\boldsymbol{k_i\rho_i \leq \frac{\eta_c}{\eta_d}\gamma_i^n \leq 1}$: In this case, the worst-case of online algorithm will buy the energy from the grid first, and then sell the extra energy to the grid. In the offline setting, since still some purchasing is needed, the cost is similar to the previous case.

$$\text{Cost}\left[\mathcal{A}_{\text{alg}}\right] \leq (1 - k_i\rho_i)\bar{a}_i^n\theta_i\frac{\eta_d}{\eta_c} + (k_i\rho_i\frac{\eta_d}{\eta_c} - \gamma_i^n)\bar{a}_i^n \alpha m$$
$$\text{Cost}\left[\mathcal{A}_{\text{ofl}}\right] \geq (1 - \gamma_i^n\frac{\eta_c}{\eta_d})\bar{a}_i^n m$$

Case 2.3. $\boldsymbol{k_i\rho_i \leq 1 \leq \frac{\eta_c}{\eta_d}\gamma_i^n}$: In this case, the online algorithm is same as the previous one.However, in the offline setting, no purchasing is needed and

all we have is selling to the grid.

$$\begin{aligned}\text{Cost}\left[\mathcal{A}_{\text{alg}}\right] &\leq (1-k_i\rho_i)\bar{a}_i^n\theta_i\frac{\eta_d}{\eta_c}+(k_i\rho_i\frac{\eta_d}{\eta_c}-\gamma_i^n)\bar{a}_i^n\alpha m\\ \text{Cost}\left[\mathcal{A}_{\text{ofl}}\right] &\geq (\frac{\eta_d}{\eta_c}-\gamma_i^n)\bar{a}_i^n\alpha m\end{aligned}$$

It is worth to mention that $\frac{\eta_c}{\eta_d}\gamma_i^n$ could be greater or less than 1 or ρ_i for some n, but $\sum_{n=1}^{N_i}\frac{\eta_c}{\eta_d}\gamma_i^n\bar{a}_i^n=\rho_i\sum_{n=1}^{N_i}\bar{a}_i^n=\rho_i a_i(t)$.

Now, let A_1, A_2, A_3, A_3 and A_5 be the indices of one-shot demands that correspond to the Case 1.1, Case 1.2, Case 2.1, Case 2.2 and Case 2.3 respectively. To ease the notation, let $k_i\rho_i=\varrho_i$ and $\frac{\eta_d}{\eta_c}=\varepsilon$. Define $\mathsf{a}\coloneqq\sum_{i=1}^{I}\sum_{n=1}^{N_i}\bar{a}_i^n$, and

$$\begin{aligned}\mathsf{a}_i^1&\coloneqq\sum_{n\in A_1}\bar{a}_i^n & \mathsf{b}_i^1&\coloneqq\sum_{n\in A_1}\frac{\eta_c}{\eta_d}\gamma_i^n\bar{a}_i^n\\ \mathsf{a}_i^2&\coloneqq\sum_{n\in A_2}\bar{a}_i^n & \mathsf{b}_i^2&\coloneqq\sum_{n\in A_2}\frac{\eta_c}{\eta_d}\gamma_i^n\bar{a}_i^n\\ \mathsf{a}_i^3&\coloneqq\sum_{n\in A_3}\bar{a}_i^n & \mathsf{b}_i^3&\coloneqq\sum_{n\in A_3}\frac{\eta_c}{\eta_d}\gamma_i^n\bar{a}_i^n\\ \mathsf{a}_i^4&\coloneqq\sum_{n\in A_4}\bar{a}_i^n & \mathsf{b}_i^4&\coloneqq\sum_{n\in A_4}\frac{\eta_c}{\eta_d}\gamma_i^n\bar{a}_i^n\\ \mathsf{a}_i^5&\coloneqq\sum_{n\in A_5}\bar{a}_i^n & \mathsf{b}_i^5&\coloneqq\sum_{n\in A_5}\frac{\eta_c}{\eta_d}\gamma_i^n\bar{a}_i^n\end{aligned}$$

Also the relation between these new variables can be seen below:

$$\begin{aligned}&\mathsf{b}_i^1\leq\mathsf{a}_i^1\\ &\varrho_i\mathsf{a}_i^2\leq\mathsf{a}_i^2\leq\mathsf{b}_i^2\\ &\mathsf{b}_i^3\leq\varrho_i\mathsf{a}_i^3\leq\mathsf{a}_i^3\\ &\varrho_i\mathsf{a}_i^4\leq\mathsf{b}_i^4\leq\mathsf{a}_i^4\\ &\varrho_i\mathsf{a}_i^5\leq\mathsf{a}_i^5\leq\mathsf{b}_i^5\end{aligned}\tag{A.5}$$

Given that $\frac{\sum_i x_i}{\sum_i y_i}\leq\max_j\frac{x_j}{y_j}$ holds for $x_i, y_i\geq 0, \forall i$, and considering the equality $\max_i\max_j\cdot=\max_j\max_i\cdot$, the CR can be reformulated as follows:

$$\text{CR}=\max_i\left\{\max\frac{\phi_1(\mathsf{a}_i^1,\mathsf{b}_i^1)+\phi_2(\mathsf{a}_i^2,\mathsf{b}_i^2)+\phi_3(\mathsf{a}_i^3,\mathsf{b}_i^3)+\phi_4(\mathsf{a}_i^4,\mathsf{b}_i^4)+\phi_5(\mathsf{a}_i^5,\mathsf{b}_i^5)}{\psi_1(\mathsf{a}_i^1,\mathsf{b}_i^1)+\psi_2(\mathsf{a}_i^2,\mathsf{b}_i^2)+\psi_3(\mathsf{a}_i^3,\mathsf{b}_i^3)+\psi_4(\mathsf{a}_i^4,\mathsf{b}_i^4)+\psi_5(\mathsf{a}_i^5,\mathsf{b}_i^5)}\right\}$$

where

$$\phi_1(\mathsf{a}_i^1, \mathsf{b}_i^1) = (\mathsf{a}_i^1 - \mathsf{b}_i^1)M\beta$$

$$\phi_2(\mathsf{a}_i^2, \mathsf{b}_i^2) = \varepsilon(\mathsf{a}_i^2 - \mathsf{b}_i^2)\alpha m$$

$$\phi_3(\mathsf{a}_i^3, \mathsf{b}_i^3) = (1 - \varrho_i)\mathsf{a}_i^3\theta_i\varepsilon + (\varrho_i\mathsf{a}_i^3 - \mathsf{b}_i^3)M\beta$$

$$\phi_4(\mathsf{a}_i^4, \mathsf{b}_i^4) = (1 - \varrho_i)\mathsf{a}_i^4\theta_i\varepsilon + \varepsilon(\varrho_i\mathsf{a}_i^4 - \mathsf{b}_i^4)\alpha m$$

$$\phi_5(\mathsf{a}_i^5, \mathsf{b}_i^5) = (1 - \varrho_i)\mathsf{a}_i^5\theta_i\varepsilon + \varepsilon(\varrho_i\mathsf{a}_i^5 - \mathsf{b}_i^5)\alpha m$$

$$\psi_1(\mathsf{a}_i^1, \mathsf{b}_i^1) = (\mathsf{a}_i^1 - \mathsf{b}_i^1)\theta_i\varepsilon$$

$$\psi_2(\mathsf{a}_i^2, \mathsf{b}_i^2) = \varepsilon(\mathsf{a}_i^2 - \mathsf{b}_i^2)\alpha m$$

$$\psi_3(\mathsf{a}_i^3, \mathsf{b}_i^3) = (\mathsf{a}_i^3 - \mathsf{b}_i^3)m$$

$$\psi_4(\mathsf{a}_i^4, \mathsf{b}_i^4) = (\mathsf{a}_i^4 - \mathsf{b}_i^4)m$$

$$\psi_5(\mathsf{a}_i^5, \mathsf{b}_i^5) = \varepsilon(\mathsf{a}_i^5 - \mathsf{b}_i^5)\alpha m$$

The location of the maximum value can be on the boundary of the feasible region or within it. If it is found within the region, it necessitates that the function's gradient, comprising all its partial derivatives, equals zero. This stipulation arises from the foundational concept that:

$$\mathsf{a}_i = \mathsf{a}_i^1 + \mathsf{a}_i^2 + \mathsf{a}_i^3 + \mathsf{a}_i^4 + \mathsf{a}_i^5$$

$$\rho_i\mathsf{a}_i = \mathsf{b}_i^1 + \mathsf{b}_i^2 + \mathsf{b}_i^3 + \mathsf{b}_i^4 + \mathsf{b}_i^5$$

we can see that the partial derivative with respect to a_i^2 ($\frac{\partial}{\partial \mathsf{a}_i^2}$) is always non-zero. This implies that the maximum cannot be within the feasible region. Thus, it must be on the boundary of the feasible region. There are 10 variables in total ($\mathsf{a}_i^1 \ldots \mathsf{a}_i^5, \mathsf{b}_i^1, \ldots \mathsf{b}_i^5$). Based on the constraints of equations A.5, we can deduce that there are 15 boundary points, and any combination of these 15 points could be critical in determining the maximum. Therefore, there are $2^{15} - 1$ possible combinations of boundary points. Many of these combinations are identical due to the relationships between them, and

many are not feasible because both the numerator and the denominator must be greater than zero. Our observations indicate that, among all combinations, there are 6 critical cases that can lead us to the competitive ratio of this algorithm.

a. $\mathbf{a_i^1 = b_i^1, a_i^2 = b_i^2, a_i^5 = b_i^5}$: Now we can rewrite the CR in this case as:

$$\begin{aligned}&\frac{\phi_1(\mathsf{a}_i^1,\mathsf{b}_i^1)+\phi_2(\mathsf{a}_i^2,\mathsf{b}_i^2)+\phi_3(\mathsf{a}_i^3,\mathsf{b}_i^3)+\phi_4(\mathsf{a}_i^4,\mathsf{b}_i^4)+\phi_5(\mathsf{a}_i^5,\mathsf{b}_i^5)}{\psi_1(\mathsf{a}_i^1,\mathsf{b}_i^1)+\psi_2(\mathsf{a}_i^2,\mathsf{b}_i^2)+\psi_3(\mathsf{a}_i^3,\mathsf{b}_i^3)+\psi_4(\mathsf{a}_i^4,\mathsf{b}_i^4)+\psi_5(\mathsf{a}_i^5,\mathsf{b}_i^5)}\\ &\leq \frac{\theta_i\varepsilon(1-\varrho_i)+\varrho_i(M\beta-\alpha\varepsilon m)(1-\rho_i)-(\rho_i-\varrho_i)\varepsilon\alpha m}{m(1-\rho_i)}\end{aligned}$$

This conclusion is derived through standard algebraic manipulations.

$$\begin{aligned}&\phi_1(\mathsf{a}_i^1,\mathsf{b}_i^1)+\phi_2(\mathsf{a}_i^2,\mathsf{b}_i^2)+\phi_3(\mathsf{a}_i^3,\mathsf{b}_i^3)+\phi_4(\mathsf{a}_i^4,\mathsf{b}_i^4)+\phi_5(\mathsf{a}_i^5,\mathsf{b}_i^5)\\ =&(1-\varrho_i)\mathsf{a}_i^3\theta_i\varepsilon+(\varrho_i\mathsf{a}_i^3-\mathsf{b}_i^3)M\beta\\ &+(1-\varrho_i)\mathsf{a}_i^4\theta_i\varepsilon+\varepsilon(\varrho_i\mathsf{a}_i^4-\mathsf{b}_i^4)\alpha m\\ &+(1-\varrho_i)\mathsf{a}_i^5\theta_i\varepsilon+\varepsilon(\varrho_i\mathsf{a}_i^5-\mathsf{b}_i^5)\alpha m\\ =&(1-\varrho_i)\mathsf{a}_i\theta_i\varepsilon+(\varrho_i-\rho_i)\mathsf{a}_i\varepsilon\alpha m+(\varrho_i\mathsf{a}_i^3-\mathsf{b}_i^3)(M\beta-\varepsilon\alpha m)\\ &\text{Since: } \varrho_i\mathsf{a}_i^3-\mathsf{b}_i^3\leq\varrho_i(\mathsf{a}_i-\mathsf{b}_i)=\varrho_i\mathsf{a}_i(1-\rho_i)\\ \Rightarrow&\phi_3(\mathsf{a}_i^3,\mathsf{b}_i^3)+\phi_4(\mathsf{a}_i^4,\mathsf{b}_i^4)+\phi_5(\mathsf{a}_i^4,\mathsf{b}_i^5)\\ &\leq(1-\varrho_i)\mathsf{a}_i\theta_i\varepsilon+(\varrho_i-\rho_i)\mathsf{a}_i\varepsilon\alpha m+\varrho_i\mathsf{a}_i(1-\rho_i)(M\beta-\varepsilon\alpha m)\end{aligned}$$

Also:

$$\begin{aligned}&\psi_1(\mathsf{a}_i^1,\mathsf{b}_i^1)+\psi_2(\mathsf{a}_i^2,\mathsf{b}_i^2)+\psi_3(\mathsf{a}_i^3,\mathsf{b}_i^3)+\psi_4(\mathsf{a}_i^4,\mathsf{b}_i^4)+\psi_5(\mathsf{a}_i^5,\mathsf{b}_i^5)\\ =&m(\mathsf{a}_i^3-\mathsf{b}_i^3)m+(\mathsf{a}_i^4-\mathsf{b}_i^4)m=m(1-\rho_i)\mathsf{a}_i\\ &\Longrightarrow\checkmark\end{aligned}$$

The proof for the other cases is straightforward and similar to this one. They are omitted for brevity.

b. $\mathbf{a_i^1 = b_i^1, a_i^4 = 0, a_i^5 = 0, b_i^3 = 0}$: We know $\mathsf{a}_i^4 = 0, \mathsf{a}_i^5 = 0 \Rightarrow \mathsf{b}_i^4 = 0, \mathsf{b}_i^5 = 0$. Now we can rewrite the CR as:

$$\frac{\phi_1(\mathsf{a}_i^1, \mathsf{b}_i^1) + \phi_2(\mathsf{a}_i^2, \mathsf{b}_i^2) + \phi_3(\mathsf{a}_i^3, 0)}{\psi_1(\mathsf{a}_i^1, \mathsf{b}_i^1) + \psi_2(\mathsf{a}_i^2, \mathsf{b}_i^2) + \psi_3(\mathsf{a}_i^3, 0)} \leq \frac{\theta_i \varepsilon(1-\varrho_i) + \varrho_i(M\beta - \alpha\varepsilon m) - (\rho_i - \varrho_i)\varepsilon\alpha m}{(1-\alpha\rho_i\varepsilon)m}$$

c. $\mathbf{a_i^1 = b_i^1, a_i^2 = b_i^2, a_i^5 = b_i^5, a_i^3 = 0}$: We know $\mathsf{a}_i^3 = 0 \Rightarrow \mathsf{b}_i^3 = 0$. Now we can rewrite the CR in this case as:

$$\frac{\phi_1(\mathsf{a}_i^1, \mathsf{b}_i^1) + \phi_2(\mathsf{a}_i^2, \mathsf{b}_i^2) + \phi_4(\mathsf{a}_i^4, \mathsf{b}_i^4) + \phi_5(\mathsf{a}_i^5, \mathsf{b}_i^5)}{\psi_1(\mathsf{a}_i^1, \mathsf{b}_i^1) + \psi_2(\mathsf{a}_i^2, \mathsf{b}_i^2) + \psi_4(\mathsf{a}_i^4, \mathsf{b}_i^4) + \psi_5(\mathsf{a}_i^5, \mathsf{b}_i^5)} \leq \frac{\theta_i \varepsilon(1-\varrho_i) - (\rho_i - \varrho_i)\varepsilon\alpha m}{m(1-\rho_i)}$$

d. $\mathbf{a_i^1 = b_i^1, a_i^4 = 0, a_i^5 = 0, b_i^3 = \varrho_i a_i^3}$: We know $\mathsf{a}_i^4 = 0, \mathsf{a}_i^5 = 0 \Rightarrow \mathsf{b}_i^4 = 0, \mathsf{b}_i^5 = 0$. Now we can rewrite the CR in this case as:

$$\frac{\phi_1(\mathsf{a}_i^1, \mathsf{b}_i^1) + \phi_2(\mathsf{a}_i^2, \mathsf{b}_i^2) + \phi_3(\mathsf{a}_i^3, \varrho_i \mathsf{a}_i^3)}{\psi_1(\mathsf{a}_i^1, \mathsf{b}_i^1) + \psi_2(\mathsf{a}_i^2, \mathsf{b}_i^2) + \psi_3(\mathsf{a}_i^3, \varrho_i \mathsf{a}_i^3)} \leq \frac{\theta_i \varepsilon(1-\varrho_i) - (\rho_i - \varrho_i)\varepsilon\alpha m}{(1-\varrho_i)m - (\rho_i - \varrho_i)\varepsilon\alpha m}$$

e. $\mathbf{a_i^2 = b_i^2, a_i^4 = b_i^4, a_i^5 = b_i^5, a_i^3 = 0}$: We know $\mathsf{a}_i^3 = 0 \Rightarrow \mathsf{b}_i^3 = 0$. Now we can rewrite the CR in this case as:

$$\frac{\phi_1(\mathsf{a}_i^1, \mathsf{b}_i^1) + \phi_2(\mathsf{a}_i^2, \mathsf{b}_i^2) + \phi_4(\mathsf{a}_i^4, \mathsf{b}_i^4) + \phi_5(\mathsf{a}_i^5, \mathsf{b}_i^5)}{\psi_1(\mathsf{a}_i^1, \mathsf{b}_i^1) + \psi_2(\mathsf{a}_i^2, \mathsf{b}_i^2) + \psi_4(\mathsf{a}_i^4, \mathsf{b}_i^4) + \psi_5(\mathsf{a}_i^5, \mathsf{b}_i^5)} \leq \frac{\theta_i \varepsilon \rho_i(1-\varrho_i) + (M\beta - \alpha\varrho_i\varepsilon m)(1-\rho_i) - (\rho_i - \varrho_i)\varepsilon\alpha m}{\theta_i\varepsilon(1-\rho_i)}$$

f. $\mathbf{a_i^3 = 0, a_i^4 = 0, a_i^5 = 0}$: We know $\mathsf{a}_i^3 = 0, \mathsf{a}_i^4 = 0, \mathsf{a}_i^5 = 0 \Rightarrow \mathsf{b}_i^3 = 0, \mathsf{b}_i^4 = 0, \mathsf{b}_i^5 = 0$. Now we can rewrite the CR in this case as:

$$\frac{\phi_1(\mathsf{a}_i^1, \mathsf{b}_i^1) + \phi_2(\mathsf{a}_i^2, \mathsf{b}_i^2)}{\psi_1(\mathsf{a}_i^1, \mathsf{b}_i^1) + \psi_2(\mathsf{a}_i^2, \mathsf{b}_i^2)} \leq \frac{M\beta - \alpha\varrho_i\varepsilon m - (\rho_i - \varrho_i)\varepsilon\alpha m}{\theta_i\varepsilon - \rho_i\alpha\varepsilon m}$$

Figure A.2 shows the competitive ratio as a function of θ_i for all these cases.

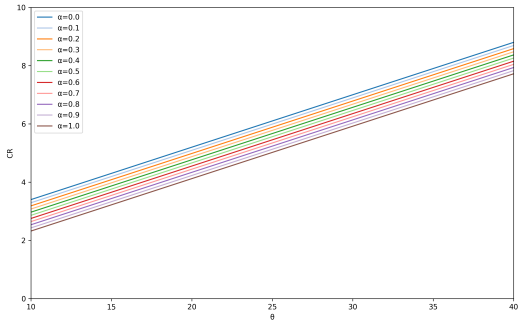

(a) $\mathsf{a}_i^1 = \mathsf{b}_i^1, \mathsf{a}_i^2 = \mathsf{b}_i^2, \mathsf{a}_i^5 = \mathsf{b}_i^5$

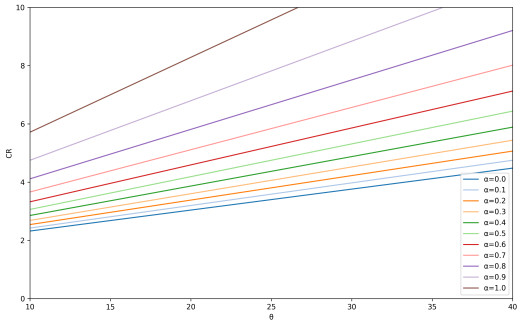

(b) $\mathsf{a}_i^1 = \mathsf{b}_i^1, \mathsf{a}_i^4 = \mathbf{0}, \mathsf{a}_i^5 = \mathbf{0}, \mathsf{b}_i^3 = \mathbf{0}$

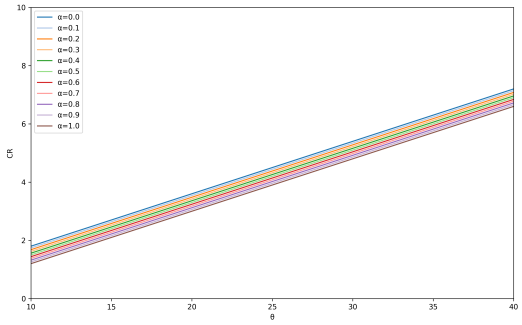

(c) $\mathsf{a}_i^1 = \mathsf{b}_i^1, \mathsf{a}_i^2 = \mathsf{b}_i^2, \mathsf{a}_i^5 = \mathsf{b}_i^5, \mathsf{a}_i^3 = \mathbf{0}$

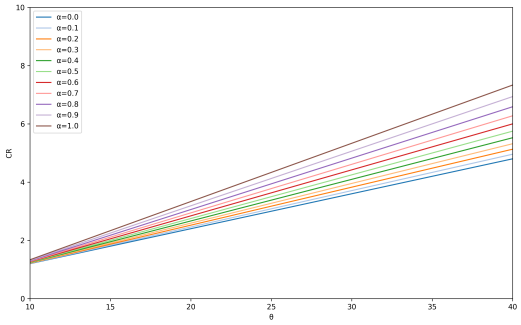

(d) $\mathsf{a}_i^1 = \mathsf{b}_i^1, \mathsf{a}_i^4 = \mathbf{0}, \mathsf{a}_i^5 = \mathbf{0}, \mathsf{b}_i^3 = \boldsymbol{\varrho}_i \mathsf{a}_i^3$

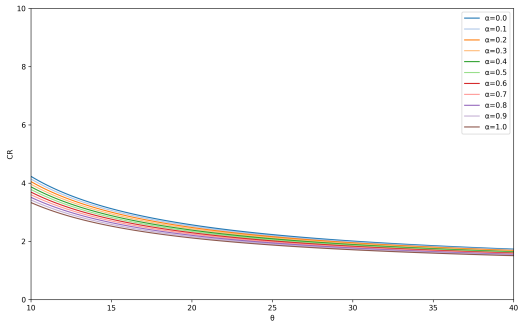

(e) $\mathsf{a}_i^2 = \mathsf{b}_i^2, \mathsf{a}_i^4 = \mathsf{b}_i^4, \mathsf{a}_i^5 = \mathsf{b}_i^5, \mathsf{a}_i^3 = \mathbf{0}$

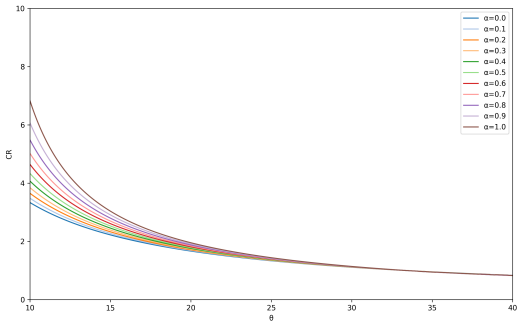

(f) $\mathsf{a}_i^3 = \mathbf{0}, \mathsf{a}_i^4 = \mathbf{0}, \mathsf{a}_i^5 = \mathbf{0}$

Figure A.2: Critical boundary cases of the competitive ratio

It is evident that case c. consistently yields lower results than case a., attributed to the premise $M\beta \geq \alpha \frac{\eta_d}{\eta_c} m$. Furthermore, it is straightforward to confirm that case d. falls below case a. when $\alpha \frac{\eta_d}{\eta_c} \leq 1$, and beneath case b. when $\alpha \frac{\eta_d}{\eta_c} \geq 1$. Consequently, these two cases can be disregarded as they are not dominant. Moreover, only two viable pairings exist between cases a., b., e., and f.: specifically, the combination of

case a. with e. and case b. with f. These lead to two distinct competitive ratio solutions, with the higher value being designated as the competitive ratio for that MG. Thus,

$$\mathrm{CR} \leq \max\left\{ \begin{array}{l} \dfrac{\theta_i^1\varepsilon(1-\varrho_i)+\varrho_i(M\beta-\alpha\varepsilon m)(1-\rho_i)-(\rho_i-\varrho_i)\varepsilon\alpha m}{m(1-\rho_i)}, \\ \dfrac{\theta_i^1\varepsilon\rho_i(1-\varrho_i)+(M\beta-\alpha\varrho_i\varepsilon m)(1-\rho_i)-(\rho_i-\varrho_i)\varepsilon\alpha m}{\theta_i^1\varepsilon(1-\rho_i)} \\ \dfrac{\theta_i^2\varepsilon(1-\varrho_i)+\varrho_i(M\beta-\alpha\varepsilon m)-(\rho_i-\varrho_i)\varepsilon\alpha m}{(1-\alpha\rho_i\varepsilon)m}, \\ \dfrac{M\beta-\alpha\varrho_i\varepsilon m-(\rho_i-\varrho_i)\varepsilon\alpha m}{\theta_i^2\varepsilon-\rho_i\alpha\varepsilon m} \end{array} \right\}$$

where θ_i^1 and θ_i^2 are the results obtained from the following equations (see Figure A.3).

$$\begin{aligned} &\frac{\theta_i^1\varepsilon(1-\varrho_i)+\varrho_i(M\beta-\alpha\varepsilon m)(1-\rho_i)-(\rho_i-\varrho_i)\varepsilon\alpha m}{m(1-\rho_i)} \\ =&\frac{\theta_i^1\varepsilon\rho_i(1-\varrho_i)+(M\beta-\alpha\varrho_i\varepsilon m)(1-\rho_i)-(\rho_i-\varrho_i)\varepsilon\alpha m}{\theta_i^1\varepsilon(1-\rho_i)} \end{aligned}$$

$$\begin{aligned} &\frac{\theta_i^2\varepsilon(1-\varrho_i)+\varrho_i(M\beta-\alpha\varepsilon m)-(\rho_i-\varrho_i)\varepsilon\alpha m}{(1-\alpha\rho_i\varepsilon)m} \\ =&\frac{M\beta-\alpha\varrho_i\varepsilon m-(\rho_i-\varrho_i)\varepsilon\alpha m}{\theta_i^2\varepsilon-\rho_i\alpha\varepsilon m} \end{aligned}$$

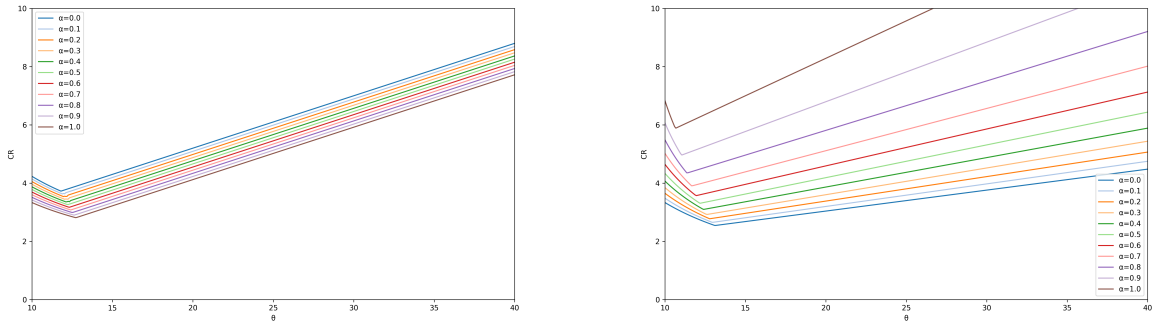

(a) θ_i^1 equations. (b) θ_i^2 equations.

Figure A.3: θ_i^1 and θ_i^2 illustration.

Now, let's consider the cases that charging and discharging rates are less than the battery capacity. With μ_c less than B, energy must be stored over multiple time slots rather than a single slot, which is possible when rates are not limited. This restriction can prevent the system from capitalizing on the lowest market prices at a given moment for energy uptake from the grid. The algorithm, which operates on a fixed threshold θ, maintains its competitive ratio; it is not worsened by limited charging rates compared to when rates are unlimited.

On the other hand, if μ_d is less than B, demands that could have been met by immediate energy release from storage must instead be fulfilled by direct grid energy during the time of need, altering the strategy for both online and offline algorithms. Nevertheless, this constraint on discharging rates does not increase the competitive ratio beyond that of the scenario with unrestricted rates.

Once the competitive ratio for each MG is calculated, the competitive ratio of the whole algorithm is determined as the maximum among them.

■